IMPERIAL COLLEGE LONDON

SIGNAL PROCESSING FOR GUIDED WAVE STRUCTURAL HEALTH MONITORING

by

Tindaro Cicero

A thesis submitted to Imperial College London for the degree of

Doctor of Philosophy

Department of Mechanical Engineering

Imperial College London

London SW7 2AZ

July 2009

Abstract

The importance of Structural Health Monitoring (SHM) in several industrial fields has been continuously growing in the last few years with the increasing need for the development of systems able to monitor continuously the integrity of complex structures. In order to be competitive with conventional non destructive evaluation techniques, SHM must be able to effectively detect the occurrence of damage in the structure, giving information regarding the damage location. Ultrasonic guided waves offer the possibility of inspecting large areas of structures from a small number of sensor positions. However, inspection of complex structures is difficult as the reflections from different features overlap. Therefore damage detection becomes an extremely challenging problem and robust signal processing is required in order to resolve strongly overlapping echoes.

In our work we have considered at first the possibility of employing a deconvolution approach for enhancing the resolution of ultrasonic time traces and the potential and the limitations of this approach for reliable SHM applications have been shown. The effects of noise on the bandwidth of the typical signals in SHM and the effects of frequency dependent phase shifts are the main detrimental issues that strongly reduce the performance of deconvolution in SHM applications.

The second part of this thesis is concerned with the evaluation of a subtraction approach for SHM when changes of environmental conditions are taken into account. Temperature changes result in imperfect subtraction even for an undamaged structure, since temperature changes modify the mechanical properties of the material and therefore the velocity of propagation of ultrasonic guided waves. Compensation techniques have previously been used effectively to overcome temperature effects, in order to reduce the residual in the subtraction. In this work the performance of temperature compensation techniques has been evaluated also in the presence of other detrimental effects, such as liquid loading and different temperature responses of materials in adhesive joints. Numerical simulations and experiments have been conducted and it has been shown that temperature compensation techniques can cope

in principle with non temperature effects. It is concluded that subtraction approach represents a promising method for reliable Structural Health Monitoring. Nonetheless the feasibility of a subtraction approach for SHM depends on environmental conditions.

Acknowledgements

I would like to express my gratitude to my supervisors Prof. Peter Cawley, Dr. Francesco Simonetti and Prof. Mike Lowe for their superb guidance and endless patience. Being in the Nondestructive Testing group I was not only part of a stimulating and lively research environment, but I felt part of an incredible group of friends. I want to extend my thanks to Daniel, Marco, Ken, Prabhu, Fred, Matt, Thomas, Giuseppe, Pierre, Remo and all the other colleagues with whom I enjoyed sharing this invaluable experience at Imperial College. I am sure you will remain friends for life.

I am deeply indebted to Prof. Stanislav I. Rokhlin for his help and precious advice and for the patience shown in our long and useful discussions.

Finally, I want to express my deepest gratitude to my family for their support and encouragement throughout my studies. I have always felt that you were close by over the years. Heartfelt thanks goes to Anna for standing by me every day and for continuously renewing my enthusiasm. Last (but not least) thanks to my little niece Antonella who has brought so much joy in the last few months of my PhD.

Contents

1 Introduction **22**

1.1 Motivation 22

1.2 Thesis outline 24

2 An introduction to Structural Health Monitoring **26**

2.1 Overview 26

2.2 Aircraft design and Structural Health Monitoring 27

2.3 Passive systems for Structural Health Monitoring: Acoustic Emission 29

2.4 Active systems for Structural Health Monitoring: Guided wave SHM systems 32

2.4.1 Single mode transduction for an active Guided wave SHM system 32

2.4.2 Guided wave SHM arrays 34

2.4.3 Single unit arrays for SHM 35

2.4.4 Distributed sparse arrays for SHM 37

2.5 Signal processing for Structural Health Monitoring 41

3 Literature Review on Deconvolution techniques 43

3.1 Introduction 43

3.2 Causality, Stability and Minimum phase properties 45

3.3 Least squares deconvolution 46

3.4 Autoregressive spectral extrapolation 48

3.5 Maximum likelihood deconvolution 49

3.6 Minimum entropy deconvolution 50

3.7 Iterative deconvolution 52

3.8 L_P-norm deconvolution 53

3.9 Deconvolution approach for phase shifted signals 54

3.10 Summary 55

4 Deconvolution Approach for Structural Health Monitoring 56

4.1 The Deconvolution approach 56

4.2 Mathematical Model for Deconvolution Approach 58

4.3 The Wiener filter approach for deconvolution 59

4.3.1 Non optimal Wiener Filter 60

4.3.2 Optimal Wiener Filter 61

4.4 A typical problem in Structural Health Monitoring 62

4.5 Effect of noise on deconvolution performance 63

4.5.1 Broadband Input wavelet: performance of the optimal Wiener filter 63

4.5.2 Hanning windowed toneburst: effect of limited bandwidth on temporal resolution 64

4.6 Effect of phase shift on deconvolution performance 65

4.6.1 Frequency independent phase shift. Reflection from the free edge of a plate 65

4.6.2 Frequency dependent phase shift. Plane strain model for a plate with a rib 67

4.7 Combined effect of noise and phase shift 69

4.7.1 Introduction to the SMLR algorithm 70

4.7.2 Performance of SMLR algorithm on a typical problem in SHM 72

4.8 Summary 73

5 Subtraction Approach for Structural Health Monitoring 75

5.1 Background 75

5.2 Detrimental factors for subtraction performance 77

5.3 Effect of temperature changes on signal subtraction 78

5.4 Temperature compensation techniques 79

5.4.1 Signal processing for the subtraction approach 80

5.4.2 Optimal Baseline method 82

5.4.3 Optimal Stretch method 83

5.4.4 Local Temporal Coherence method 86

5.4.5 Combination of compensation techniques 86

5.5 SHM applications of Temperature Compensation Techniques 87

5.6 Summary 90

6 Effects of Liquid Loading on Subtraction approach 91

6.1 Background 91

6.2 Guided waves in bilayered plates 92

6.3 Parameters affecting guided wave propagation in a fluid-solid bilayer . 94

6.4 Comparing Liquid Loading to Temperature changes 96

6.4.1 S_0 mode in Aluminium-water bilayer 97

6.4.2 A_0 mode in Aluminium-water bilayer 99

6.5 Performance of Optimal Baseline and Optimal Stretch with liquid loading 101

6.6 Infinite water layer on an aluminium plate 103

6.6.1 Amplitude compensation for the S_0 mode 104

6.6.2 Performance of Optimal Baseline and Optimal Stretch with liquid loading: Infinite water layer 106

6.7 Subtraction approach in presence of an epoxy layer 107

6.7.1 Performance of Optimal Baseline and Optimal Stretch with a thin epoxy layer 108

6.8 Experimental work 112

6.9 Experiment with an infinite water layer 113

6.9.1 Experimental setup 113

6.9.2 Measurement procedure 115

6.9.3 Results 117

6.10 Experiment with a thin uniform viscoelastic layer 121

6.10.1 Results 122

6.11 Experiment with a non uniform viscoelastic layer 125

6.12 Summary 126

7 Effects of different temperature responses in adhesive joints on Subtraction approach 128

7.1 Background 128

7.2 Different temperature responses of materials and Temperature Compensation techniques 129

7.3 Experimental setup and 3D FE model 130

7.3.1 Experimental setup 130

7.3.2 3D FE model 132

7.4 Results of numerical simulations 133

7.5 Preliminary experiments: performance of Optimal Stretch method . . 136

7.5.1 Optimal Stretch performance 136

7.5.2 Optimal Baseline performance 138

7.6 Second series of experiments on the bonded stringer 140

7.6.1 Optimal Stretch performance 141

7.6.2 Optimal Baseline performance 143

7.7 Temperature compensation strategy and damage detection [1] 143

7.7.1 Compensation strategy performance: undamaged structure . . 144

7.7.2 Compensation strategy performance: damaged structure . . . 145

7.8 Summary 149

8 Conclusions **151**

8.1 Thesis Review 151

8.2 Brief summary of the main contributions 153

8.3 Future work 155

References **157**

List of Publications **171**

List of Figures

1.1 *Aerospace, oil and gas industry, chemical and power generation plants are potential fields of application for SHM.* 23

2.1 *Schematic representation of an airframe structure [3].* 28

2.2 *Dispersion curves for a steel plate. a)Phase Velocity, b)Group Velocity.* 30

2.3 *a)Single unit array, b)Distributed sparse array.* 34

3.1 *Convolution process in nondestructive evaluation.* 44

4.1 *Time trace recorded in a 1000 × 1000 × 5 mm aluminium plate.* . . . 57

4.2 *a) Pitch catch inspection of a plate. The typical recorded signal contains strongly overlapping echoes. b) Ideal deconvolution: the wave packets of the received signals have been compressed to sharp spikes, allowing the identification of the different echoes.* 58

4.3 *Generation of strongly overlapping signals. The two reflections are not resolvable.* 62

4.4 *Broadband input wavelet: detection of a small reflection by means of the optimal Wiener filter.* 63

4.5 *Comparison between Hanning toneburst and broadband input wavelet.* 64

4.6 *Hanning toneburst: detection of a small reflection by means of the optimal Wiener filter.* 65

4.7 *Wavelet modification caused by a $\pi/2$ rad phase shift on a 3 cycle Hanning toneburst (the propagated distance for the reflected signal is 50 mm).* 66

4.8 *Deconvolution of $\pi/2$ rad phase shifted signal.* 67

4.9 *Plane strain model of a steel plate with a rib.* 68

4.10 *Input and reflected signals from the rib for the incident A_0 mode.* . . 68

4.11 *Reflection coefficient from a rib. Ideal deconvolution.* 69

4.12 *Reference and test sequences for the SMLR algorithm.* 71

4.13 *Typical problem in SHM. Deconvolution of two strongly overlapping signals (SNR = 40 dB). Detection and estimation of arrival times and amplitudes by means of SMLR algorithm.* 72

4.14 *Received signal with a $\pi/2$ rad frequency independent phase shift, SNR = 40 dB. Detection and amplitude estimation by means of the SMLR algorithm.* 73

5.1 *Ideal Baseline subtraction for SHM. The subtraction of the baseline from the current signal leads to a subtracted signal from which the presence of a defect can be determined.* 76

5.2 *Schematic of the time shift and maximum residual in the subtraction for a 5 cycle Hanning toneburst.* 80

5.3 *Optimal Baseline subtraction for SHM. The temperature difference of the two time traces is 0.1 °C. The maximum residual is -38 dB [103].* 82

5.4 *Amplitude of the subtracted signal on a dB scale relative to the amplitude of the first arrival in figure 5.3 [103].* 83

5.5 *Uncompensated subtraction with a 5 °C temperature difference. The maximum residual is -10 dB [103].* 85

5.6 *Optimal Stretch subtraction for SHM. The temperature difference of the two time traces is 5 °C. The maximum residual is -38 dB [103].* . 85

5.7 *Amplitude in dB scale of the subtracted signal relative to the amplitude of the first arrival in figure 5.6 [103].* 86

6.1 *Schematic of an aluminium-water bilayer. τ is the ratio of liquid thickness to plate thickness.* 92

6.2 *a)Comparison of the dispersion curve for an aluminium-water bilayer and a free aluminimim plate. b)Difference between the two phase velocities. The plate thickness is 10 mm and $\tau = 0.01$.* 95

6.3 *a) Uncompensated subtraction for a 10 °C temperature change for the S_0 mode. The maximum residual is -11 dB. b)Uncompensated subtraction with liquid loading. The maximum residual is -28.5 dB.* . 98

6.4 *S_0 mode. Comparison of the dispersion curve for the aluminium water bilayer at 20 °C with the dispersion curves for the free plate at 20 and 30 °C. The values of the corresponding phase velocities at centre frequency are indicated.* 99

6.5 *a) Uncompensated subtraction for a 10 °C temperature change for the A_0 mode. The maximum residual is -16 dB. b) Uncompensated subtraction with liquid loading. The maximum residual is -19 dB.* . . 100

6.6 *A_0 mode. Comparison of the dispersion curve for the aluminium water bilayer at 20 °C with the dispersion curves for the free plate at 20 and 30°C. The values of the corresponding phase velocities at centre frequency are indicated.* 101

6.7 *Compensation of the subtraction for the S_0 mode. Performance of Optimal Baseline and Optimal Stretch in presence of a uniform water layer, $\tau = 0.01$, d=10mm.* 103

6.8 *Compensation of the subtraction for the A_0 mode. Performance of Optimal Baseline and Optimal Stretch in presence of a uniform water layer.* 104

6.9 *Attenuation curve for a 10 mm thick aluminium plate bordered by an infinite water. The frequency range is shown is typical for S_0 mode inspection.* 105

6.10 *Amplitude compensation in frequency domain. The original signals are shown on the top left corner. The amplitude of the signal measured in the liquid loaded plate is compensated in frequency domain (right). The amplitude compensated signal is compared with the reference signal obtained from the free plate (bottom left corner).* 106

6.11 *S_0 mode. Comparison of the dispersion curve for the aluminium water bilayer ($\tau = \infty$) at 20 °C with the dispersion curves for the free plate at 20 and 30° C. The values of the corresponding phase velocities at centre frequency are indicated.* 107

6.12 *Compensation of the subtraction for the S_0 mode. Performance of Optimal Baseline and Optimal Stretch in presence of an infinite water layer.* 108

6.13 *Uncompensated subtraction for the propagation of the S_0 mode in presence of a thin epoxy layer ($\tau = 0.01$). The maximum residual is -12.5 dB.* 109

6.14 *S_0 mode. Comparison of the dispersion curve for the aluminium epoxy bilayer ($\tau = 0.01$) at 20 °C with the dispersion curves for the free plate at 20 and 30 °C. The values of the corresponding phase velocities at centre frequency are indicated.* 110

6.15 *Compensation of the subtraction for the S_0 mode. Performance of Optimal Baseline and Optimal Stretch in presence of a thin epoxy layer.* 111

6.16 *Uncompensated subtraction for the propagation of the A_0 mode in presence of a thin epoxy layer ($\tau = 0.01$). The maximum residual is -21 dB.* 111

6.17 *A_0 mode. Comparison of the dispersion curve for the aluminium epoxy bilayer ($\tau = 0.01$) at 20 °C with the dispersion curves for the free plate at 20 and 30 °C. The values of the corresponding phase velocities at centre frequency are indicated.* 112

6.18 *Compensation of the subtraction for the A_0 mode. Performance of Optimal Baseline and Optimal Stretch in presence of a thin epoxy layer.* 113

6.19 *Pitch-catch inspection of an aluminium plate.* 114

6.20 *Schematic of a piezoelectric transducer encapsulated with waterproof silicone. The electrical insulator avoids electrical contact between the transducer and the plate.* 114

6.21 *Aluminium plate instrumented with transducers on 3 adjustable height, point supports.* 115

6.22 *Cross section of the experimental setup immersed in a water tank.* . . . 116

6.23 *Leakage phenomenon in a plate immersed by water. Energy radiates in the surrounding fluid creating a leaky bulk wave at a characteristic angle θ.* 116

6.24 *Comparison of a current signal measured from the immersed plate with the reference signal recorded from the free plate at the same temperature. The dashed line represents the first arrival of the water surface reflection.* 118

6.25 *Amplitude ratio between current signal measured from the immersed plate and baseline. Multiple reverberations are responsible for peaks and troughs in the actual trend. Running averages can be used to smooth the curve.* 119

6.26 *Zoomed view of area enclosed in the dashed rectangle of figure 6.25.* . 119

6.27 *Compensation of the subtraction for the S_0 mode. Performance of Optimal Baseline and Optimal Stretch in presence of an infinite water layer.* 120

6.28 *Top view of the aluminium plate coated with a thin epoxy layer. The transducers (dotted circles) are bonded to the back surface of the plate.* 122

6.29 *Comparison of a current signal measured from the plate coated with a thin epoxy layer with the reference signal recorded from the free plate at the same temperature.* 123

6.30 *Amplitude ratio between current signal measured from the plate coated with an epoxy layer and baseline. Multiple reverberations are responsible for peaks and troughs in the actual trend. Running averages can be used to smooth the curve.* 123

6.31 *Compensation of the subtraction for the S_0 mode. Performance of Optimal Baseline and Optimal Stretch in presence of a thin uniform epoxy layer.* 124

6.32 *Non uniform viscoelastic layer on an aluminium plate. The area enclosed in the dashed square represents the adhesive patch removed from the former uniform layer.* 125

6.33 *Compensation of the subtraction for the S_0 mode. Performance of Optimal Baseline and Optimal Stretch in presence of a thin non uniform epoxy layer.* 126

7.1 *Detailed view of the adhesive joint in the experimental setup.* 131

7.2 *Top view of the plate with bonded stringer. The transducers are operated in pitch-catch mode.* 132

7.3 *Compensation by Optimal Stretch for the 3D FE model. Optimal Stretch can compensate for 2 °C temperature change, achieving a maximum residual level of -37 dB.* 133

7.4 *Compensation by Optimal Stretch for the 3D FE model. In the presence of 1.5 °C temperature change, the maximum residual is always lower than -40 dB. Optimal Stretch can compensate for 2 °C temperature change, achieving a residual level of -37 dB.* 134

7.5 *Amplitude of the residual as function of the temperature difference between baseline and current signal for the FE model of a free plate and the FE model of a plate with bonded stringer.* 135

7.6 *Compensation by Optimal Stretch for the first series of experiments with the bonded stringer. Optimal Stretch can compensate for 0.5 °C temperature change, achieving a maximum residual level of -36 dB.* . 136

7.7 *Compensation by Optimal Stretch for the first series of experiments with the free plate. Optimal Stretch can compensate for 2 °C temperature change, achieving the target residual level.* 138

7.8 *Maximum residual in the subtraction as function of the temperature difference between baseline and current signal for the free plate. Optimal Stretch can compensate for 2 °C temperature variation, achieving the target residual level.* 139

7.9 *Amplitude of the residual as function of the temperature difference between baseline and current signal for the free plate and the plate with bonded stringer.* 139

7.10 *Compensation by Optimal Baseline for experiment with the bonded stringer. Optimal Baseline can achieve a maximum residual of -28.5 dB. The temperature of the baseline and current signals was 15 °C.* . 140

7.11 *Compensation by Optimal Stretch for the second series of experiments with the bonded stringer. Optimal Stretch can compensate for 1.5 °C temperature change, achieving a residual level of -38 dB.* 141

7.12 *Amplitude of the subtracted signal on a dB scale relative to the amplitude of the first arrival for the plate with bonded stringer. Optimal Stretch is able to achieve a residual level of -41 dB for the entire time trace in the presence of 1 °C temperature change. A maximum residual close to the target is achieved for 1.5 °C temperature change.* 142

7.13 *Performance of the compensation strategy for the undamaged structure. A maximum residual of -55 dB was achieved.* 144

7.14 *Drilled hole in the region of the bond, simulating an artificial defect. The hole is placed at 130 mm from the bottom side of the plate.* . . . 145

7.15 *Performance of the compensation strategy for the damaged structure with a 5 mm diameter drilled hole.* 146

7.16 *Pitch-catch inspection using the transducers pair 1-2. Amplitude of the residual in the subtraction for different hole diameters compared to the residual for the undamaged structure. Increasing the defect size is responsible for higher residual level.* 147

7.17 *Pitch-catch inspection using the transducers pair 3-4. Amplitude of the residual in the subtraction for different hole diameters compared to the residual for the undamaged structure.* 148

List of Tables

5.1 *Diameter of a through-thickness hole corresponding to a -30 dB reflector in a steel plate.* 77

Nomenclature

c_{gr}	Group velocity
c_{ph}	Phase velocity
c_{H_2O}	Bulk velocity in water
d	Plate thickness
D	Propagation distance
f	Frequency
Δf	Frequency step
F·d	Frequency-thickness product
G	Propagator function
t	Time
T	Temperature
W	Wiener filter

Greek letters:

α	Coefficient of thermal expansion
λ	Wavelength
δ	Dirac delta function
η	Dynamic viscosity
κ	Coefficient of change in phase velocity
ω	Angular frequency
τ	Ratio of liquid thickness to plate thickness
θ	Leakage angle

Acronyms:

AE	Acoustic Emission
ARMA	Auto Regressive Moving Average
DTLTI	Discrete Time Linear Time Invariant
FWHM	Full Width Half Maximum

continue on next page

continue from previous page

LTI	Linear Time Invariant
MED	Minimum Entropy Deconvolution
MLD	Maximum Likelihood Deconvolution
NDE	Non Destructive Evaluation
NDT	Non Destructive Testing
PSD	Power Spectrum Density
RMS	Root Mean Square
SHM	Structural Health Monitoring
SMLR	Single Most Likely Replacement
SNR	Signal to Noise Ratio

Chapter 1

Introduction

1.1 Motivation

The main objective of Nondestructive Evaluation (NDE) is the detection and characterization of defects that may compromise the integrity and the operability of a structure. Conventional inspection can be expensive and time consuming and, very often, the normal service of complex structures may be significantly affected. In the last few decades the possibility of assessing continuously the integrity of complex structures has fostered intense research in the field of Structural Health Monitoring (SHM) and several SHM approaches based on different inspection techniques have been proposed [1]. The basic concept of SHM consists in inspecting a structure using permanently attached or embedded sensors.

It is evident that a reliable SHM system can potentially alter the way complex structures are operated and maintained, because an optimal functionality can be guaranteed minimizing the time in which the structure is out of service and reducing significantly plant outage, as well as the costs associated with conventional inspection. SHM can also be useful in estimating the remaining life of components and can be used to assess whether their replacement is needed. Hence SHM appears extremely attractive for a wide number of engineering applications ranging from the aerospace industry (e.g. health monitoring of the fuselage of aircraft while in

service) to the chemical and power generation industries (e.g. inspection of storage tanks, pressure vessels and pipelines). Figure 1.1 shows some possible engineering applications for SHM.

Figure 1.1: *Aerospace, oil and gas industry, chemical and power generation plants are potential fields of application for SHM.*

The feasibility of an SHM methodology is strongly dependent on the possibility of effectively inspecting the structure from only a few locations. Furthermore, it is crucial that the data recorded can be reliably interpreted to make damage detection possible. In addition, the development of a reliable SHM technology poses new challenges in several different fields, such as development of smart materials, integration of sensors with the structure to be inspected, acquisition and transmission of large amounts of data [1, 2].

Ultrasonic guided waves offer the possibility of inspecting large areas from a small number of sensor positions and guided wave inspection is now an established approach in NDE. In addition, it has been demonstrated that acoustic emission signals in typical aircraft structures are a combination of the fundamental A_0 and S_0 modes and that long propagation distances can be achieved [3, 4]. Guided wave inspection is therefore attractive for the development of an SHM system for the inspection of complex structures. However, guided wave inspection of complex structures is difficult as the reflections from different features overlap. Hence the ultrasonic time traces become very complicated and damage detection is a difficult task (e.g. the reflection from the damage site can be masked by reflections coming from benign features).

The main objective of this work is to enhance the detectability of defects in complex structures and in order to make damage detection possible two different approaches have been considered. In the first part of this project the performance of deconvolution has been evaluated. Deconvolution aims to enhance the resolution of ultrasonic time traces in order to distinguish different wave packets for achieving damage detection. Subsequently, considering that deconvolution, although very promising, shows some important limitations for SHM applications, the need for an alternative approach arose. Therefore considering that recent progress has been made in the application of a Subtraction approach for SHM [5], this method was investigated. The goal of Subtraction is to detect the presence of damage by comparing ultrasonic signals recorded in the structure in service with reference signals obtained when the structure was undamaged. Subtraction performance can be affected by environmental conditions, such as temperature variations. Compensation techniques have been proposed [6, 7] to overcome the effects of temperature changes and in this work the performance of these techniques will be evaluated also in presence of other changes.

1.2 Thesis outline

The structure of this thesis broadly follows the sequence in which research was conducted during this work.

Chapter 2 provides background information on the field of guided wave SHM and different methodologies are discussed. In particular, the concepts of single unit and sparsely distributed arrays are illustrated and several applications of these two approaches found in literature are introduced. Subsequently the desirable requirements for robust signal processing of complicated ultrasonic time traces are described.

In Chapter 3 the Deconvolution approach is introduced and a review of the most commonly used techniques is presented. Our attention is mainly devoted to the Wiener filter and Single Most Likely Replacement (SMLR) algorithms. These two techniques have been extensively applied for the solution of inverse problems in different fields. Hence these two approaches will be considered for the evaluation of

the Deconvolution approach for SHM.

The potential and limitations of the Deconvolution approach for SHM are presented in Chapter 4. The performance of the Wiener filter and SMLR is evaluated on the detection of a small signal in typical configurations for damage detection in SHM. The effects of phase shift on deconvolution performance are also evaluated.

Chapter 5 describes the Subtraction approach for SHM and the detrimental issues for the performance of this method are briefly introduced. Temperature Compensation techniques are introduced and a review of their applications is presented.

In Chapter 6 the effects of liquid loading on subtraction is considered. Firstly, numerical simulations on fluid-solid bilayers were carried out to compare the effects of the presence of a thin liquid layer with the effects of temperature change in a free plate. Subsequently, Temperature Compensation techniques were used in the presence of liquid loading and it is shown that subtraction can be used to compensate for uniform liquid loading. Experimental work was conducted to study the case of an aluminium plate bordered by an infinite water layer and the case of an aluminium plate coated with a thin layer of viscoelastic material.

The performance of the Subtraction approach with signals recorded in structures comprising materials with different temperature responses is evaluated in Chapter 7. An FE model of an aluminium plate with an epoxy bonded stringer has been designed and the different temperature responses of aluminium and epoxy have been taken into account in evaluating the performance of Temperature Compensation techniques. A stringer has been bonded to an aluminium plate via high temperature curing adhesive in order to evaluate experimentally the performance of subtraction on a real structure with different temperature responses of materials.

Finally the major outcomes of the present thesis are presented in Chapter 8, where general conclusions are drawn and suggestions for future work are outlined.

Chapter 2

An introduction to Structural Health Monitoring

2.1 Overview

In the last few decades Structural Health Monitoring (SHM) has attracted considerable attention with the increasing need for the development of systems able to monitor continuously the structural integrity of complex structures. Damage detection in the structure by visual inspection or by conventional nondestructive techniques can be prohibitive for many reasons, such as the inaccessibility of some areas. In addition, conventional nondestructive techniques can be quite demanding in terms of the time required for the inspection which results in a prolonged period in which the structure to be monitored is not available. This problem is particularly important in the aerospace industry and chemical and nuclear plants. To address these issues considerable effort is currently focused on the development of convenient SHM equipment that can effectively detect the occurrence of damage in the structure and can provide information regarding the location and the severity of damage and possibly about the remaining life of the structure. An SHM system, able to continuously assess the health of a structure, can potentially change the way in which safety critical structures are monitored and maintained over their lifetimes, reduc-

ing significantly the duration of the period in which the structure to be inspected is out of service. Therefore the development of an efficient SHM system is crucial for the opportunity of maintaining a continuous assessment of the integrity of the structure, in order to facilitate the detection of critical defects and the observation of the growing of pre-existing cracks, originally below the critical size. The purpose of this Chapter is to specify the main features of a guided wave SHM system and the requirements to make this kind of equipment competitive with traditional inspection methods. The concept of SHM can be applied to several industrial fields; without loss of generality we will be especially oriented to the description of a monitoring system for structures of interest in aerospace industry. The issues related to the integration of an SHM system with the aircraft structure will be discussed next.

2.2 Aircraft design and Structural Health Monitoring

A typical example of a complex structure of interest for SHM is shown in figure 2.1 [3]. This structure can be regarded as a schematic approximation of a real fuselage of an aircraft and presents a high density of different structural features. In particular the fuselage of an aircraft is characterized by the presence of ribs and stiffeners which constitute the fundamental elements of the framework of the aircraft. We can observe also the presence of drilled holes and other structural features that further complicate the geometry of the structure.

A very good summary of the issues related to the design of an aircraft with respect to its operational environment and the integration of an SHM system can be found in Boller [2]. Here it is sufficient to stress that the main prerequisite in structural design is represented by the capability of the structure to withstand the operational loads over its design life. To account for the negative effects of missing knowledge about material properties, manufacturing technology and operational loads an increase in inspection effort is required. On the basis of the geometry of the damage observed,

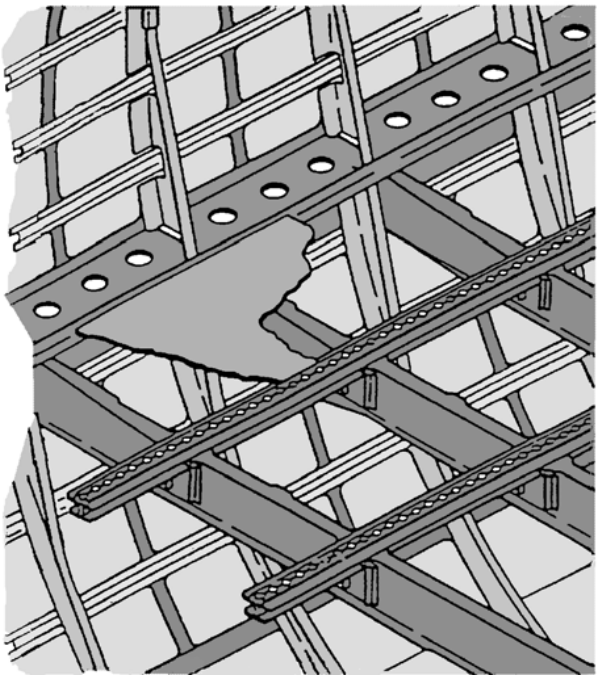

Figure 2.1: *Schematic representation of an airframe structure [3].*

it is possible to estimate the fatigue life using fracture mechanics models combined with standard loading sequences. However, this procedure is efficient only when the critical fatigue locations are well known. In addition nondestructive evaluation can have a significant impact on operational cost, due to the periods in which the aircraft is out of operation. Therefore it is very important to achieve automation and integration of sensing elements with the structural components. Furthermore robust signal processing is required for the correct interpretation of the signals recorded by an SHM system. This is the reason why several studies in SHM are currently focused in the smart materials research field and in devising convenient techniques suitable for the signal processing.

Taking advantage of the unceasing improvements in sensor technology, signal processing and smart materials, an SHM system for aircraft could be able in the future to make NDT techniques an integral part of the structure to be monitored, reducing significantly the cost of man-powered inspection [2]. The fundamental principle of such an SHM system is to have sensors placed on the more critical areas of the structure under inspection. The sensors will evaluate the integrity of the structure

in a nondestructive fashion and if the information gathered is conveniently processed it is possible to decide whether the severity of damage is such as to compromise the operability and the integrity of the structure.

According to their operational strategy SHM systems can be divided in two main groups that in the following will be termed passive SHM and active SHM systems. A passive SHM system is based on detecting changes in a chosen property of the structure in a passive way. Typical examples are given by the detection of strain fields induced by crack growth, of changes in the vibration characteristics, or of cyclically-operating structures due to growth of defects. The main difference between a passive and an active SHM system is represented by the fact that in the latter the sensors are directly excited and the excitation is therefore transmitted to the structure. The response of the structure to this excitation represents the information to be measured and evaluated in order to obtain information regarding the integrity of the structure. An example of this approach is provided by the vibration based techniques in which the structure is excited with a pulse and the vibration modes are evaluated by response measurements in the structure with accelerometers placed at strategic positions [8]. The two different approaches for the design of a Structural Health Monitoring system will be further discussed in the following sections. In particular the next section will describe briefly the application of passive systems for SHM and subsequently our attention will be concentrated on the application of active systems for the monitoring of complex structures.

2.3 Passive systems for Structural Health Monitoring: Acoustic Emission

Among the passive SHM systems, Acoustic Emission (AE) represents the most extensively used technique for defect detection on complex structures [9]. The basic idea is that crack propagation and the growth of a pre-existing defect, including corrosion [10], generates waves which can propagate in the structure and can be

received by sensors located several metres away from the source with sufficient amplitude. The successful reception of these waves by sparsely distributed sensors shows the signals are propagating across several features in the structure; hence a study of acoustic emission is also a good starting point for better understanding of the issues related to an active guided wave SHM system. In particular, fundamental work which describes the propagation of guided waves in plates is reported by Gorman [11]. In this work acoustic emission signals were conveniently simulated experimentally both in an aluminium plate and in a composite plate. The velocity of the waves propagating in the structure were comparable with the theoretical values for the fundamental flexural mode (A_0) and the fundamental extensional mode (S_0). In particular, the results showed good agreement for the S_0 mode and some discrepancy for the A_0 mode, especially for the composite plates. This is essentially due to the fact that the A_0 mode is dispersive at low frequencies and especially in composite structures. The phenomenon of dispersion is the dependence of phase velocity on frequency and it is in general responsible for an increase in the time duration of a signal and therefore in a more difficult detection of different echoes in a time trace. A typical example of the dispersion curves for phase and group velocity is shown in figures 2.2a and 2.2b respectively. The dispersion curves have been obtained using the software DISPERSE [12].

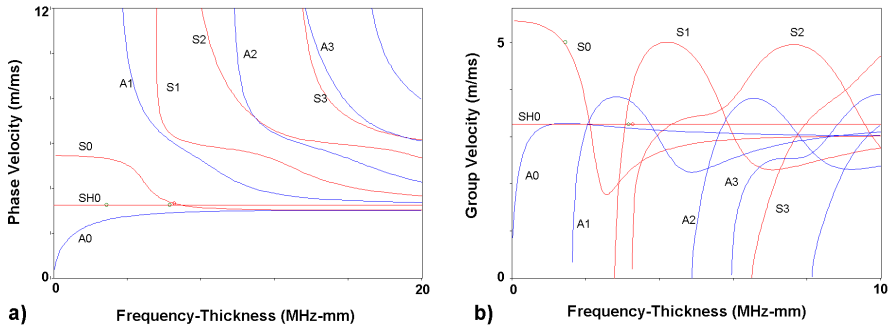

Figure 2.2: *Dispersion curves for a steel plate. a)Phase Velocity, b)Group Velocity.*

Another study on the propagating modes observed in AE has been presented by Dalton et al. in [3]. The results of this work confirmed the prediction made by Gorman, observing that generally a combination of the fundamental symmetric and

anti-symmetric S_0 and A_0 modes represents typical AE signals. Experiments were undertaken on a 1.2 mm thick aluminium plate and signals were generated in a similar fashion as in [11]. The authors also identified the frequency range where the energy of the signals is concentrated. For both modes, the peak energy of the signal is centred around 65-70 kHz. This work also demonstrates that acoustic emission signals can effectively propagate long distances through aircraft structure and therefore are attractive for potential use in SHM. Several applications using the principle of the AE technique based on guided wave analysis have been considered. An example of AE systems incorporating guided wave analysis signal processing can be found in [13]. An AE system which can detect impact of high speed debris on the space shuttle wing leading edge was developed recently by NASA [14]. AE analysis has been used successfully in a wide range of applications including: detecting and locating faults in pressure vessels or leakage in storage tanks or pipe systems, monitoring welding applications and detection of corrosion patches. One of its advantages is represented by the possibility of observing the damage processes during the entire load history. Although potentially attractive and widely used for investigation of complex structures, AE presents some relevant drawbacks which restrain its application in SHM. In particular it is important to stress that AE is highly sensitive to noise or background noise interference, which are especially severe in aircraft applications [15]. More importantly, many damage types, such as failure in ductile materials, give very low sound emission, making impractical reliable application of the AE technique [9]. In addition commercial AE systems cannot estimate quantitatively the severity of the damage in the structure; hence other NDE methods are required for a complete examination of the structure under inspection in order to provide quantitative results.

2.4 Active systems for Structural Health Monitoring: Guided wave SHM systems

Among the active SHM systems used to evaluate complex structures the most studied are those based on vibration mode analysis and on the use of sound waves (either guided waves or bulk waves) [2]. Both use sensors to transmit an excitation to the structure and to gather information on the integrity by analyzing the response. Since ultrasonic guided waves can propagate for long distances they offer the possibility of inspecting large areas from a small number of sensor positions. The main idea is to measure and evaluate the reflections of these waves from features or from defects through convenient signal processing techniques making possible the location of defects and the assessment of the effective integrity of the structure. The sensors employed in guided wave-based systems are generally used both as emitters and receivers of sound waves. The inspection strategies for SHM are based on the conventional NDT techniques of inspection in pitch-catch mode or pulse echo mode. Different concepts of sensor arrays have been proposed and some examples will be discussed in the following sections. There are several cases of successful guided wave inspection systems developed for the inspection of structures that are characterized by their relative simplicity and low feature density, such as pipes, rails, plates and small structures, which will be discussed in the next sections. These systems allow the operator to detect the location of damage in the structure. Although these structures are fairly simple, they can be considered a good idealisation for the design of an SHM system which could be also employed for the inspection of complex structures.

2.4.1 Single mode transduction for an active Guided wave SHM system

The choice of which guided wave mode to use in any inspection system and over what frequency range is of crucial importance. In particular when the feature density is

quite high as in an airframe (figure 2.1), the classical strategy is to increase the inspection frequency so that the wavelength is reduced, in order to obtain discrete echoes from successive features. Initial work on this strategy has been conducted at Imperial College [4] and unfortunately it has been demonstrated that the modes propagating in typical aircraft structures in the high frequency range (high order modes, see figure 2.2) are very complex and that it was not possible to obtain reliable propagation across a succession of typical stiffeners and joints. However, it has been shown that acoustic emission signals propagate long distances through aircraft structure and are usually a combination of A_0 and S_0 Lamb waves in the relatively low acoustic emission frequency regime below the cut-off frequency of the A_1 mode. Therefore the low frequency region appears the more suitable for the excitation of an SHM system. Hence the choice of the excitation is restricted to three possible modes (S_0, SH_0 and A_0). The S_0 mode has been employed [16] to detect corrosion patches and is attractive from the point of view of having low attenuation in structures in contact with liquid. However, the S_0 mode suffers from an increasingly long wavelength at low frequencies, and hence lower defect resolution. The slower SH_0 mode has a correspondingly shorter wavelength, but is difficult to excite in a simple fashion for SHM applications. The A_0 mode is commonly regarded as being highly attenuated in structures in contact with liquid and therefore of limited applicability for long range testing. However, there is a low frequency regime where it is not attenuated by surrounding liquid because its phase velocity is too low to allow energy leakage. In addition, the wavelength for the A_0 mode in the region of interest is always lower than the wavelengths of the S_0 and SH_0 modes and therefore the A_0 mode can still offer reasonably high resolution in detection capability. An SHM system operating at low frequencies will be excited by transducers by applying localized forces in the same direction as the characteristic displacement of the mode to be excited. When an harmonic point force is applied to the surface of the structure, guided waves will be produced and will propagate in circular wave-fronts centred in the transducers.

2.4.2 Guided wave SHM arrays

SHM systems based on guided waves can be divided in two main groups with respect to the concept of transducer arrays adopted. The two groups can be termed as (i) single unit arrays, (ii) sparsely distributed arrays. Single unit arrays contain a relatively large number of individual transducers in a single housing and typically each element is used as a transmitter and receiver. If the response at each element is measured when each element in turn is switched as a transmitter, focusing techniques can be used to propagate a beam in each direction around the array, as reported in [17]. Several projects have been conducted on the development of single unit arrays for SHM and some of them will be discussed in the next section. The second conceptual design for SHM arrays is represented by a distributed sparse array of simple elements. According to this approach, point source transducers will be distributed throughout the structure, in order to create a network of simple elements permanently attached to the structure. The advantages of this approach compared with the previous one can be observed in figures 2.3a and 2.3b.

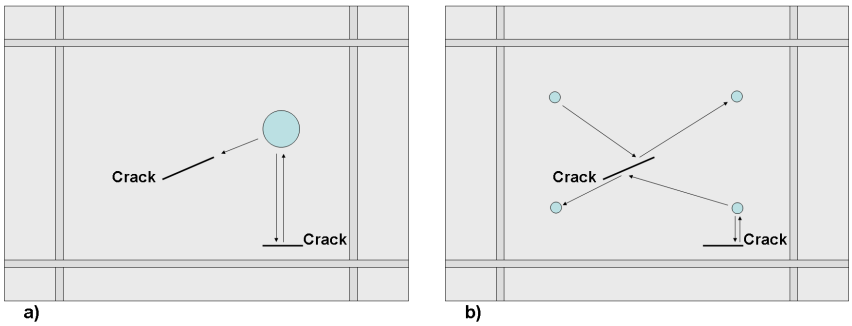

Figure 2.3: *a)Single unit array, b)Distributed sparse array.*

A sparsely distributed array is able in principle to detect the presence of a crack regardless of its geometry and relative position with respect to the elements of the array. Damage location can be achieved through triangulation, since theoretically the information from three independent sensors regarding the arrival time of the reflected wave from the crack is required. In addition, information from more sensors can be combined to improve damage location; an example is reported in [18] where Beard and Chang report how to efficiently combine the information from 9 sensors

for reliable detection of damage in a filament wound composite tube. In contrast, a permanently attached single array would encounter detection problems for defects lying along certain orientations (e.g. parallel to the direction of propagation of the guided waves), or in the case of a deployable single array several different inspection positions would be required in order to identify the presence of a defect; a sparsely distributed array would allow several different sensors to receive signals from a single transmitter, so there would be a combination of transmitter-receiver for every crack orientation. However, since the amplitude of the reflections coming from a defect is dependent on the angle of incidence of the guided waves, it is still possible to have detection problems, especially in correspondence of those angles of incidence for which the reflectivity is null. In addition, the performance of distributed sparse arrays can be strongly dependent on the environmental conditions, such as temperature variations and surface conditions of the structure under inspection. There are other practical advantages in using a sparsely distributed array for SHM instead of a single unit array. An element in a sparsely distributed array is a single channel device which requires relatively straightforward electronics compared to the electronics needed by a multi-element deployable array. In addition, for the coverage of a given area the number of distributed sensor elements required is lower than the number of elements required in a single array unit. As reported in [17], damage localisation with a single array unit is necessarily based on beam steering, which requires the array to be several wavelengths in diameter and to contain a minimum number of elements per wavelength and consequently the exciting and receiving routines and the correct phasing between the transducers can become extremely complex.

2.4.3 Single unit arrays for SHM

Several studies have been carried out on SHM systems based on guided waves using arrays of transducers assembled in a single unit, which is supposed to be attached to the structure when periodical inspection is required. Intense work has been conducted in the Non-Destructive Testing (NDT) group at Imperial College on the inspection of pipes and rails [19–21], which can be considered as mono-dimensional

structures from the guided wave point of view. These studies have resulted in the development of equipment commercially used in different industrial fields. The research activity of the NDT group has also led to the development of single unit arrays for the inspection of large plate-like structures. An example is reported in [17] where the authors describe the design of a novel electromagnetic acoustic transducer (EMAT) array and discuss issues related to mode selectivity, the design and the lay-out of the elements and the instrumentation required. The array was realized using non-contact pancake coil point-source EMATs, disposed on two concentric circles; the inner circle contains 16 transmitter and 32 receivers are placed on the outer circle. The data received are simultaneously processed using a phased addition algorithm [22]. The time taken to perform a test, including acquisition, processing and data transfer was less than one minute. The array was tested experimentally on several plates with different thicknesses, surface conditions and artificial defects. The sensitivity of the equipment allowed the authors to detect different morphologies of defects and the results demonstrate the feasibility of using a guided wave EMAT array for rapid inspection of large areas of steel plate structures. More recently another prototype of a guided ultrasonic wave array has been developed as result of the efforts of the NDT group at Imperial College [23]. In this work the description of the entire process of design, construction and testing of the single unit array has been reported. The proposed array consists of 32 transducers for the excitation and the measurement of the fundamental A_0 mode. The transducers are placed on a ring inside a compact housing which also hosts the required electronics. Unlike the array described in [17] this system has been designed in order to be permanently attached to the structure. The A_0 mode is excited in the low frequency region, in particular in the 0.5 MHz·mm to 1.2 MHz·mm range. Although the A_0 mode is strongly dispersive at these frequencies (figure 2.2), it has the advantage of being characterized by a short wavelength which is desirable for improving the resolution and the sensitivity of the system to defects. The problem of dispersion can be overcome by means of a convenient signal processing technique, such as the dispersion compensation approach described by Wilcox in [24]. Dispersion compensation was used in conjunction with a phased-addition algorithm in order to process the data

of the array in the wavenumber domain. The array was tested on a 5-mm thick steel plate for the detection of various artificial defects. Although, due to limitations of transducer performance, the overall dynamic range was limited to 27 dB, the defects were clearly visible and the work conducted indicates how further investigations on transducer design and manufacturing can potentially lead to an improvement of the dynamic range, thus resulting in a better detection of small defects. Other groups have been extensively working on projects similar to the single units previously described. An example is reported in [25] where a compact sensor configuration comprising a single transmitter and multiple receivers has been proposed for SHM of large isotropic plate structures. The receivers are arranged in a circle, while the transmitter is placed in the centre of the array. The signal processing is similar to the approach proposed in [23]. A prototype has been experimentally tested to reconstruct the profile of circular holes drilled in plates, obtaining good agreement between the position of the reconstructed hole and its actual location. Another example of a single unit array for SHM is reported in [26]. It is based on the "difference of time of flight" technique and it has been employed for the detection of linear cracks in plates. A deployable grid of piezoelectric transducers in a square configuration is used to scan the plate to identify the location of a crack. On the basis of the time of flight technique, elliptical loci of possible crack positions are determined and the position of the crack can be approximately estimated by the intersection of at least three ellipses. Once the position of the crack has been detected, length and orientation can be estimated from measurements of the energy of the reflected signal from the crack, moving the grid of sensors in the area where the damage has been detected.

2.4.4 Distributed sparse arrays for SHM

Whereas activity in the development of single unit array is a well established research field in SHM, the development of a sparse distributed array of simple elements for SHM represents a relatively new area of investigation and poses new challenges in terms of miniaturization and integration of the sensor elements with the structure

and in terms of efficient signal processing techniques able to treat the amount of data recorded by the sensors. A feasibility study [27] about the possibility of using a distributed array of guided wave sensors to monitor an entire structure has been conducted at the University of Bristol. A distributed array was created by bonding 15 piezoelectric transducers to a 1500 $\times$ 750 $\times$ 3 mm aluminium plate. A reference data set was collected from all 210 possible pairings of transmit and receive sensors and by means of a simple imaging algorithm a map of the reflected energy amplitude as a function of position on the structure was obtained. Immediately after the reference data was collected, an artificial defect was introduced into the structure and a second set of data was recorded and processed in the same manner to obtain a second image. Coherent noise, due to a combination of reflections from the plate edges and the presence of multiple wave modes, was observable in both images. Therefore it was not possible to distinguish the reflection from the defect in the second image. However, subtraction of the reference image from the second image yields a new image with a clear indication of the defect at its correct location. The defect signal amplitude and level of coherent noise (around -40 dB) represent reasonable values for a guided wave inspection system. This work clearly demonstrates the potential of the proposed technique, but also indicates some of the major issues that must be addressed for the technique to be reliably applied to real structures. For instance, signals of unknown origin were observed, despite the experiment being conducted under laboratory conditions and on a very simple structure. These signals complicate further the interpretation of the data and can cause false alarms in the integrity assessment of a real structure. Another major issue is represented by sensor density, that in this experiment was higher than reasonable values for practical applications. Therefore it is important to decrease the number of sensors required while maintaining acceptable standards of sensitivity and coverage.

An interesting work on quantitative optimization of the number of sensors and their location in an ultrasonic guided wave network is reported in [28]. The authors demonstrated that there is a trade-off between the overall network performance, number of sensors and the performance of each individual sensor. Specifically, the probability of mis-detection decreases with the number of transducers and the trend

is affected by the individual sensor performance. Once the optimal performance for each transducer has been specified, the total number of transducers in the network and their placement can be obtained. Another recent piece of work on sparse array approach for SHM of critical structures is reported in [29]. In particular, the authors propose a method to detect and approximately locate damaged regions by analyzing signals recorded from a permanently mounted array of transducers. Subsequently, follow-up inspections can be performed using an external ultrasonic transducer to scan the suspected damaged areas; the external transducer is acting as receiver while the *in situ* sensors are the emitters. This method can be implemented in many cases also with the structure in service. In addition it simplifies the scanning hardware requirements and provides sensitivity comparable with conventional ultrasonic inspections. Another study of spatially distributed array for *in situ* location of defects in large plate-like structures has been proposed by Michaels [30]. The approach proposed is based on the use of broadband Lamb waves and in the continuous monitoring of the received signals, in order to achieve damage location. In particular several signals were recorded for different frequencies and for all the possible transmitter-receiver pairs; the signal were conveniently combined for generating several images for the same structural state. The combination of several images result in an improved damage detection. Another piece of work conducted by Michaels [31] is based on the generation of two dimensional images of plate-like structures by means of tomographic and phased array methods. The images are obtained combining the signals recorded by a sparse array of distributed ultrasonic transducers. This approach has been used for damage detection problems in aluminium plates by comparing the image obtained for the undamaged plate with the image obtained after small drilled holes have been introduced as artificial defects. An approach based on the use of guided wave tomographic techniques and permanently installed transducers has been proposed by Gao et al. for the SHM of an aircraft wing [32]. In this work 8 piezoelectric sensors were placed on a circle on an aircraft wing and the area inside the circle was continuously monitored. With this approach it was possible to detect the presence and the progression of an artificial defect introduced in proximity of one of the rivets. Another example of guided wave

system for SHM of an aircraft wing is reported by Zhao et al. in [33]. In this work it is observed that although large area inspections are difficult due to strong attenuation, it was possible to achieve the approximate location of cracks and corrosion using small piezoelectric discs attached in some parts of the wings in order to create relatively sparse arrays. The localisation of the defects was obtained by means of correlation analysis based on the assumption that the probability of a defect occurrence is related to the changes observed in the time trace recorded by a pair of transducers.

Significant effort has been also devoted to the integration of SHM system with the structure to be inspected. An interesting work, proposed by Giurgiutiu [34], is based on the use of piezoelectric wafer active sensors (PWAS) that can be directly mounted on the surface of plate-like structures or even embedded between layers of composite structures. These transducers were used in both pitch-catch and pulse-echo configurations to generate/receive Lamb wave modes and were used successfully for crack detection also on a real aircraft panel [35]. An important step in the integration of SHM system with complex structure is represented by the SMART layer developed by Acellent Technologies Inc. in collaboration with Stanford University [36]. The layer can be mounted on existing structure or integrated into composite structures providing built-in nondestructive assessment of the internal and external integrity of the structure. The SMART layer consists of a network of piezoelectric elements supported on a flexible printed circuit substrate. In this way a whole array of sensors can be embedded in the structure and issues related to the integration of the monitoring system are significantly reduced. In addition, by exploiting the flexibility of the printed circuit technique, a large variety of size, shapes and complexity are possible for the SMART layer. Basic shapes include a circular and three-dimensional shell [37]. Furthermore the printed circuits guarantee a very good integration because they are able to deform with the structure. Following the pioneering work on the SMART layer, an interesting project for the development of a hybrid piezoelectric-fibre optical diagnostic system for aerospace structures has been proposed by Qing et al [38]. A more complex SMART layer, containing a network of piezoelectric elements and fibre gratings, is used in the same fashion as

the system described in [36] to evaluate the integrity of metallic and complex structures. Piezoelectric actuators input a controlled excitation to the structure and fibre optical sensors are used for monitoring the corresponding structural response. With this approach decoupling between input and output signals can be achieved, since the piezoelectric transducers use electrical channels and the fibre optical sensors use optical means. This equipment can be used to perform *in situ* detection of structural defects and damage including delaminations and corrosion.

2.5 Signal processing for Structural Health Monitoring

From what has been previously reported we can deduce that SHM is an attractive research field of continuously growing importance and it can potentially modify the way in which complex structures are designed, operated and maintained during their lifetimes. We observed that ultrasonic guided waves offer the possibility of inspecting large areas from a small number of sensor positions, since they can propagate over long distance. Therefore guided waves represent a promising means for the inspection of complex structures and their characteristics have been extensively studied in conventional nondestructive evaluation. However, inspection of complex structures is difficult as the reflections from different features overlap. Estimating the number and amplitude of the wave packets contained in ultrasonic time traces is therefore crucial for the development of a successful guided wave inspection system, in order to enable damage to be detected and located by identifying changes in the measured signal over time. Therefore an appropriate and robust signal processing tool for Structural Health Monitoring must be able to resolve closely spaced events and to distinguish reflections due to the presence of a defect from reflections caused by structural features. Other desired requirements for signal processing algorithms to be applied in SHM, can be briefly listed as follows [39]:

- Ability to reduce the noise on the damage estimate;

- Capability of enhancing the SNR in the data, for instance removing distortion introduced by the measurement channel;
- Robustness to modelling error, since material properties, noise characteristics and other variables may be only approximately known and therefore the algorithms should be able to cope with the related uncertainties;
- High flexibility and easy implementation for handling the signal processing of large amounts of data recorded at sensors embedded in the structure.

The main objective of this work is to devise suitable signal processing techniques that can be effectively used to retrieve useful information about the integrity of a complex structure monitored by a sparse distributed array of piezoelectric sensors.

Several methods have been proposed as potential candidates for SHM. In this work we will examine the performance of two possible methods: Signal Deconvolution and Signal Subtraction.

The first approach has been extensively applied for the solution of inverse problems in different fields, such as geophysical prospecting, oil exploration and seismology. Due to the similarities between the problems tackled in these fields with the typical problems encountered in guided waves inspection, Signal Deconvolution appears as a promising approach for SHM and its performance with ultrasonic signals will be evaluated in Chapter 4.

Signal Subtraction relies on the possibility of gathering information about the integrity of a structure from the observation of changes in the measured ultrasonic signals over time. The simple subtraction of a baseline obtained from the undamaged structure from a signal recorded from the structure in operating conditions should provide in principle a reliable means for detecting the appearance of a defect. However, several issues (such as changes of environmental conditions and temperature variations) prevent Subtraction approach from being efficiently employed for SHM in the simple and intuitive manner previously described. The application of this approach to SHM will be considered in Chapter 5.

Chapter 3

Literature Review on Deconvolution techniques

3.1 Introduction

Several physical phenomena can be described by the methods of Linear Time Invariant (LTI) systems theory. When the LTI theory is applicable, the underlying physical process is usually described as the response of an LTI system to some physical source excitation. The corresponding mathematical model is composed of an input (the source excitation), an impulse response (the LTI system function), and an output (the physical process) [40]. The process of convolution transforms the input into the output by the LTI impulse response. The convolution process is described by the following convolution integral:

$$y(t) = \int_{-\infty}^{+\infty} h(\tau)x(t-\tau)d\tau \tag{3.1}$$

which is usually written briefly as:

$$y(t) = h(t) * x(t) \tag{3.2}$$

where the symbol $*$ indicates the convolution operation between $h(t)$ and $x(t)$. Equation 3.1 can be used to express how the input $x(t)$ is transformed into the output

$y(t)$ by means of the impulse response $h(t)$. For instance in a typical nondestructive evaluation problem, the recorded ultrasonic time trace $y(t)$ is the result of the convolution process between the input signal $x(t)$ and the impulse response $h(t)$ of the structure under inspection.

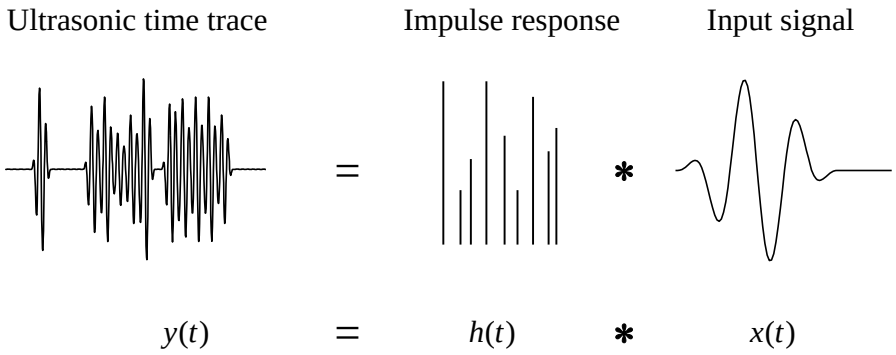

Figure 3.1: *Convolution process in nondestructive evaluation.*

Let us now consider the inverse problem of trying to evaluate $h(t)$ when $x(t)$ and $y(t)$ are known. From equation 3.2 we observe that the convolution of $y(t)$ with a function $q(t)$:

$$y(t) * q(t) = h(t) * x(t) * q(t) \tag{3.3}$$

would be equal to $h(t)$ if

$$x(t) * q(t) = \delta(t) \tag{3.4}$$

In the previous equation $\delta(t)$ is the Dirac delta function. If equation 3.4 is satisfied, then equation 3.3 gives $h(t)$ and problem of the determination of the impulse response can be solved. The function $q(t)$ is called a deconvolution filter, since it unravels the input $x(t)$ from the output $y(t)$. Deconvolution plays an important role in the identification of physical systems. This problem is concerned with the development of robust and stable algorithms in order to produce accurate deconvolution filters. Several deconvolution techniques have been proposed in the literature in order to tackle this problem, especially in geophysical exploration, oil and gas industry and seismology. For any process of deconvolution we need to consider a physical model that takes into account both known and unknown factors. An example of the application of model based filtering techniques in NDE has been proposed

by Challis et al. for measuring the acoustic impedance of adhesive and for detecting void-disbond in adhesive joints [41]. The main purpose of this Chapter is to provide an overview of the most popular deconvolution approaches that have been proposed in the literature and that have been considered suitable for solution of inverse problems in different fields.

3.2 Causality, Stability and Minimum phase properties

A Discrete Time Linear Time Invariant (DTLTI) system is characterized by its impulse response $h(n)$, where n is the discrete index for the variable time. The corresponding z-transform, indicated in the following by $H(z)$, represents the system transfer function [40]. We assume that $h(n)$ is a causal sequence and therefore $h(n) = 0$ for $n < 0$. In addition, we assume that $H(z)$ can be described as an Autoregressive Moving Average (ARMA) system:

$$H(z) = \frac{B(z)}{A(z)} \tag{3.5}$$

where $B(z)$ and $A(z)$ are polynomials in the negative powers of z given by:

$$B(z) = b_0 + b_1 z^{-1} + \cdots + b_M z^{-M} \tag{3.6}$$

$$A(z) = a_0 + a_1 z^{-1} + \cdots + a_N z^{-N} \tag{3.7}$$

with $M \geq 0$ and $N > M$.

It is possible to demonstrate that $h(n)$ is a stable and causal sequence if the corresponding transfer function $H(z)$ has no poles outside or on the unit circle in the complex z-plane. Therefore all the zeros of the $A(z)$ must lie inside the unit circle [42]. We can observe at this point that the location of the zeroes of the $B(z)$ does not have to be specified for the stability of $H(z)$. However, the location of the zeroes of $B(z)$ is important for the definition of another property often encountered in deconvolution and inverse problems, the concept of minimum phase. A DTLTI is

called minimum phase if its transfer function $H(z)$ has no zeroes outside or on the unit circle in the complex z-plane. From what has been previously stated and considering equation 3.5, we can observe that if a system $H(z)$ satisfies the minimum phase property, then the inverse system $H^{-1}(z)$ has no poles outside or on the unit circle and therefore is stable and causal.

3.3 Least squares deconvolution

Least squares deconvolution is a well established approach for signal processing of seismic reflection data and it has been extensively applied to improve the temporal resolution and to remove short-period reverberations in geophysical recorded time traces [43, 44]. The origin of this approach goes back to the pioneering work of Norbert Wiener who developed a statistical process to separate signals from noise [45]. The process was originally known as smoothing or prediction filtering. The inverse process of prediction filtering was formerly called decomposition and later deconvolution [46]. The approach based on the Wiener filter has also been termed predictive deconvolution and it constitutes the keystone of many current deconvolution methods. The application of the least-squares deconvolution approach consists of the design of a convenient Wiener filter which attempts to shape the raw data into the desired output by minimizing the mean squared error. As reported by Peacock and Treitel in their fundamental work [47], the Wiener filter has been widely used to deconvolve reverberating pulse trains in a series of spike-like impulses (reflectivity). More generally it is possible to consider the Wiener filter as a suitable method for removing repetitive events having specified periodicity and for the suppression of rather complex reverberation patterns. A more exhaustive discussion of the general properties of the digital Wiener filter has been provided by Robinson and Treitel in [48]. This method is based on the design of a deconvolution filter able to minimize the mean squared error between the desired output and the actual output of the filter. Once the expression of the least squares error has been formulated, it can be minimized by setting its partial derivatives equal to zero with respect to the unknown filter coefficients. These equations, also known as Wiener-Hopf equa-

tions, can be efficiently solved by means of the iterative Levinson algorithm [49]. A more detailed mathematical description of the prediction filtering will be given in Chapter 4, where the formulation in both time and frequency domains will be derived. At this point it is sufficient to stress the two fundamental hypotheses of this approach: the underlying reflectivity is assumed to be random and white, and the input wavelet is assumed to be minimum phase. Several studies have been conducted on the evaluation of least squares deconvolution for geophysical applications and as observed in [50], standard Wiener deconvolution proved to be robust in terms of performance under a variety of different input wavelets and signal distortions, although the performance can be significantly degraded if the input signal is not minimum phase [50, 51]. A detailed study on the accuracy of the Wiener filter for enhancing the resolution of seismic events is reported in [52], where the effects of noise on bandwidth and temporal resolution are also taken into account. The applicability of the Wiener filter as a suitable method for the solution of inverse problems has been evaluated in a wide range of applications. In particular the Wiener filter has often been employed for the improvement of blurred images. An example of this application can be found in [53] where the authors described how the Wiener filter can be used for the restoration of degraded images, through an iterative estimation of their autocorrelation matrix. In addition, issues related to the convergence of the iterative process are considered and a possible approach to ensure the convergence of the iterative process is also presented. The Wiener filter in combination with regularization techniques has been applied to the enhancement of astronomical images as reported in [54]. An example is reported in [55] where a study of different parametric versions of the Wiener filter is considered for image restoration in astronomical applications. The Wiener filter has also been used in the speech enhancement as reported in [56]. In this work both the iterative and non iterative formulations of the Wiener filter have been considered as suitable means for the estimation of speech signals in noisy environments. In addition, generalizations of the Wiener filter taken from the context of image restoration have been proposed for speech enhancement. Recently a non iterative method based on the Wiener filter has been proposed for improvement of speech signals in noisy environments [57].

This approach employs a time-varying parameter for the suppression of the noise; in this way it is possible to suppress those components of the frequency spectrum of the signal where speech is not likely to be present and to enhance the components of the spectrum where speech signal is predominant. The formulation of the Wiener filter in the frequency domain has also been proposed for nondestructive evaluation.

An interesting application for the estimation of the scattering amplitude of flaws by removing the effect of the measurement system in the presence of noise can be found in [58]. The potential of Wiener filtering for image processing applications in NDE is described in [59] where the limitations and the problems that can occur have also been considered. A possible drawback, essentially due to the implicit cyclical assumption of the FFT algorithm, is the edge effect which can corrupt the edge of the image being processed. Another problem is represented by the introduction of ripples that can mask subtle features present in the image. More recently Honarvar et al. [60] proposed an interesting application of the Wiener filter in combination with Autoregressive (AR) spectral extrapolation for improving the resolution of ultrasonic time traces. A brief description of the AR spectral extrapolation and its applications for NDE is given in the next section.

3.4 Autoregressive spectral extrapolation

Autoregressive spectral extrapolation has been used in several studies in combination with different deconvolution techniques, in order to improve the performance of the inversion process. Some applications in ultrasonic NDE can be found in [61, 62]; in particular it has been observed that using AR spectral extrapolation can improve significantly the performance of the Wiener filter in ultrasonic applications [63]. The combination of AR spectral extrapolation and Wiener filter has been used by Honarvar et al. [60] for resolving overlapping echoes and for improving the resolution of ultrasonic time traces with low signal to noise ratio. It has been observed that the application of the autoregressive spectral extrapolation enhances significantly the results obtained by the Wiener filter, providing a better time resolution of the

deconvolved signal. The method of the AR spectral extrapolation is based on the following principle: once the deconvolved signal is obtained, it is assumed that the part of the deconvolved spectrum with high signal to noise ratio can be represented by an AR process [64]; the remaining part of the spectrum is therefore extrapolated on the basis of this assumption, starting from the frequency window where the signal to noise ratio is high. This procedure provides a broadband spectrum that should be reasonably flat and, therefore, representative of an impulse response consisting of a number of delta functions. However, some limitations of this approach need to be considered. The performance of this method is dependent on the order of the AR model used for the interpolation of the part of the deconvolved spectrum with high signal to noise ratio; in addition the detrimental effects of the frequency window chosen for the extrapolation of the spectrum can be significant and they cannot be easily compensated. These limitations as well as the difficulties introduced by the arbitrary selection of some parameters involved in the AR spectral extrapolation can limit significantly the practical application of this approach [60].

3.5 Maximum likelihood deconvolution

Maximum Likelihood Deconvolution (MLD) represents a promising approach to deconvolution. This method was developed by J. M. Mendel and co-workers in the early 1980s for geophysical applications. This approach can estimate simultaneously an input wavelet as well as statistical parameters and detect spike locations, providing the estimation of the reflectivity sequence. With respect to the input wavelet, it is important to observe that the assumption of minimum phase is not required. This technique is based on a state variable model for the noisy data and a sparse spike-train model for the sequence of reflectors to be detected. As reported in [65] the estimation of the unknown parameters is obtained by means of suitable detectors in the framework of a Bayesian approach. The inverse problem is formulated as an estimation problem where on the basis of the "a priori" information available a likelihood function is obtained and the estimation of the unknown variables is achieved by maximizing the likelihood function with respect to the unknown vari-

ables. The Single Most Likely Replacement (SMLR) [66], which will be described more in detail in Chapter 4, represents the fundamental detector for MLD. This detector is designed to estimate iteratively a sequence of event locations, in such a way that a likelihood function always increases. On the basis of this method, successive improvements have been considered in order to enhance its performance and some examples are reported in [67]. In this paper two detection algorithms are proposed in order to correct problems sometimes observed in deconvolution by SMLR, such as splitting of the estimated event or slight shifting of the estimated events. By means of the application of these more advanced detectors in different configurations, a better estimation of the reflectivity can be achieved, reducing also the occurrence of false alarms (location of events in wrong position). The SMLR algorithm has been the key technique for the development of other MLD detectors and a comparative study of some procedures based on the SMLR algorithm can be found in [68]. In addition, other techniques based on MLD have originated from the SMLR and some examples can be found in [69]. More recently, Kaaresen has developed an algorithm which allows more complicated transitions than SMLR. By means of this method an initial configuration is iteratively improved through a number of small changes in the set of positions where events are expected [70]. This method has been proposed for non destructive evaluation of layered media containing a limited number of abrupt impedance changes [71].

3.6 Minimum entropy deconvolution

Minimum entropy deconvolution (MED) is one of the most recent approaches to the deconvolution problem and has been proposed by Wiggins [72] with the purpose of separating the different components of a signal. The advantages claimed for this method are that MED does not need strong hypotheses over the components and it is based on the concept of *simplicity* of the output. The degree of simplicity is measured by the varimax norm introduced in [73], which can be considered as a measure of "spikiness" of a time trace; in fact its maximum value for any time series is 1 and occurs only when the time series consists only of a single spike. On the basis of the

varimax norm an iterative algorithm is derived for the computation of a deconvolution filter. The method does not require any phase assumptions about the input signal and searches for a deconvolved output which consists of the smallest number of large spikes consistent with the input data. An improvement to this method has been proposed by Ooe and Ulrych [73]. They observed that the efficiency of MED can be improved when an exponential transformation is incorporated into the algorithm. This is particularly true when the input traces contain additive noise. In this case the noise suppression characteristics of MED are considerably enhanced by the exponential transformation, and the identification of smaller spikes is enhanced. This paper also presents a kurtosis criterion of simplicity instead of the varimax norm introduced by Wiggins. A different approach has been suggested in [74] where on the basis of the geometrical analysis of the varimax norm a new criterion (the D-norm) for simplicity is assumed. One of the most remarkable characteristics of this criterion is that on its basis a non iterative algorithm for the computation of the deconvolution filter can be obtained. Wang et al. [75] proposed a faster and more efficient algorithm called D-norm. They pointed out that for the MED method the result can be dependent on the initial value of the iterative method and the filters are not unique. The D-norm criterion, on the other hand, provides a unique solution and can be very useful in overcoming the problem of the non-unique solution of MED. The possibility of employing the MED approach to deconvolve time traces containing phase shifted wavelets has been examined in [76] where the design of a MED filter has been used in combination with a seismic model based on the convolution of a complex reflectivity (in order to take in account the phase shift) and the analytic representation of the input wavelet. As observed by Wiggins in [77] MED has not found many applications due to difficulties caused essentially by the nature of the varimax function or other similar nonlinear norms and by the excessive sensitivity of the estimated deconvolution filter to the probability distribution of the underlying random series.

3.7 Iterative deconvolution

Iterative deconvolution techniques have been proposed in the literature for many applications in signal processing, based on the method described in [78]. The most important advantages of iterative deconvolution are represented by:

- A priori knowledge of the statistics of the data is usually not required;
- Constraints can be easily incorporated into the algorithm;
- The iterative process can be ended when a certain error criterion is accomplished.

An iterative approach to deconvolution of seismic time traces has been proposed by LaCoste in [79]. In this paper the author introduces a successive approximation method that operates in the time domain and is based on a simple procedure based on the design of zero-phase shift filters. Such filters have the same phase shift for all frequencies and their weighting coefficients are symmetrical with respect to time. In each iteration the effect of the filter is to multiply each frequency component by the corresponding gain factor for that particular frequency, without affecting the phase. Under these assumptions, an estimation of the deconvolved signal can be obtained via successive approximations and the iterative procedure can be terminated when any undesired frequencies begin to appear. Another technique used in geophysical applications is reported in [80], where the authors present an iterative method, based on successive substitutions to design a stable filter in time domain. The same technique has been used later in [81] where the authors compared the results to the corresponding results of the Wiener filter, observing that the latter produces more unwanted high frequency noise in the deconvolved signal.

3.8 L_P-norm deconvolution

$L_P - norm$ deconvolution has been proposed as a possible alternative approach to inverse filtering for geophysical applications. It is based on the general idea of finding the parameters that provide the best linear curve fit for a generic set of data, according to a criterion that minimizes the error between the actual data and the fit. The deconvolution problem is usually solved within iterative constrained minimization schemes for statistical distributions of noise and reflectivity. Depending on the value of P, it is possible to distinguish different methods. According to Debeye et al. [82], for practical applications the range of the possible $L_P - norm$ deconvolution methods is narrowed to the following three possibilities:

- $P = 1$ ($L_1 - norm$, least absolute value)
- $P = 2$ ($L_2 - norm$, least squares)
- $P = 1$ and $P = 2$ (mixed scheme)

The first approach ($P = 1$) is one of the most widely used and an interesting application is reported in [83]. In this work the authors show that, given a wavelet and a noisy time trace, an estimation of the spike train can be obtained using the $L_1 - norm$ or, alternatively, it is possible to extract the original input wavelet from a received time trace when the spike train is known. Different techniques, based on linear programming procedures, have been proposed to solve problems in the frame of the $L_1 - norm$ and some examples can be found in [84, 85]. Barrodale et al. [86] compared the performance of L_1 and L_2 schemes for a deconvolving seismic trace by extracting spikes one at time in different configurations. The authors observed that the $L_1 - norm$ generally performs better than the $L_2 - norm$ and they also implemented a fast algorithm for the $L_1 - norm$ approach. In [82] it is reported that under the assumptions of sparsely distributed reflectivity and Gaussian noise the mixed scheme $L_1 - norm$ (reflectivity) $L_2 - norm$ (noise) performs the best and that, in general, the maximum likelihood estimate of reflectivity, for a range of density functions of reflectivity and noise, can be obtained by means of the corresponding

$L_P - norm$ scheme. In [82] it is also observed that the performance of $L_P - norm$ deconvolution can also be limited by the data bandwidth and sometimes only the well separated events are resolved.

3.9 Deconvolution approach for phase shifted signals

In geophysical applications, it is usually assumed that the received signal is represented by the convolution of an input wavelet with a series of real impulses. In other words it is assumed that the received signal is composed of scaled versions of the original wavelet. This assumption breaks down when the input wavelet is phase shifted after reflection from boundaries or structural elements. Little attention has been given to the issue of phase shift of the input signal and its effects on signal deconvolution. The problem of estimating the arrival time of phase-shifted pulses for geophysical problems has been considered by Levy et al. in [87]. The authors observe that the estimation of the arrival time of pulses which have been significantly phase shifted can be very difficult due to the strong differences between the altered waveform and the original input wavelet. Based on the deconvolution approach described in [88] the authors address the deconvolution of pulses which have undergone a frequency independent phase shift. The approach proposed, termed analytic deconvolution, is based on the analytic formulation of the convolution process described by equation 3.2. In particular the received signal will be the real part of the convolution between a complex reflectivity sequence and the analytic representation of the input wavelet. The deconvolution is carried out in the frequency domain by means of an inverse analytic filter, whose expression is similar to the formulation of the non optimal Wiener filter. By means of this technique it is possible to estimate the arrival times of the phase shifted pulses contained in the received signal and to determine the phase of each reflector.

3.10 Summary

The solution of inverse problems represents a key issue in many fields and several deconvolution techniques have been proposed in the literature as possible means for the estimation of unknown quantities in the solution of inverse problems. In this Chapter we have described the most popular deconvolution techniques in a brief survey that does not claim to be exhaustive. Due to the strong similarities between the typical problems of nondestructive evaluation and the problems encountered in geophysical prospecting and oil exploration, it seems convenient to evaluate the applicability of the Deconvolution approach for SHM applications.

The performance of the Deconvolution approach for SHM is evaluated in the next Chapter, where two of the methods previously introduced will be examined:

- Wiener filter (Least squares deconvolution)
- SMLR algorithm (Maximum likelihood deconvolution)

The Wiener filter has been recommended as the most successful technique used in oil exploration and geophysical applications and the possibility of employing this approach for deconvolution of ultrasonic signals in SHM will be evaluated. In addition, SMLR algorithm has also been considered, due to the promising results obtained with this technique in detecting strongly overlapped wave packets in ultrasonic signals.

Chapter 4

Deconvolution Approach for Structural Health Monitoring

4.1 The Deconvolution approach

The development of a robust SHM system is one of the most challenging problems currently tackled in the research field of nondestructive evaluation. A very important task assigned to a guided wave SHM system is the capability of detecting the presence of damage even in configurations where the corresponding reflection is overlapping with reflections coming from benign structural features. To illustrate the grade of complexity that it is reasonable to expect in a typical SHM problem we can consider the time trace shown in figure 4.1. Two piezoelectric transducers were attached to the plate and operated in pitch-catch mode [89]. The input signal was a 5 cycle Hanning windowed toneburst, 20 kHz centre frequency and the A_0 mode was generated. The monitoring time was chosen in order to record the multiple reflections coming from the edges of the plate. The time trace is complicated by the presence of strongly overlapping echoes. Although this time trace has been recorded on a simple plate, it is very complicated and can be considered representative of the typical signals that would be recorded in the inspection of a complex structure.

In conventional nondestructive evaluation the presence of a defect can be detected

because different wave packets in the ultrasonic signals are well separated and it is possible to discriminate between structural features and defects without a baseline (signal obtained when the structure was not defective). However, standard NDT techniques cannot be successfully applied in SHM since signals in complex structures are strongly overlapping.

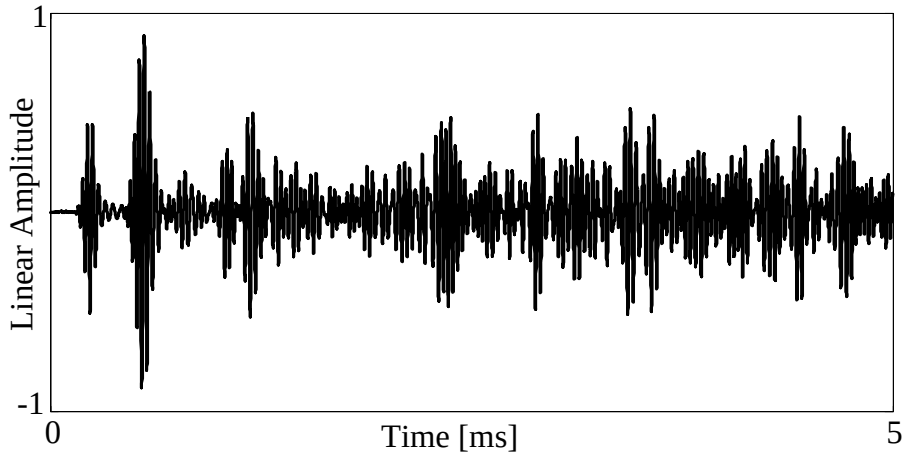

Figure 4.1: *Time trace recorded in a 1000 × 1000 × 5 mm aluminium plate.*

The idea suggested by the deconvolution approach is to compress the temporal duration of individual pulses in order to make it possible to separate them in time. This approach is very attractive because in principle defect detection can be achieved without baseline information using triangulation.

Figure 4.2a illustrates schematically the pitch-catch inspection of a plate; the reflection coming from a defect can be masked by the multiple reflections from structural features. Figure 4.2b shows how deconvolution could enhance significantly the resolution of the original time trace, making it possible to determine the amplitudes and the arrival times of the wave packets contained in the original time trace. Therefore the integrity assessment of the structure becomes easier because the presence of a defect would produce an additional reflection which appears as an extra spike in the deconvolved signal. The benefit of the deconvolution depends on the sharpness of the spikes or resolution. This approach will be effective only if the maximum achievable resolution represents a significant improvement with respect to the original data. The feasibility of deconvolution is affected by two main factors: (i) noise

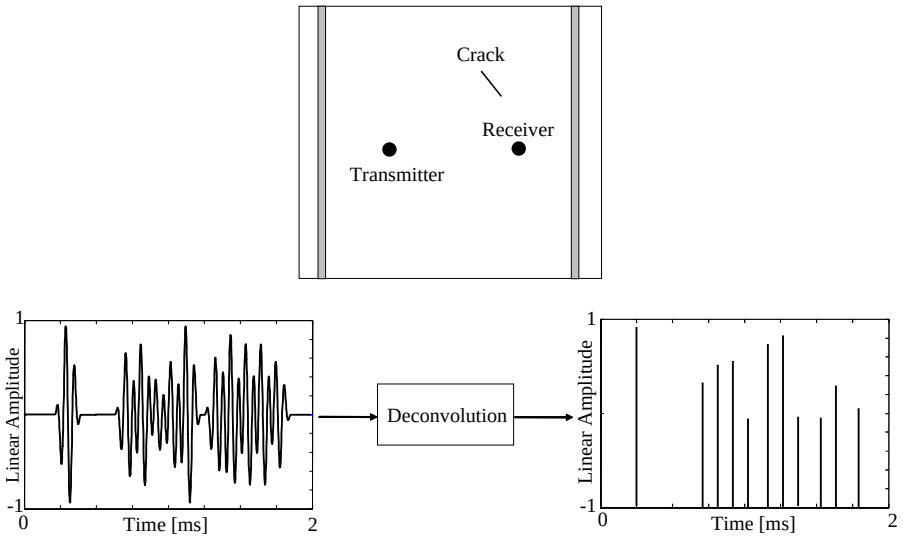

Figure 4.2: *a) Pitch catch inspection of a plate. The typical recorded signal contains strongly overlapping echoes. b) Ideal deconvolution: the wave packets of the received signals have been compressed to sharp spikes, allowing the identification of the different echoes.*

and (ii) complexity of the reflection coefficient from structural features. These two aspects will be discussed separately as they are independent of each other.

4.2 Mathematical Model for Deconvolution Approach

A simple model for the received ultrasonic signal is required in order to study the deconvolution approach and it will be derived in the following. Under the assumption of uncorrelated noise and considering the convolution model introduced in section 3.1 the received ultrasonic time trace can be represented in the time domain as:

$$s(t) = s_0(t) * g(t) + n(t) \tag{4.1}$$

where $s(t)$ is the received time trace, $s_0(t)$ is the input wavelet, $n(t)$ is the noise and $g(t)$ is the propagator function which defines the response measured at the receiver location due to an impulse at the position of the transmitter. The propagator which corresponds to the result of deconvolution in figure 4.2b provides the arrival times of all the individual wave packets contained in the received signal $s(t)$. According

to the convolution theorem [64] convolution in the time domain is equivalent to multiplication in the frequency domain and *vice versa*, therefore equation 4.1 can be written in the frequency domain as:

$$S(\omega) = S_0(\omega)G(\omega) + N(\omega) \tag{4.2}$$

where $S(\omega)$, $S_0(\omega)$, $G(\omega)$ $N(\omega)$ are the Fourier Transforms of the corresponding quantities previously defined in the time domain. Equation 4.2 is very important because inverse problems are usually tackled in the frequency domain and the estimation of an unknown quantity can be obtained by means of convenient inverse filtering. From equation 4.2 it is possible to observe that in a noise free case, infinite bandwidth deconvolution for the estimation of the propagator simply corresponds to spectral division in the frequency domain between the received time trace $S(\omega)$ and the input signal $S_0(\omega)$. However, due to the presence of noise, the design of a stable inverse filter or inversion algorithm is required in order to estimate the propagator in practical SHM applications. Several deconvolution methods have been proposed for the solution of inverse problems; the first approach that we evaluated is the optimal Wiener filter, as it represents the most well established technique for digital inverse filtering [44, 45].

4.3 The Wiener filter approach for deconvolution

The Wiener filter is based on the minimization of the mean square error between the estimated signal and the actual signal, providing the optimal trade-off between bandwidth and Signal to Noise Ratio (SNR) [49]. The Wiener filter in the frequency domain is given by:

$$W(\omega) = \frac{P_G(\omega)S_0^\star(\omega)}{P_G(\omega)|S_0(\omega)|^2 + P_N(\omega)} \tag{4.3}$$

where $P_G(\omega)$ $P_N(\omega)$ are the the Power Spectrum Densities (PSD) of the propagator $G(\omega)$ and noise $N(\omega)$ respectively and S_0^* is the complex conjugate spectrum of the input wavelet. The previous expression can also be written as:

$$W(\omega) = \frac{S_0^\star(\omega)}{|S_0(\omega)|^2 + Q(\omega)} \tag{4.4}$$

where

$$Q(\omega) = \frac{P_N(\omega)}{P_G(\omega)} \tag{4.5}$$

It is important to note that the propagator $G(\omega)$ and therefore $P_G(\omega)$ are unknown and thus an estimation of $P_G(\omega)$ and $P_N(\omega)$ is required for the determination of the factor $Q(\omega)$. Depending on how the estimation of $Q(\omega)$ is achieved, two different forms of the Wiener filter are obtained: the non optimal and the optimal formulations; the differences between the two formulations will be discussed in the following. Once the Wiener filter has been designed, the estimated propagator, indicated in the following by $\hat{G}(\omega)$, will be determined in the frequency domain as:

$$\hat{G}(\omega) = W(\omega)S(\omega) \tag{4.6}$$

The time domain representation of $\hat{G}(\omega)$, which is easier to interpret for the evaluation of structural integrity, can be obtained by means of the inverse Fourier Transform.

4.3.1 Non optimal Wiener Filter

In this formulation the factor $Q(\omega)$ is assumed to be a constant, Q, that can be estimated from the variance of the noise. Q is an offset factor that is used in order to avoid ill conditioned division in the determination of the filter and to minimize the distortion caused by high frequency noise [90]. The chosen value will affect the performance in terms of noise suppression and exploitable bandwidth and, therefore, the resolution of the filtered signal. The value of Q is sometimes determined experimentally by means of a trial and error procedure: small values of Q would lead to poor noise suppression, whereas large values yield filtered signals with high SNR but with significant blurring and poor resolution [90]. Other authors have suggested a different criterion for choosing the constant Q [58]:

$$Q(\omega) = const \approx 10^{-2}|S_0(\omega)|^2_{max} \tag{4.7}$$

The same value is suggested also in [60] where the factor Q is termed noise desensitizing factor.

4.3.2 Optimal Wiener Filter

In the optimal formulation the factor $Q(\omega)$ is assumed to be a function of frequency. In order to design the optimal Wiener filter it is necessary to estimate $P_G(\omega)$ and $P_N(\omega)$. $P_N(\omega)$ can be estimated from the variance of the noise and $P_G(\omega)$ can be obtained via an iterative procedure:

1. Obtain a propagator estimate $G(\omega)$ via the non optimal Wiener filter; an initial guess $P_G^1(\omega)$ is then:

$$P_G^1(\omega) = G(\omega)G^*(\omega) \tag{4.8}$$

2. Therefore $Q^1(\omega) = \frac{P_N(\omega)}{P_G^1(\omega)}$ and the Wiener filter is:

$$W^1(\omega) = \frac{S_0^\star(\omega)}{|S_0(\omega)|^2 + Q^1(\omega)} \tag{4.9}$$

3. The new estimate of the propagator $G(\omega)$ is:

$$\hat{G}^1(\omega) = W^1(\omega)S(\omega) \tag{4.10}$$

4. $\hat{G}^1(\omega)$ can be used to update the estimation of $P_G(\omega)$, giving $P_G^2(\omega)$

5. Iteration of the steps 1-4 yields an optimal estimation of $P_G(\omega)$.

This procedure has been used in several applications; see e.g. [53], where a detailed study on the convergence of the iterative process is also presented. In general few iterations are needed for the convergence of the process [53]. Some results of the application of the optimal Wiener filter to typical SHM problems are shown in the following sections. It is obvious that the two formulations of the Wiener filter are equivalent in noise free conditions. In this case deconvolution is equivalent to simple spectral division.

4.4 A typical problem in Structural Health Monitoring

A typical test problem in SHM is the detection of a small signal from damage in the presence of a large reflection from a nearby feature. Figure 4.3 shows a simple example of this problem using synthetic data generated in Matlab containing two strongly overlapping wave packets obtained by the convolution of an input wavelet with two Dirac delta functions (the second signal is 10% of the magnitude of the first); the two reflections are not resolvable. This configuration is representative of typical detection problems in NDE. In our initial numerical examples only one mode is propagating, whereas in real guided wave SHM applications more modes are likely to be present. This simplified case is therefore a first test of the deconvolution approach: if the technique is promising in the simple case, more complex cases would then be considered.

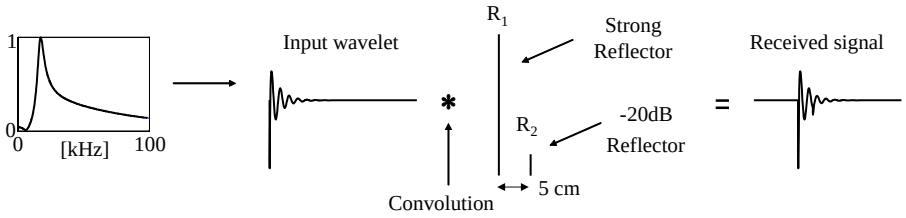

Figure 4.3: *Generation of strongly overlapping signals. The two reflections are not resolvable.*

The wavelet of figure 4.3 is a broadband signal with its centre frequency at 20 kHz, which is typical for excitation of A_0 mode [89]. The expression for the wavelet is given in equation 4.11.

$$s_0(t) = -1360t\exp^{-500t} + 0.5\sin(33.3\pi t)\exp^{-15.3t} \tag{4.11}$$

where the time t is expressed in ms [44]. However, inspection systems use narrowband inputs. The effect of noise when the bandwidth of the input signal is reduced is addressed in the following section.

4.5 Effect of noise on deconvolution performance

The presence of noise does not allow the propagator function to be estimated by the spectral division between the received signal and the input wavelet. Therefore the detrimental effect of noise needs to be investigated in order to evaluate the deconvolution performance. In this section we compare the performance of the optimal Wiener filter for the same level of noise when two different input wavelets have been used (broadband and narrowband inputs).

4.5.1 Broadband Input wavelet: performance of the optimal Wiener filter

In order to evaluate the performance of the optimal Wiener filter with a broadband input wavelet, white Gaussian noise was added to the synthetic data of figure 4.3; the SNR (relative to the largest amplitude in the signal) being 40 dB, which is a realistic noise level for SHM applications. The sampling frequency for the synthetic data was 1 MHz.

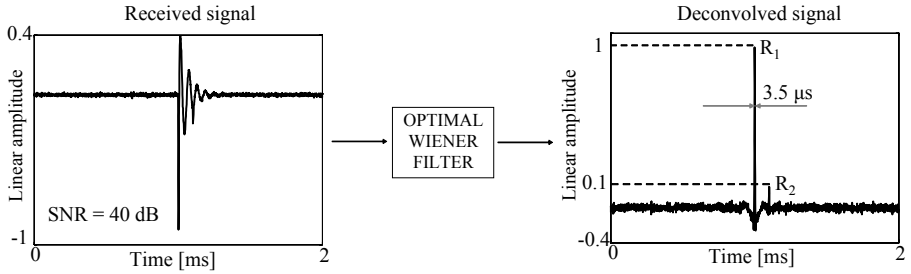

Figure 4.4: *Broadband input wavelet: detection of a small reflection by means of the optimal Wiener filter.*

The results shown in figure 4.4 clearly demonstrate the capability of the Wiener filter to enhance the resolution of overlapping echoes. The two wave packets are not resolvable in the original time trace, whereas the corresponding amplitudes and arrival times are clearly identified in the deconvolved signal; high temporal resolution is achieved, the Full Width Half Maximum (FWHM) of the deconvolved spike being 3.5 μs. The FWHM is defined as the difference between the two times on either side

of the peak at which the amplitude is half its maximum value. Convergence of the iterative process described in section 4.3.2 was achieved after 50 iterations.

4.5.2 Hanning windowed toneburst: effect of limited bandwidth on temporal resolution

Since excitation signals provided by transducers in an SHM system are narrowband for practical reasons (e.g. for limiting the dispersion of the input signal and for avoiding the presence of multiple modes), the effects of limited bandwidth on temporal resolution must be evaluated. A typical input signal used in NDE and SHM applications is the Hanning windowed toneburst [91]. Figure 4.5 shows that the spectrum of the Hanning windowed toneburst is similar to that of the broadband wavelet at low frequencies, but has much less energy at higher frequencies. Therefore, considering the same level of noise, it is reasonable to expect a decrease in temporal resolution compared to the results obtained with the broadband input wavelet because the exploitable bandwidth of the deconvolved signal is significantly reduced. Figure 4.6 shows that the small reflection is not easily resolvable and its amplitude is comparable to the side lobes of the first reflection. The FWHM of the spike is increased from 3.5 to 18 μs, which corresponds to 24 % of the FWHM of the envelope of the original wavelet. Convergence of the iterative process was again achieved after 50 iterations, as in the test shown in figure 4.4.

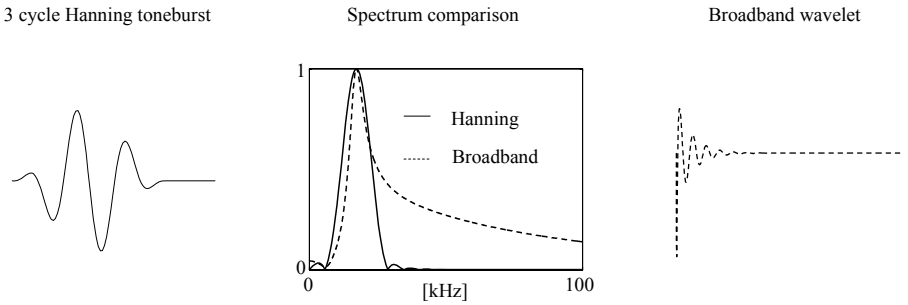

Figure 4.5: *Comparison between Hanning toneburst and broadband input wavelet.*

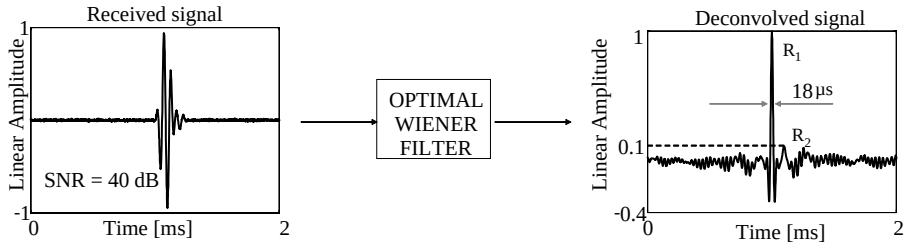

Figure 4.6: *Hanning toneburst: detection of a small reflection by means of the optimal Wiener filter.*

4.6 Effect of phase shift on deconvolution performance

Reflection from structural features can produce phase shifts in the input signal, so it is important to evaluate the influence of phase shift on deconvolution performance. This issue has not been studied in depth in the past and it has been addressed only in a few papers [76, 87]. First we will consider the case in which the phase shift is constant and frequency independent (e.g. reflection from the free edge of plate for the anti-symmetric A_0 mode at low frequencies [92]); subsequently we will consider the more general case in which the phase shift is a function of frequency [93]).

4.6.1 Frequency independent phase shift. Reflection from the free edge of a plate

The estimation of the arrival time of a wavelet which has been significantly phase shifted is difficult due to the alteration of the wavelet shape [94]. Figure 4.7 shows the effect of a $\pi/2$ rad phase shift on a 3 cycle Hanning toneburst.

This example is important for SHM because when the low-frequency anti-symmetric A_0 mode is reflected at the free edge of a plate, the reflected signal exhibits a frequency independent $\pi/2$ rad phase shift [92]. The problem of a frequency independent phase shift for deconvolution in reflection seismology has been addressed in [87]. When an input wavelet $s_0(t)$ is phase shifted by a frequency independent

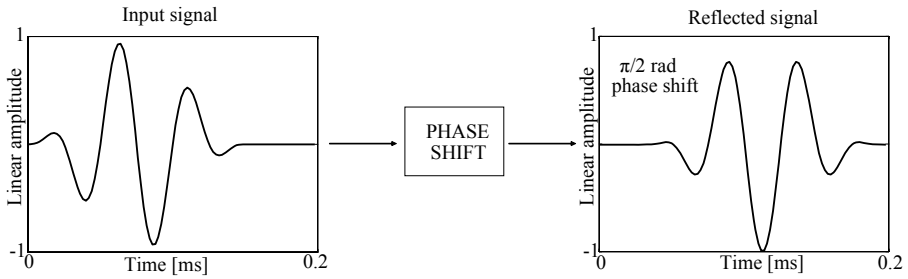

Figure 4.7: *Wavelet modification caused by a $\pi/2$ rad phase shift on a 3 cycle Hanning toneburst (the propagated distance for the reflected signal is 50 mm).*

angle, α, the phase shifted wavelet $s(t)$ can be written as a linear combination of $s_0(t)$ and its corresponding Hilbert Transform [94]:

$$s(\alpha, t) = s_0(t)\cos\alpha + \tilde{s_0}(t)\sin\alpha \tag{4.12}$$

where $\tilde{s_0}(t)$ represents the Hilbert Transform of the original wavelet $s_0(t)$. The case when $s_0(t) = \delta(t)$ where $\delta(t)$ is the Dirac delta function and $\alpha = \pi/2$ is particularly important. Here equation 4.12 gives:

$$s(\alpha, t) = \tilde{s_0}(t) = (-\pi\, t)^{-1} = -\frac{1}{\pi\ t} \tag{4.13}$$

since the hyperbola $(-\pi\, t)^{-1}$ is the Hilbert Transform of the Dirac delta function. The Hilbert Transform can be interpreted as a *quadrature* filter which is responsible for a $\pi/2$ phase shift [95]. The signal $(-\pi\ t)^{-1}$ is non causal and it is also the result that would be obtained in attempting the ideal deconvolution of a signal with infinite bandwidth that has undergone a frequency independent $\pi/2$ rad phase shift in noise-free conditions. It is important to stress that in this case deconvolution by means of the Wiener filter is equivalent to simple spectral division in the frequency domain. Therefore, even under these ideal conditions the presence of the phase shift results in resolution degradation as shown in figure 4.8 (the result is no longer a simple Dirac delta function). It is important to observe that the absence of causality stems from the idealization of the system, as discussed for the reflection of acoustic waves [94]. In a real experimental test where causality is respected, significant further distortion of the reflected signal would be observed.

This result is clearly unsatisfactory and an alternative solution has been suggested in [87]. This approach is based on the analytic formulation of the Wiener filter and

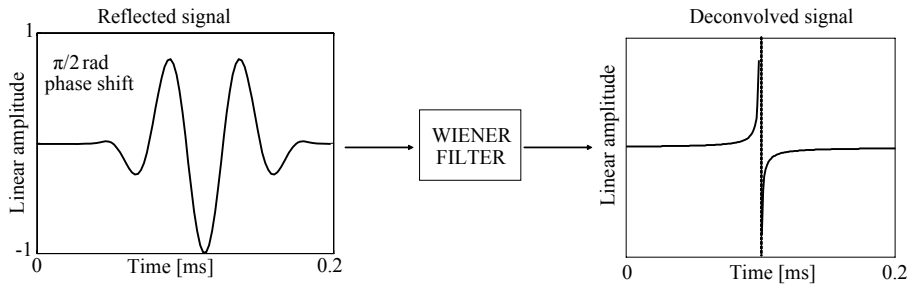

Figure 4.8: *Deconvolution of $\pi/2$ rad phase shifted signal.*

on the introduction of a complex model for the reflectors (where each reflector is characterized by amplitude and phase). The signal $s(\alpha, t)$ is expressed as:

$$s(\alpha, t) = s_0(t)\cos\alpha + \tilde{s_0}(t)\sin\alpha = Re\left\{\hat{s_0}(t)\exp(i\alpha)\right\} \tag{4.14}$$

where Re indicates the real part of a complex number and $\hat{s_0}(t)$ is the analytic representation of the input wavelet given by [95]:

$$\hat{s}(t) = s_0(t) - i\tilde{s_0}(t) \tag{4.15}$$

Equation 4.14 is important because it allows us to express a constant, frequency independent phase shift in a simple way by multiplying the analytic formulation of the original wavelet by a complex number. According to this approach it is possible to retrieve the arrival time, amplitude and phase shift α of the signal. The result in a noise-free case is represented by perfect deconvolution. Therefore a zero width spike located at the exact arrival time of the phase shifted signal would be obtained and the exact phase shift α would also be retrieved [87].

4.6.2 Frequency dependent phase shift. Plane strain model for a plate with a rib

In order to evaluate the performance of deconvolution on a system that is more representative of a typical complex structure for SHM, a plane strain FE model has been designed to simulate a 5 mm thick steel plate with a rib. Figure 4.9 shows a schematic of the model.

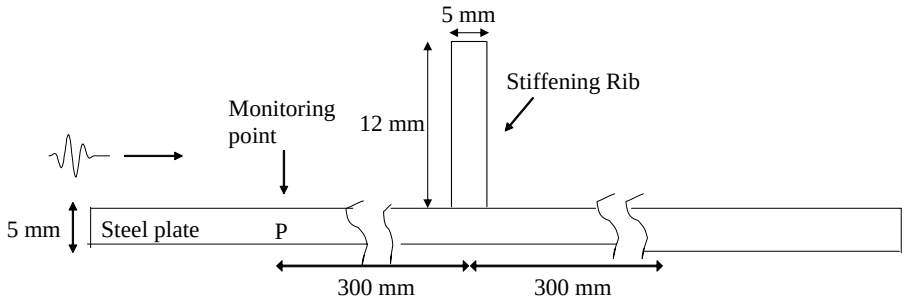

Figure 4.9: *Plane strain model of a steel plate with a rib.*

The rib is 12 mm long which is equivalent to a quarter of the wavelength at the centre frequency of the excitation used. The model has been meshed with CPE4R elements from the ABAQUS element library. The input signal is a 5 cycle Hanning windowed toneburst, 20 kHz centre frequency and it is applied to all the nodes at the left edge of the plate in order to generate the A_0 mode. The received signal is the signal reflected from the rib and recorded at the monitoring point P, as shown in figure 4.9. Figure 4.10 shows the reflected signal from the rib and the original input wavelet. Once the reflection coefficient has been estimated, it is possible to obtain the ideal (noise-free) deconvolved signal by means of the Inverse Fourier Transform.

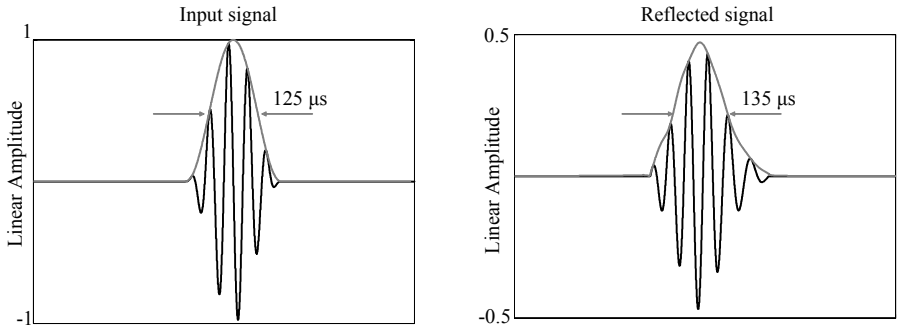

Figure 4.10: *Input and reflected signals from the rib for the incident A_0 mode.*

Figure 4.11 shows the result of the deconvolution of the reflected signal. The spectrum of the reflection coefficient has been band pass filtered to include only the 40 dB bandwidth of the excitation signal. Figure 4.11 shows that the resolution of the deconvolved signal is very poor and little benefit is obtained from deconvolution. The FWHM for the deconvolved signal is 100 μs, which corresponds to approximately 75 % of the FWHM of the envelope of the reflected signal.

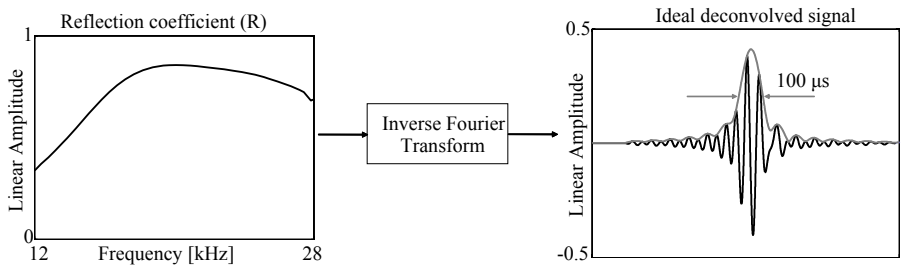

Figure 4.11: *Reflection coefficient from a rib. Ideal deconvolution.*

4.7 Combined effect of noise and phase shift

Before we consider a test in which the detrimental effects of noise and phase shift on deconvolution performance are simultaneously taken into account, it is convenient to highlight the two main results achieved so far:

- Noise reduces the resolution of the deconvolved signal because it is responsible for a decrease of the exploitable bandwidth of the signal;
- Phase shift is responsible for a further reduction in resolution because it alters the original shape of the input signal. Although frequency independent phase shifts can be overcome, no significant benefit is obtained for the more general case of frequency dependent phase shift.

Since the performance of the Wiener filter is strongly affected by the presence of noise and phase shift, it is important to investigate an alternative approach for deconvolution. Maximum likelihood approach has performed very well in deconvolving noisy signals without phase shifts, yielding zero width spikes with a better resolution than the optimal Wiener filter. We therefore investigated adopting this approach and in particular the Single Most Likely Replacement (SMLR) algorithm for the deconvolution of noisy signals when phase shifts are also present. The SMLR algorithm will be briefly introduced next.

4.7.1 Introduction to the SMLR algorithm

The Maximum Likelihood (ML) approach [65] has been applied to the solution of several inverse problems, especially in seismology and oil exploration [66, 96]. Maximum Likelihood techniques are claimed to be able to resolve closely spaced events and to efficiently handle backscatter effects and reflections from small features. In order to assume a Maximum Likelihood approach to the deconvolution problem it is necessary to consider the following steps:

- Specify a probability model for the measured output;
- Determine an expression for the likelihood function;
- Maximize the likelihood function with respect to the unknown parameters of the function in order to find the corresponding maximum likelihood estimators.

The SMLR is an iterative search detector originally developed for deconvolution of geophysical time traces [97]. This approach is based on the specific convolution model introduced in [66]. According to this model the propagator $g(t)$ introduced in equation 4.1 is modelled as a Bernoulli-Gaussian sequence [97]. As a consequence, the propagator will be expressed as the following product model:

$$g(t) = r(t)q(t) \tag{4.16}$$

where the function $r(t)$, containing the amplitude information, is a white Gaussian sequence and $q(t)$ is a Bernoulli sequence (random sequence of 0 and 1) for which $q(t) = 1$ corresponds to the presence of a wave packet. Event detection consists of finding the maximum likelihood estimation of the sequence $q(t)$ and the amplitude estimation of the events is provided by the maximum likelihood estimation of the sequence $r(t)$. In the estimation of the number of wave packets contained in a time trace, the SMLR algorithm will first solve the event detection problem determining the best estimate of the sequence $q(t)$ by means of an iterative process that will be briefly outlined below. Once the event detection problem has been solved the sequence of the amplitude of the detected wave packets can be estimated in a closed

form solution [97]. In order to estimate the sequence $q(t)$, the SMLR algorithm compares the likelihood of an initial sequence $q_i(t)$ with only a limited number of the 2^N possible test sequences $q_{pos}(t)$ in each iteration (N is the length of the data to be processed). Specifically, it is assumed that each $q_{pos}(t)$ differs from $q_i(t)$ at only one location, so that there are only N possible test sequences for a given reference sequence. Beginning with some initial reference sequence $q_i(t) = q^0(t)$ the SMLR detector computes N likelihood ratios corresponding to the N different $q_{pos}(t)$ sequences. Among these, the sequence which maximizes the likelihood ratio will be used as the reference sequence $q_i(t) = q^1(t)$ for the next iteration [98]. If, after K iterations a reference sequence $q_i(t) = q^K(t)$ is more likely than any of the corresponding $q_{pos}(t)$ sequences, the iterative search terminates and $q^K(t)$ is the final detected sequence. Figure 4.12 shows an example of a reference sequence and corresponding test sequences for the simple case when $N = 4$ and $q_i(t)$ contains only two non zero elements. The SMLR detector is similar to the CLEAN algorithm, a deconvolution technique widely used in astronomical applications, especially in high resolution interferometry [99].

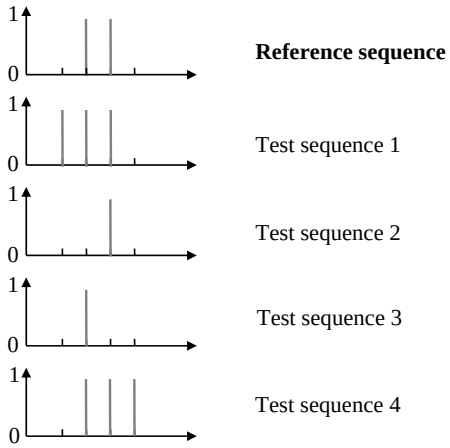

Figure 4.12: *Reference and test sequences for the SMLR algorithm.*

4.7.2 Performance of SMLR algorithm on a typical problem in SHM

SMLR performance has been evaluated on the signal shown in figure 4.6. Figure 4.13 shows that that SMLR technique is able to correctly estimate the arrival times and amplitudes of the two wave packets contained in the original time trace. The amplitude of the second signal has been estimated with an error of less than 2% with respect to the actual value. The arrival times have been exactly estimated and each wave packet is represented by a zero width spike in the deconvolved signal. The performance of the SMLR in detecting the presence of the small reflection is significantly better than Wiener filter performance. Figure 4.13 shows that SMLR is potentially suitable for the deconvolution of ultrasonic time traces. However, satellite or split spikes are sometimes seen [63], especially when the arrival time of the wave packet to be detected does not correspond to an integer number of time steps. Furthermore, this approach is computationally intensive; the maximum number of data points that it was possible to process with Matlab simulations on a normal desktop computer was approximately 300.

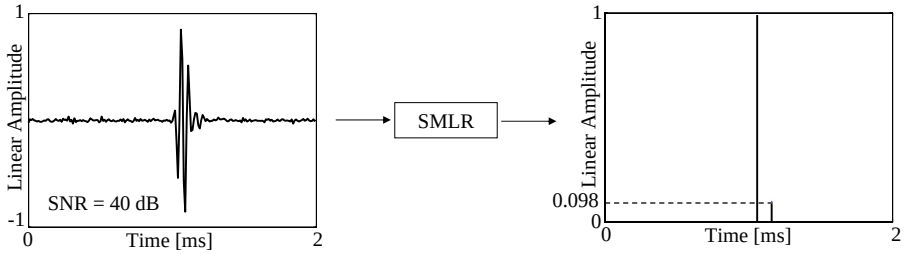

Figure 4.13: *Typical problem in SHM. Deconvolution of two strongly overlapping signals (SNR = 40 dB). Detection and estimation of arrival times and amplitudes by means of SMLR algorithm.*

Having shown that SMLR performs better than the Wiener filter on simple overlapping signals without phase shifts, it is important to investigate how the performance of the SMLR algorithm is affected by a constant frequency independent phase shift. The deconvolution of a noisy signal which has undergone a frequency independent $\pi/2$ rad phase shift has been considered. This test is also important because the effects of noise and phase shift on deconvolution performance are simultaneously

taken into account. The performance of the SMLR algorithm will be evaluated when random Gaussian noise (SNR = 40 dB) is added to the phase shifted signal already considered in figures 4.7 and 4.8. Figure 4.14 shows that the deconvolution of the phase shifted signal is represented by several spikes, so the gains of figure 4.13 are lost. The reason for this is that the iterative process described in section 4.7.1 corresponds to an attempt to match the phase shifted signal with the original input wavelet. Since the two waveforms are significantly different due to the phase shift (see figure 4.7), the SMLR is not able to correctly match the phase shifted signal with the original input wavelet and this results in split spikes and incorrect amplitude estimation in the deconvolved signal. It therefore appears that SMLR is very sensitive to changes in the form of the wavelet and this makes it unattractive for deconvolution in SHM.

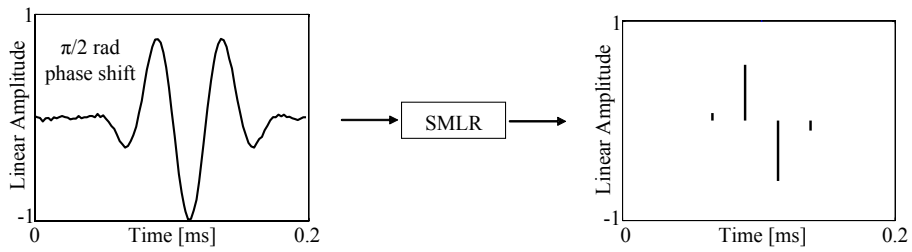

Figure 4.14: *Received signal with a $\pi/2$ rad frequency independent phase shift, SNR = 40 dB. Detection and amplitude estimation by means of the SMLR algorithm.*

4.8 Summary

The possibility of employing deconvolution in Structural Health Monitoring applications in an attempt to increase the temporal resolution of ultrasonic time traces has been evaluated. A significant improvement in resolution is achieved by using the Wiener filter when the input signal is broadband. However, it has been seen that the detection capability of the Wiener filter is strongly dependent on the bandwidth of the input signal and on the SNR. Phase shifts caused by structural features are also crucial in affecting deconvolution performance. Frequency independent phase shifts can be accommodated by employing the analytical form of the Wiener filter, though

at the expense of a decrease in temporal resolution. No significant improvement in temporal resolution is obtained for reflections from features such as ribs where reverberations can occur. The SMLR method gives better temporal resolution than the Wiener filter on signals without phase shifts. Specifically, very good results have been obtained in the detection of a small signal overlapping a large one. However, SMLR is very sensitive to the exact form of the input wavelet and does not perform well with phase shifts. It is therefore concluded that, although promising results have been obtained in different configurations by the Wiener filter and SMLR algorithm, deconvolution is unlikely to be useful in practical SHM applications where limited bandwidth signals are employed and different wave packets will have different phase shifts. An alternative method for SHM is baseline subtraction, but it is essential to account for changes in environmental conditions between the baseline and the current signals. This approach will be introduced in Chapter 5.

Chapter 5

Subtraction Approach for Structural Health Monitoring

5.1 Background

In conventional guided wave inspection the presence of a defect can be detected because different wave packets in the ultrasonic time traces are well separated and it is possible to discriminate between structural features and defects. Guided wave inspection has been successfully applied in several industrial applications to approximately one dimensional structures (relative to the wavelength), characterized by their low feature density (e.g. pipes and rails) [21]. The reliable inspection of these one dimensional structures can be effectively achieved because echoes from structural features are in general well separated and therefore the presence of defects can easily be detected by the appearance of extra reflections or by observing changes in the reflections coming from structural features. If these assumptions are satisfied, this method can be effectively employed for the integrity assessment of the structure. However, adopting this approach for the inspection of a complex structure like the one shown in figure 2.1 would be impractical because the reflections from different features are strongly overlapping making it impossible to observe changes in the signal coming from a single reflector.

An alternative approach for complex structures is to subtract a baseline obtained in the undamaged structure from the current signal [5]. The subtraction approach relies on the hypothesis that the recorded signal is stable if damage is not present [100]. If it were possible to achieve perfect subtraction between the current signal and the baseline signal, the presence of a defect could be deduced from the observation of changes in the residual of the subtraction, as shown in figure 5.1.

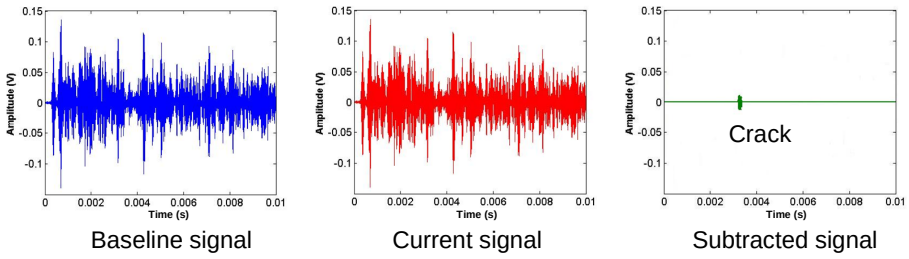

Figure 5.1: *Ideal Baseline subtraction for SHM. The subtraction of the baseline from the current signal leads to a subtracted signal from which the presence of a defect can be determined.*

In a real inspection problem, where perfect subtraction is not achievable, the occurrence of a new defect or the growth of a pre-existing defect can be detected only when the amplitude of the reflection coming from a damage location is sufficiently higher than the residual after subtraction in the absence of damage. In order to be able to detect the presence of small defects, a residual level of -40 dB is considered a desired target to be achieved for an undamaged structure [100]. The reason for this is that defects of interest in large area inspection are responsible, in general, for reflections of approximately -30 dB [93, 101]; therefore, achieving a residual level of -40 dB at the receiver location ensures a 10 dB margin that makes it possible to detect the presence of the defect. Following the approach proposed by Diligent et al. in [101], it is possible to determine approximately the diameter of a through-thickness circular hole that is responsible for a -30 dB reflection compared to the amplitude of the incident S_0 mode in a steel plate for a given distance between the centre of the hole and the receiver location. Table 5.1 shows the hole diameters obtained for typical values of the frequency-thickness product used in the inspection of plates with the S_0 mode for two centre of hole to transducer distances ($d_1 = 0.5m$ and $d_2 = 1m$, respectively).

Table 5.1: *Diameter of a through-thickness hole corresponding to a -30 dB reflector in a steel plate.*

Frequency-thickness [MHz·mm]	**Hole diameter [mm]** $d_1 = 0.5m$	**Hole diameter [mm]** $d_2 = 1m$
0.1	7	14
0.5	1.4	2.8
1	0.7	1.4

5.2 Detrimental factors for subtraction performance

Several factors are responsible for making it impossible to achieve perfect subtraction, even in an undamaged structure. The main factor that will be considered here is the effect of temperature change. Signal subtraction of ultrasonic time traces is strongly affected by temperature variations because temperature changes modify the mechanical properties of the material and therefore the velocity of propagation of the guided waves. As a result significant time shifts can be observed between signals measured in the same structures at different temperatures and this leads to a significant residual in the subtraction. Other issues that need to be considered as detrimental for a subtraction approach for SHM are:

- Loading conditions;
- Instrumentation drift;
- Boundary conditions;
- Structural changes;
- Other environmental conditions.

However, a complete discussion of these issues goes beyond the scope of this work. A more detailed explanation of the effects of temperature on signal subtraction is

given in section 5.3. Subsequently, methods designed for overcoming the detrimental effects of temperature changes on subtraction will be introduced in section 5.4.

5.3 Effect of temperature changes on signal subtraction

An important study on the effects of temperature variations on diffuse ultrasonic waves has been conducted by Weaver and Lobkis [102]. In this work it is shown that the main effect of a temperature change is a stretch or a compression of the ultrasonic signal. Temperature changes also affect the shape of the time traces, because the original shape of the pulses can be distorted. In order to gain a better insight on how guided wave signals are affected by temperature variation, it is possible to follow the approach proposed in [5]. Let us consider two Hanning windowed tonebursts $s_0(t)$ and $s_1(t)$ that have propagated for a distance d with velocity v in the same structure at two different temperatures, the temperature difference being δT. The signals $s_0(t)$ and $s_1(t)$ can be considered as the baseline and the current signal, respectively. Due to temperature change, the arrival times of the two signals will differ by δt. Our aim is to relate the difference in the arrival time of the two waveforms to the change in temperature of the structure δT. Partial differentiation of $t = \frac{d}{v}$ with respect to both d and v yields

$$\frac{\delta t}{\delta T} = \frac{1}{v}\frac{\delta d}{\delta T} - \frac{d}{v^2}\frac{\delta v}{\delta T} \tag{5.1}$$

Considering that

$$\frac{\delta d}{\delta T} = \alpha d \tag{5.2}$$

where α is the coefficient of thermal expansion and that

$$\frac{1}{v}\frac{\delta v}{\delta T} = \frac{\kappa}{v} = \gamma \tag{5.3}$$

κ being the coefficient of change in phase velocity with temperature and v the phase velocity, the relationship 5.1 can be written as

$$\delta t = \frac{d}{v}(\alpha - \gamma)\delta T \tag{5.4}$$

Since γ is generally significantly greater than α, from the previous equation we can observe that the main contribution to the time shift due to temperature variations is given by the change in the wave velocity. Furthermore, the time shift is directly proportional to the propagation distance and since the propagation velocity v appears in the denominator of equation 5.4, faster modes would be less affected than the slower ones. The subtraction of the two signals can be expressed as

$$s_1(t) - s_0(t) = u_0 h(t)[\sin \omega(t + \delta\, t) - \sin \omega\, t] \tag{5.5}$$

where u_0 is the amplitude of the signals $s_0(t)$ and $s_1(t)$ and $h(t)$ is the Hanning window function [103]. If the time shift $\delta\, t$ is small enough for the small angle approximation to be valid, it is possible to demonstrate that the maximum residual ε_{max} is given by

$$\varepsilon_{max} = |s_1(t) - s_0(t)|_{max} = 2\pi\, f\, u_0\, \delta\, t \tag{5.6}$$

where f is the excitation frequency. Figure 5.2 illustrates the time shift due to temperature variation for a 5 cycle Hanning toneburst. Equation 5.6 suggests that the residual in the subtraction is proportional to time shift (and therefore to the temperature difference) and to the excitation frequency and amplitude of the signals. However, considering that $\lambda = \dfrac{v}{f}$ the combination of equations 5.4 and 5.6 yields

$$\varepsilon_{max} = 2\pi \frac{d}{\lambda} u_0\, (\alpha - \gamma)\delta\, T \tag{5.7}$$

The last equation shows that the residual is proportional to the number of wavelengths $\dfrac{d}{\lambda}$ that signals have propagated and not simply to the inspection frequency. The residual would be simply proportional to the frequency only when the velocity is constant with frequency (e.g. non-dispersive modes) [103].

5.4 Temperature compensation techniques

Methods designed for the mitigation of the temperature effects on the performance of SHM systems have been studied in the past and some examples can be found in [104, 105]. The possibility of employing suitable signal processing techniques to

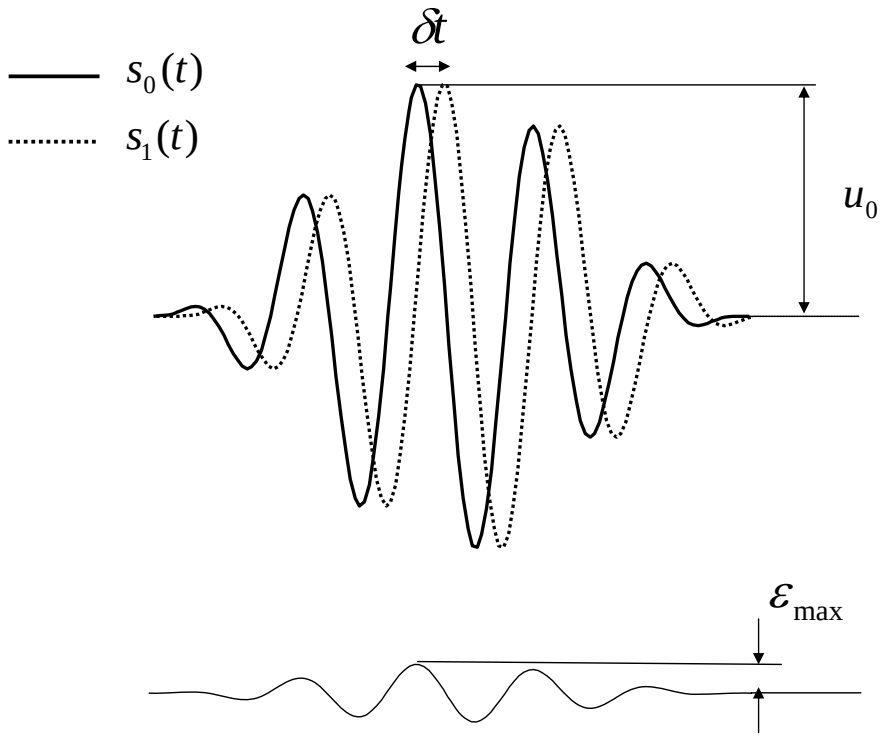

Figure 5.2: *Schematic of the time shift and maximum residual in the subtraction for a 5 cycle Hanning toneburst.*

compensate for the effects of temperature variations on ultrasonic time traces is extremely important for making the subtraction approach feasible for SHM applications, and much research has been recently conducted in this field. In this section we will discuss first the Optimal Baseline [100] and Optimal Stretch methods [6]. Subsequently an approach similar to the Optimal Stretch technique, namely the method of the Local Temporal Coherence [7] will be described. Optimal Baseline and Optimal Stretch are the temperature compensations techniques that have been used for the application of the subtraction approach. A brief description of the signal processing used in this work is given in the next subsection.

5.4.1 Signal processing for the subtraction approach

In order to achieve damage detection it is crucial to minimize the residual in the subtraction between the current signal measured from the structure in service and a

reference signal obtained from the undamaged structure. In this work, a combination of Optimal Baseline and Optimal Stretch has been considered and the overall signal processing can be written as follows:

- Firstly the Optimal Baseline method has been used in order to select the best matching baseline among the available reference signals of the undamaged structure. The optimal baseline is the reference signal for which the subtraction from the current signal yields the residual with the minimum Root Mean Square (RMS);
- Subsequently the Optimal Stretch technique has been applied in order to further reduce the residual of the subtraction between the current signal and the optimal baseline;
- Distance amplitude correction has been applied to the residual obtained after using the temperature compensation techniques in order to compensate for beam spreading.

Optimal Baseline and Optimal Stretch will be described in the next subsections as they represent the crucial part of the subtraction approach. A brief description of the distance amplitude correction algorithm is given here [106]. Let $R(t)$ be the envelope of the residual, normalized to the amplitude of the first arrival, that has been obtained after application of the temperature compensation techniques. The distance amplitude correction is carried out as follows:

$$R_{dac}(t) = \sqrt{\frac{t}{p/c_{gr}}} \cdot R(t) \tag{5.8}$$

where R_{dac} is the envelope of the residual compensated for beam spreading, p is the distance between transmitter and receiver and c_{gr} is the group velocity at the centre frequency of the guided wave mode taken into account.

5.4.2 Optimal Baseline method

The Optimal Baseline approach is based on the possibility of comparing the current signal with each one of the available baselines recorded over a wide range of operating conditions [5]. This technique relies on the hypothesis that when two ultrasonic time traces are recorded in the undamaged structure in similar environmental conditions, a low level of residual would be achieved in the subtraction. The detection of damage in the structure would be possible if the reflection from a defect location is responsible for a signal whose amplitude is above the residual level. The main aim of this approach is to extract the optimal baseline from the set of available baselines in order to achieve efficient subtraction with the current signal. The optimal baseline is the time trace that is responsible for the minimum residual in the subtraction from the current signal. It is intuitive that for reliable applications, this method requires a large number of baselines covering all the environmental conditions that are likely to be experienced by the structure in service. For instance, limiting our attention to the effects of temperature variations, baselines must be recorded with a temperature step of less than 1 °C [100].

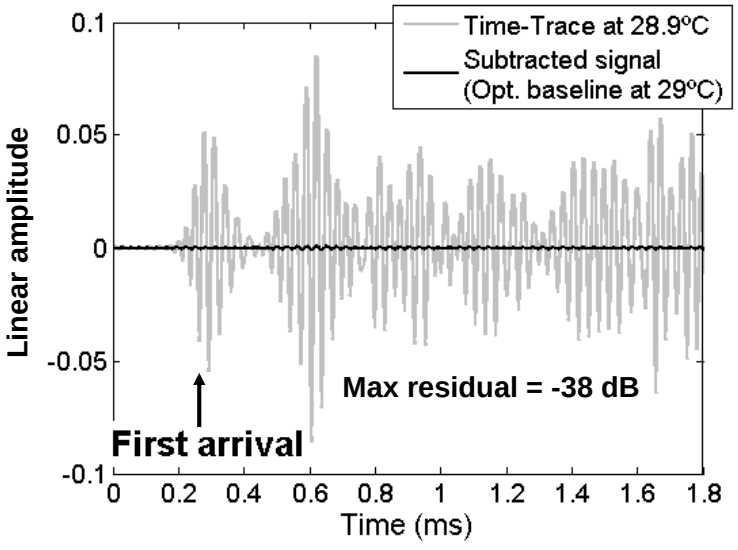

Figure 5.3: *Optimal Baseline subtraction for SHM. The temperature difference of the two time traces is 0.1 °C. The maximum residual is -38 dB [103].*

Figure 5.3 shows the result of subtraction after selection of the optimal baseline

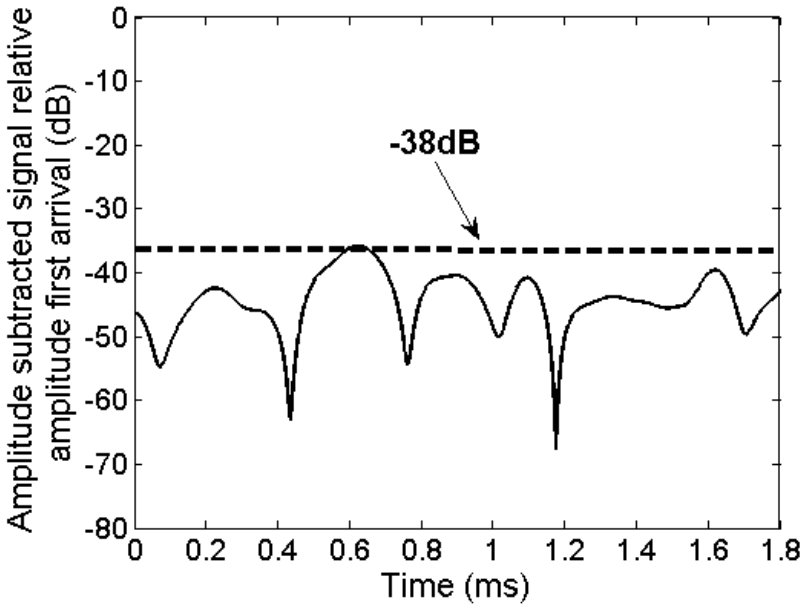

Figure 5.4: *Amplitude of the subtracted signal on a dB scale relative to the amplitude of the first arrival in figure 5.3 [103].*

for the time trace obtained from a 1000 × 1000 × 5 mm steel plate, inspected in pitch-catch mode [103]. The temperature difference between the baseline and the current signal was 0.1 °C and a maximum residual level of -38 dB relative to the first arrival was achieved, very close to the target residual level previously defined. This result confirms that very small temperature gaps among the recorded baselines are required in order to achieve good subtraction performance. Figure 5.4 shows the residual level in the subtracted signal compared to the amplitude of the first arrival on a dB scale.

5.4.3 Optimal Stretch method

In section 5.3 we have observed that temperature variations affect the velocities of guided waves propagating in a structure. This is responsible for pulses arriving later or earlier in time and therefore for a time delay between a current signal and a reference signal, recorded at two different temperatures. In addition, from equation 5.4 it is observed that the effects of temperature variations increase with propagation distance. Therefore the subtraction of the reference signal from the current signal

can lead to a large residual, especially in the later parts of the time traces. Stretch methods for compensating this effect are based on the idea of stretching or compressing either the baseline or the current signal in order to achieve a best match between the two signals to be subtracted. The compensation methods can be applied in the time domain [107] or in the frequency domain [6]. However, perfect compensation cannot be achieved because the frequency content of the signals is altered, since compensation is responsible for dilation or compression of the wave packets as well as the corresponding arrival times. The technique that we will consider is similar to the approach described in [6], where the compensation was carried out in the frequency domain. Let us consider the spectra of two signals that have been recorded at two different temperatures. In order to compensate for the effects of temperature change, the frequency step Δf of the second signal is increased or reduced until a minimum in the residual of the subtraction of the two signals is achieved. At each frequency the spectrum of the second signal is multiplied by the ratio between the spectrum of the first signal and the second one. This operation is required for correcting distortion effects in the spectrum, as explained in [6]. Iterating the process just described yields the Optimal Stretch between the two spectra, that corresponds to obtaining the minimum residual in the subtraction of the two signals in the time domain. Optimal Stretch requires only one baseline measurement, in contrast with the Optimal Baseline method of section 5.4.2.

An application of the Optimal Stretch method is reported in [103], where the performance of this technique was evaluated for a temperature difference of 5 °C between the current signal and the baseline. The reference signal was measured at 21.5 °C and the current signal was recorded at 26.5 °C from the same steel plate discussed in section 5.4.2. Figure 5.5 shows that the uncompensated subtraction between the two time traces yields a very high error, the maximum residual relative to the first arrival being -10 dB. However, when the reference signal is stretched by using the Optimal Stretch method, a significant improvement can be achieved, as shown in figure 5.6. After compensation the maximum residual relative to the first arrival was reduced to -38 dB, value very close to the target residual of -40 dB. The residual level in the subtracted signal compared on a dB scale to the amplitude of the first

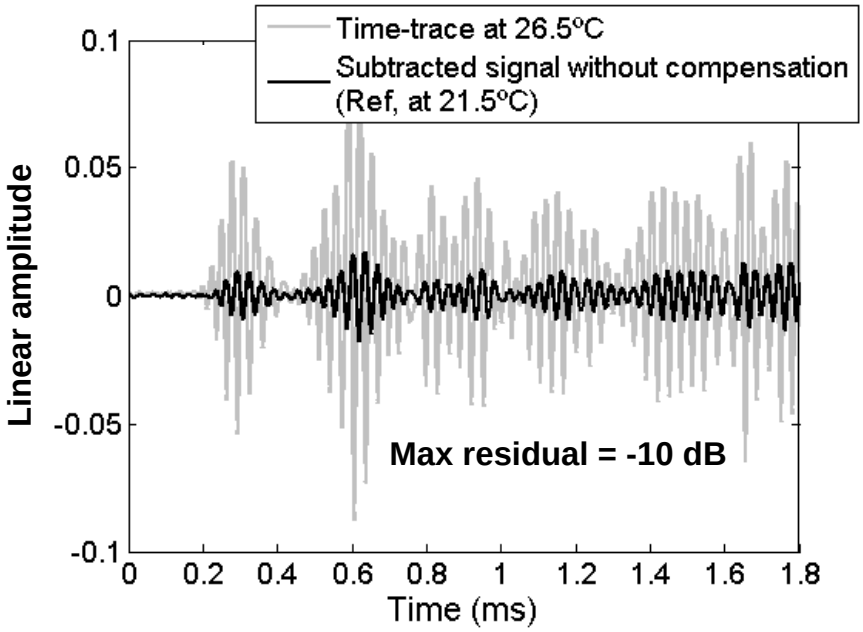

Figure 5.5: *Uncompensated subtraction with a 5 °C temperature difference. The maximum residual is -10 dB [103].*

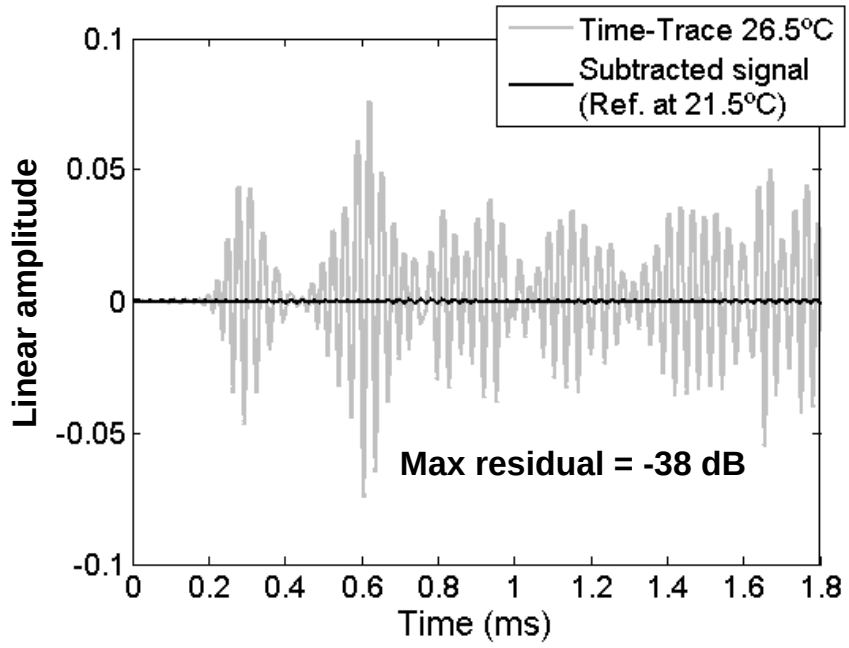

Figure 5.6: *Optimal Stretch subtraction for SHM. The temperature difference of the two time traces is 5 °C. The maximum residual is -38 dB [103].*

arrival is shown in figure 5.7.

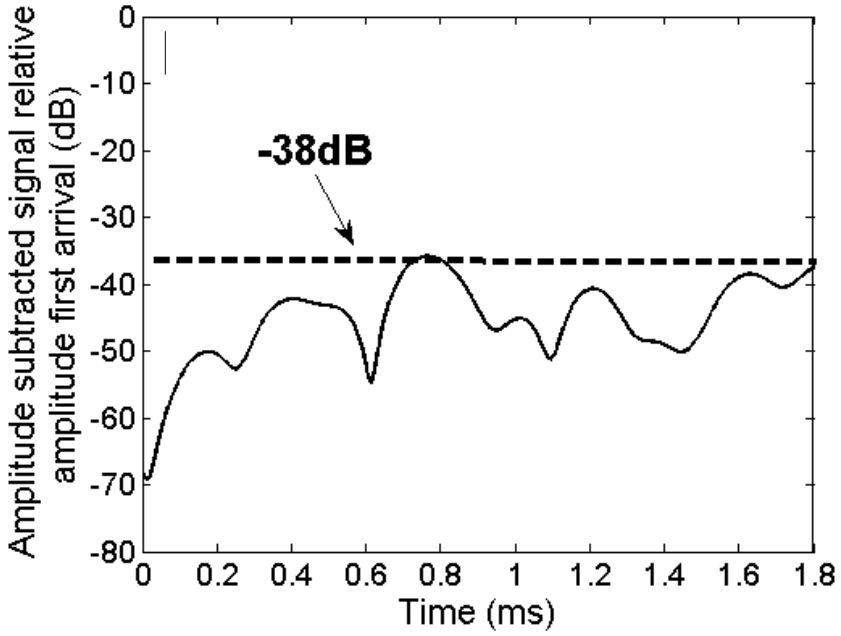

Figure 5.7: *Amplitude in dB scale of the subtracted signal relative to the amplitude of the first arrival in figure 5.6 [103].*

5.4.4 Local Temporal Coherence method

It has been already observed in section 5.3 that the time shift of two waveforms recorded at different temperatures is linear dependent on the propagation distance and that larger time shifts are expected for pulses arriving at later times (section 5.4.3). The Local Coherence, that can be calculated from the cross correlation between the two waveforms, is a means to estimate the slope of the linear relationship between the time delay of the two waveforms and the arrival time of the individual pulses [7]. Once this slope has been estimated, it is possible to stretch the selected baseline in order to minimize the mean squared error in the subtraction from the current signal.

5.4.5 Combination of compensation techniques

We can observe that Temperature Compensation techniques rely on the selection of a reference signal (Optimal Baseline method) or on signal stretch (Optimal Stretch and

Local Temporal Coherence methods). It is reasonable to combine baseline selection and stretch in order to improve the overall performance of the compensation [7]. For instance using Optimal Stretch can increase the maximum temperature gap at which the baselines need to be recorded. As a consequence, the acquisition of the baselines becomes more feasible and the size of the set of reference signals can be significantly reduced [103]. Some applications of temperature compensation techniques are presented in the next section.

5.5 SHM applications of Temperature Compensation Techniques

The temperature compensation techniques previously described appear very attractive for reducing the residual of the subtraction between two waveforms. Significant progress has been recently made in using temperature compensation techniques for typical detection problems in SHM. In this section an overview of experimental work on the application of compensation techniques for the subtraction approach is presented.

Interesting work on the feasibility of subtraction approach for SHM can be found in [100], where the Optimal Baseline method has been applied to reduce the detrimental effects of coherent noise on subtraction. In this work a method based on image subtraction was tested for the detection of a simulated defect in an aluminium plate, instrumented with three piezoelectric transducers operated in pitch-catch mode. The presence of the simulated defect was detected by simple subtraction of the images obtained combining the datasets taken immediately before and after the introduction of an artificial defect, represented by a small steel ball bearing attached to the plate [100]. However, it was observed that after increasing the time interval between the acquisition of the two datasets, significant noise was found after the subtraction. It was demonstrated that this problem was caused by the variations of temperature and the Optimal Baseline method was employed in order to improve the

result of the subtraction. A reduction of the residual in the subtraction was observed both for the A_0 and S_0 modes. In subsequent work, the influence of the size of the baseline set on the error in the subtraction was investigated and it was observed that increasing the range of conditions covered by the baseline set can be very beneficial for subtraction performance [108]. This study confirms that the Optimal Baseline can significantly improve the temperature stability of a subtraction approach for SHM. Moreover, by combining Optimal Baseline and a localization algorithm it was possible to localize simulated damage in presence of temperature variations with good accuracy. The Optimal Baseline method has also been used in [5], where a detailed study of the requirements for a sparse sensor array system for SHM has been presented. It has been observed that by using this approach, the residual in the subtraction can be reduced to -40 dB and, in addition, the number of sensors required per unit area can be decreased.

Important work on the evaluation of the performance of Temperature Compensation techniques is reported in [109]. In this paper, the methods previously discussed in this Chapter have been compared with simple subtraction in the inspection of an aluminium plate, instrumented with 6 piezoelectric transducers acting in pitch-catch mode and optimized for the excitation of the S_0 mode. Several heating cycles were applied to the plate and damage was introduced by drilling a small hole in the area covered by the transducers. Compensation techniques enabled reliable damage detection by observing changes in the residual. It was observed that for small temperature variations, Optimal Stretch provides good compensation; however, for large temperature changes, the frequency distortion (section 5.4.3) may be significant, leading to large residuals after subtraction. Similar considerations are reported in [110], where it was observed that the best performance of subtraction is achieved by selecting the best matching baseline from the set of the available reference signals and then applying stretch to improve the matching of the two signals. Therefore the combination of Optimal Stretch and Optimal Baseline can be extremely beneficial. The combination of Optimal Baseline and Optimal Stretch has been used in [103] and this strategy was tested for the compensation of temperature effects on signals measured on plate-like structures and in an airframe panel. This strategy was able

to achieve a residual level of -38 dB relative to the first arrival when the temperature difference between the current signal and the optimal baseline was 0.5 °C. Another interesting application of the combination of Optimal Baseline and Optimal Stretch is reported in [111], where this approach has been used for the inspection of a container panel both with the A_0 and S_0 modes. Low residual after subtraction was observed and it was possible to detect the presence of a small drilled hole, introduced to simulate damage, by observing an increase in the residual at the expected arrival time.

The method introduced in 5.4.4 has been used for detecting the presence of damage in aluminium plates by observing the variation in the mean squared error of the subtraction between the current signal and the optimal baseline [112]. For instance in one of the tests reported in this paper, a notch was introduced into the specimen and an increase in the mean squared error in the subtraction was observed compared to the error measured when the structure was undamaged. An imaging method based on the Local Temporal Coherence has been effectively used for damage localization in plates and is reported in [113, 114]. An aluminium plate was inspected in pitch-catch mode using six transducers with broadband excitation; the time traces recorded by all the possible transmitter-receiver combinations were combined in order to create images of the plate. After baseline images had been obtained, a small hole was drilled into the plate in order to simulate damage. Subsequently a notch starting from the left side of the hole was introduced to simulate a crack. The presence of the hole was clearly identified by subtraction, after the optimal baseline data set from the undamaged structure was selected. On the other hand, when the baseline data set was recorded with a mismatch of 2 °C from the current data set damage detection was not possible. After introduction of the notch it was observed that the area of damage localized by the imaging algorithm was shifted to the left of the centre of the hole. These results are important because damage localization was achieved in presence of temperature changes and in a typical SHM configuration. Furthermore, these tests confirm how the availability of a good matching baseline among the reference signals is crucial for efficient subtraction.

5.6 Summary

The Subtraction approach is an attractive method for SHM of complex structures and Temperature Compensation techniques can be used to overcome the negative effects of temperature variations. Specifically the combined use of Optimal Baseline and Optimal Stretch appears promising for efficient compensation of temperature effects on ultrasonic time traces. However, the effects of other detrimental issues need to be investigated in order to provide a more complete evaluation of the potential of a Subtraction approach for SHM. The presence of liquid loading, for instance is a typical condition to be expected in many situations when the structure is in service. The effects of the presence of liquid loading will be discussed in chapter 6 and they will be compared to the effects of temperature change. The performance of the combined use of Optimal Baseline and Optimal Stretch will be therefore evaluated in the presence of uniform liquid loading on plates. Subsequently the performance of temperature compensation on structures comprising materials with different temperature responses will be evaluated in chapter 7.

Chapter 6

Effects of Liquid Loading on Subtraction approach

6.1 Background

Variations in environmental and operational conditions can be extremely detrimental for damage detection because the recorded ultrasonic time traces can change and therefore the capability of detecting the presence of damage can be significantly jeopardized especially in complex structures [115]. The inspection of structures in the presence of liquid loading is a typical problem to be considered for SHM: fuel tanks, pipelines and several other components in chemical and nuclear plants are just an example of the importance of considering the presence of liquid for the reliable SHM of complex structures for industrial applications. In all these systems the presence of liquid plays a key role in the boundary conditions that need to be considered for an effective application of the Subtraction approach. For instance, in a huge storage tank the liquid level may vary according to operational conditions and the physical properties of the liquid are also temperature dependent. In addition, the signals recorded by an SHM system in complex structures can be affected by the occasional presence of liquid loading in several operating conditions. For instance rain, grease and loss of coolant and fuel can be responsible for total

or partial coverage of large plate-like structures with a thin liquid layer. Although the effects of temperature changes have been investigated and various compensation techniques have been proposed (Chapter 5), less attention has been devoted to the effects of liquid loading on subtraction techniques. In this Chapter our aim is to establish whether temperature compensation techniques are also able to cope with the changes caused by liquid loading, in order to specify under which conditions the subtraction approach can be applied also in the presence of liquid loading. In order to provide some fundamental information, the effects of liquid loading on the propagation of guided waves in plates will be briefly outlined in section 6.2.

6.2 Guided waves in bilayered plates

The problem of liquid loading is difficult to express in a mathematical context because several factors (such as physical properties of the fluid, location of the fluid on the structure and corresponding extent) should be taken into account [116]. In our study we will consider a simple system represented by a fluid-solid bilayer, as shown in figure 6.1, where a uniform liquid layer is covering the top surface of an aluminum plate. The system is completely characterized when the material properties of the plate and the fluid are known, as well as the ratio τ of liquid layer thickness to the plate thickness.

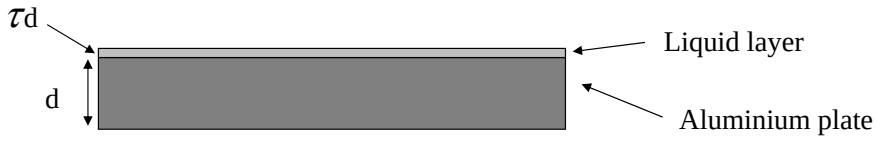

Figure 6.1: *Schematic of an aluminium-water bilayer. τ is the ratio of liquid thickness to plate thickness.*

The presence of a layer of fluid coupled with a plate increases the complexity of the modes that can propagate inside the structure. Specifically this is caused by the fact that the propagating guided modes in the bilayer are the result of the interaction between the modes propagating in the free plate and the modes propagating in the

liquid layer [117]. In other words the coupling between the fluid and the free plate is responsible for a continuous transition of the propagating wave mode through the modes characteristic of the fluid layer and those of the free plate as the frequency increases. This phenomenon is called "mode jumping" and it has been observed in higher order modes also by Yapura and Kinra in [118], where the equation for determining the dispersion curves for a fluid-solid bilayer has been obtained from the Navier's displacement equations of motion. The numerical results for an aluminium-water bilayer are presented and the transition of the guided wave mode from the liquid branch to the plate branch is studied in detail.

In order to study the effect of the liquid loading on subtraction techniques it is important to consider how the dispersion curve of the free plate is modified due to the presence of the liquid layer because this will affect the propagation characteristics of the individual pulses and therefore the error in the subtraction. An interesting study has been reported in [118] for an aluminium-water bilayer. It is observed that in a configuration characterized by $\tau = 0.125$ in the low frequency region the dispersion curves for the modes propagating in the bilayer are almost identical to those corresponding to the fundamental A_0 and S_0 modes propagating in the free plate. This is important because it suggests that the characteristics of the wave propagation in the free plate are not strongly affected by the presence of thin liquid layers in the frequency region of interest of Structural Health Monitoring.

Another interesting piece of work on guided wave propagation in bilayers is reported in [119], where the dispersion equations for an aluminium plate surrounded on both sides by a viscous liquid are presented and solved numerically. In particular, two different configurations are examined:

- plate bordered with viscous fluid layers;
- plate bordered with semi infinite viscous fluid layers.

It is observed that in both cases the phase velocity of the guided wave modes is mainly determined by the loading effect due to the presence of the liquid, whereas

the effect of the viscosity is negligible. The attenuation in the presence of thin layers for the A_0 and S_0 modes is affected by the viscosity, whereas when semi infinite layers are considered the attenuation is mainly caused by radiation to of energy towards the fluid (leaky Lamb wave [119]).

6.3 Parameters affecting guided wave propagation in a fluid-solid bilayer

The propagation of the guided waves in the presence of a uniform liquid layer is mainly affected by the physical properties of the liquid and the geometric parameters of the bilayer considered. Considering the system shown in figure 6.1, the most important factors to be considered are:

- F·d, Frequency-thickness product of the plate [MHz·mm]
- τ, ratio of liquid thickness to plate thickness
- D, propagation distance, expressed as number of wavelengths [nλ]
- η dynamic viscosity of the liquid [Pa·s]

In our work we will consider separately the propagation of the fundamental S_0 and A_0 modes in a bilayer in different configurations. The simulation of the signals has been obtained using the software DISPERSE [12]. Our objective is to estimate the error in the subtraction between the signals measured in the fluid loaded plate and in the free plate, respectively. For this purpose it is important to compare the dispersion curve of the unloaded plate with the dispersion curve of the bilayer obtained by loading the free plate with a uniform thin liquid layer. Firstly, the case in which the liquid in the bilayer is a thin water layer will be examined. Let us consider the propagation of the S_0 mode in a 10 mm thick aluminium plate loaded with a uniform water layer ($\tau = 0.01$). Figure 6.2a shows the dispersion curve for the S_0 mode in the aluminium water bilayer compared to the corresponding

dispersion curves for the unloaded plate, both at 20 °C. The two curves are close to each other and it is not possible to observe the velocity difference on this scale. Therefore the difference Δv between the phase velocity in the free plate and the phase velocity in the bilayer is plotted in figure 6.2b. It has to be noted that the maximum difference is approximately 18 m/s, which corresponds to approximately 0.32 % of the maximum phase velocity in figure 6.2a.

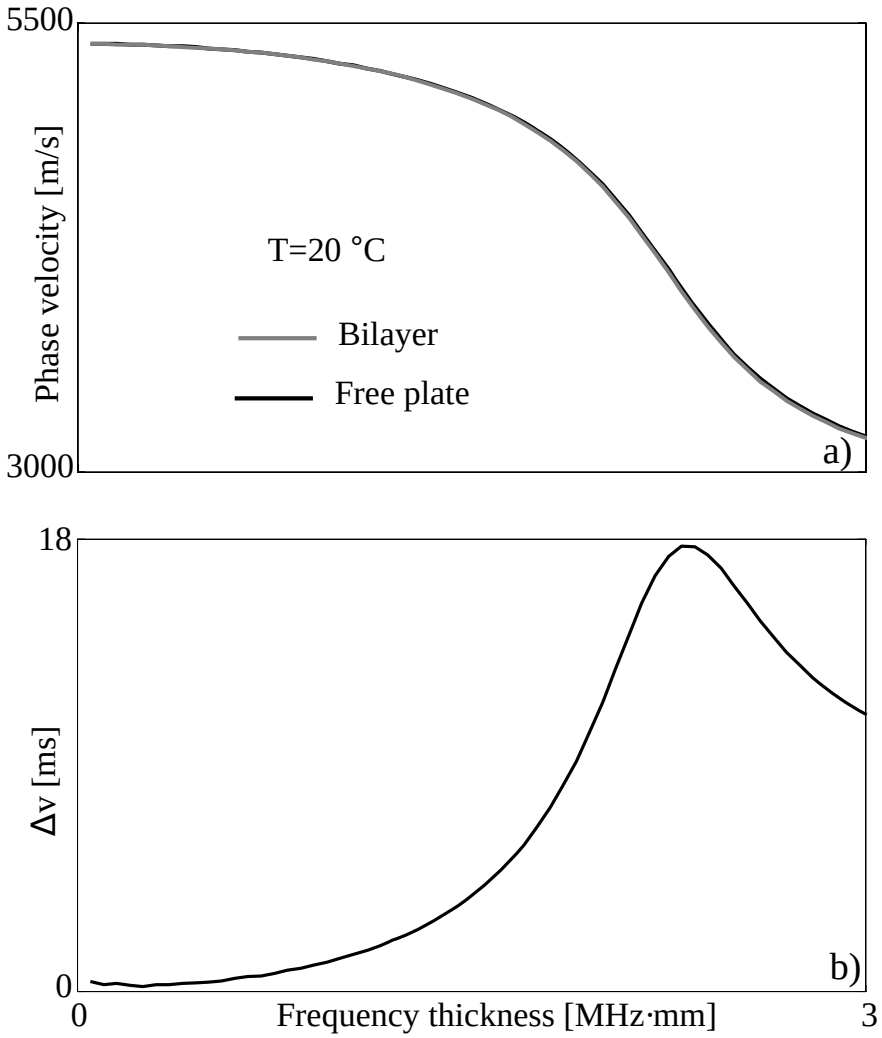

Figure 6.2: *a)Comparison of the dispersion curve for an aluminium-water bilayer and a free aluminimim plate. b)Difference between the two phase velocities. The plate thickness is 10 mm and* $\tau = 0.01$.

.

The attenuation of S_0 mode in the bilayer is negligible, as both aluminium and water have very low attenuation at these frequencies; hence the signals recorded

in the unloaded plate and in the bilayer can be directly compared to evaluate the performance of subtraction approach in presence of a thin liquid layer on plate-like structures. The considerations made so far are also valid for the A_0 mode propagating in aluminium water bilayers. In the next section the effects of liquid loading on subtraction will be compared with the effects of temperature variations for the two fundamental modes.

6.4 Comparing Liquid Loading to Temperature changes

Since the compensation techniques introduced in Chapter 5 have been proposed mainly for the compensation of temperature variations, it is interesting to compare the effects of liquid loading on simple subtraction with the effects of a typical temperature change. In this work the effects of a uniform liquid layer will be compared with the effects of a 10 °C temperature change for a free plate, in order to assess whether temperature compensation techniques can also be used to compensate for the presence of uniform liquid loading. When temperature change is considered the baseline signal and the current signal will be the time traces recorded in the free plate at 20 °C and at 30 °C, respectively. When the presence of a fluid is taken into account, the baseline will be, as before, the signal recorded in the the free plate at 20°C, whereas the the current signal will be the time trace recorded in the fluid-solid bilayer at the same temperature of 20 °C. In order to directly make a comparison between the effects of liquid loading and temperature change, an aluminium-water bilayer is now considered. The parameters defined in section 6.3 need to be provided in order to completely characterize the fluid-solid bilayer for the S_0 and A_0 modes. In particular, the values of frequency-thickness product considered for the two modes are typical for practical guided-wave nondestructive evaluation [91]. In the following the results of the subtraction in the presence of liquid loading are compared to the results obtained in presence of a 10 °C temperature change.

6.4.1 S_0 mode in Aluminium-water bilayer

For the propagation of the S_0 mode, a 10 mm thick aluminium plate is considered and for this plate thickness a typical inspection frequency is 100 kHz and therefore the frequency-thickness product is Fd = 1 MHz·mm; the propagation distance is D=20λ which at the frequency-thickness product considered corresponds to approximately 1 m. The thickness of the uniform water layer is 0.1 mm ($\tau = 0.01$) and the viscosity of the water is $\eta = 10^{-3}$ Pa·s. A number of different thicknesses of the liquid layer were also considered and it was observed that the resultant velocity change is insensitive to the thickness of the liquid layer; therefore the results that will be shown are approximately general for any thickness of the liquid layer. The input signal is a 5 cycle Hanning windowed toneburst at 100 kHz centre frequency. The geometry of the unloaded plate and of the bilayer can be easily defined in DISPERSE, as well as the mechanical properties of the aluminium at 20 and 30 °C. A lossless liquid layer is modelled in DISPERSE as an isotropic solid, characterized by the density and the bulk compression wave speed. Subsequently, it is possible to simulate the propagated signals in each system for a given propagation distance, by using the appropriate function in DISPERSE [120].

Figure 6.3a shows the result of the uncompensated subtraction between the current signal and the baseline for the case when a 10 °C temperature change is considered for the S_0 mode. The result for the uncompensated subtraction in the bilayer for the same propagation distance (D=20λ) is shown in figure 6.3b.

In the case of the temperature variation the maximum residual compared to the current signal level is -11 dB which is significantly higher than the target level of -40 dB, discussed in Chapter 6. However, it has been demonstrated that by using temperature compensation techniques the target residual level can be achieved. Considering the bilayer we can see that the maximum residual in the subtraction is -28.5 dB, which is significantly lower than that for a 10 °C temperature change.

Figure 6.4 shows the dispersion curve for the unloaded plate at 20 and 30 °C and for the bilayer at 20 °C, zoomed around the centre frequency of the input signal (0.1

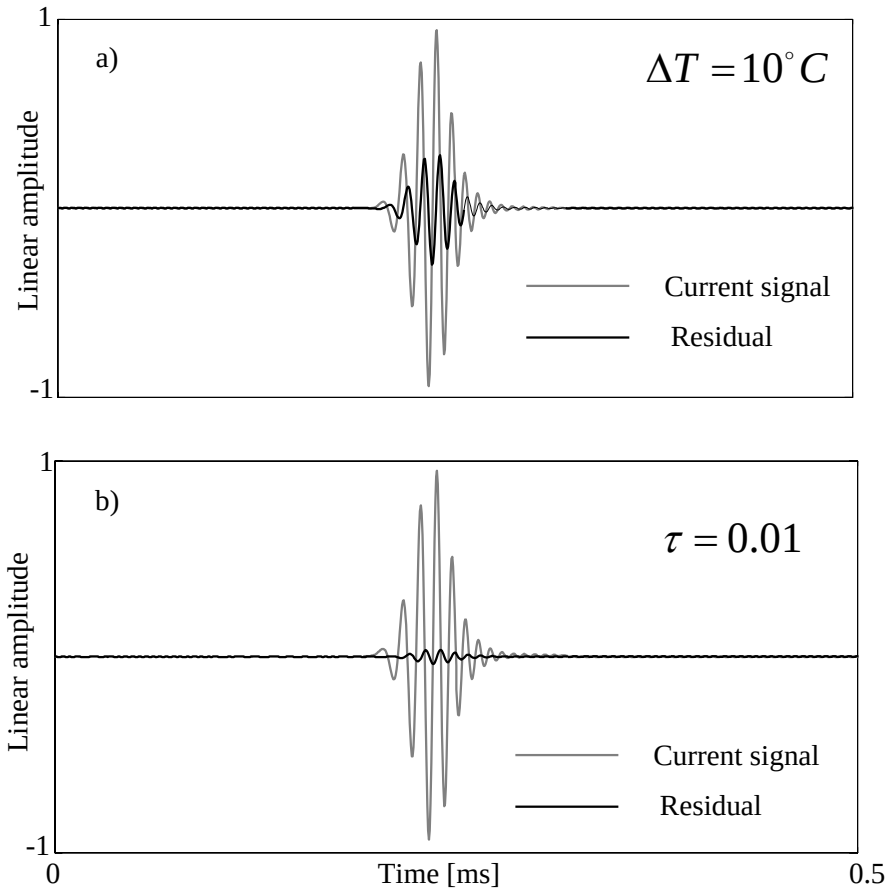

Figure 6.3: *a) Uncompensated subtraction for a 10 °C temperature change for the S_0 mode. The maximum residual is -11 dB. b)Uncompensated subtraction with liquid loading. The maximum residual is -28.5 dB.*

MHz).

The dispersion curve for the bilayer is closer to the corresponding curve for the free plate at 20 °C than the dispersion curve for the free plate at 30 °C. Specifically the difference between the values of phase velocity for the bilayer and the free plate at 20 °C is 1 m/s, which corresponds to a percentage variation of -0.018 %. The percentage variation for the phase velocity at centre frequency for the free plate from 20 to 30 °C is -0.24 %.

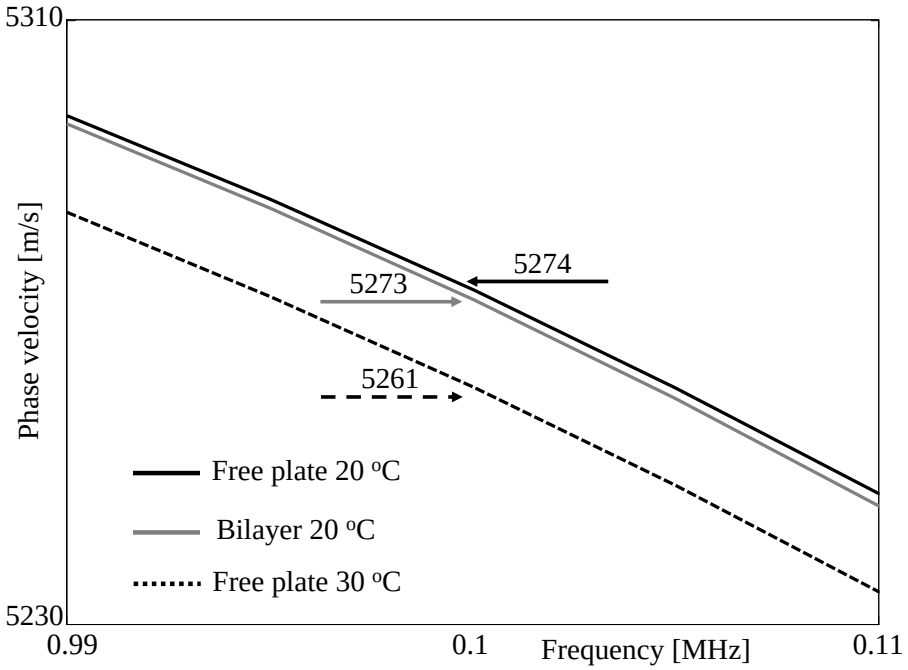

Figure 6.4: *S_0 mode. Comparison of the dispersion curve for the aluminium water bilayer at 20 °C with the dispersion curves for the free plate at 20 and 30 °C. The values of the corresponding phase velocities at centre frequency are indicated.*

6.4.2 A_0 mode in Aluminium-water bilayer

The propagation of the A_0 mode in a 5 mm thick Al plate is considered and for this plate thickness a typical inspection frequency is 20 kHz and therefore the frequency-thickness product is Fd = 0.1 MHz·mm; the propagation distance is D=20λ which at the frequency-thickness product considered corresponds to approximately 1 m, similar to the absolute propagation distance for the S_0 mode. The parameter τ has the same value considered for the S_0 mode. The input signal is a 5 cycle Hanning windowed toneburst at 20 kHz centre frequency.

Figure 6.5 illustrates the comparison of the uncompensated subtraction in the presence of 10 °C temperature change with the corresponding subtraction in the bilayer for the A_0 mode. Again the values of the maximum residual are higher than the target residual level, -16 dB and -19 dB respectively. The maximum residual of the subtraction for the A_0 mode in the bilayer is comparable to that of a 10 °C temperature change.

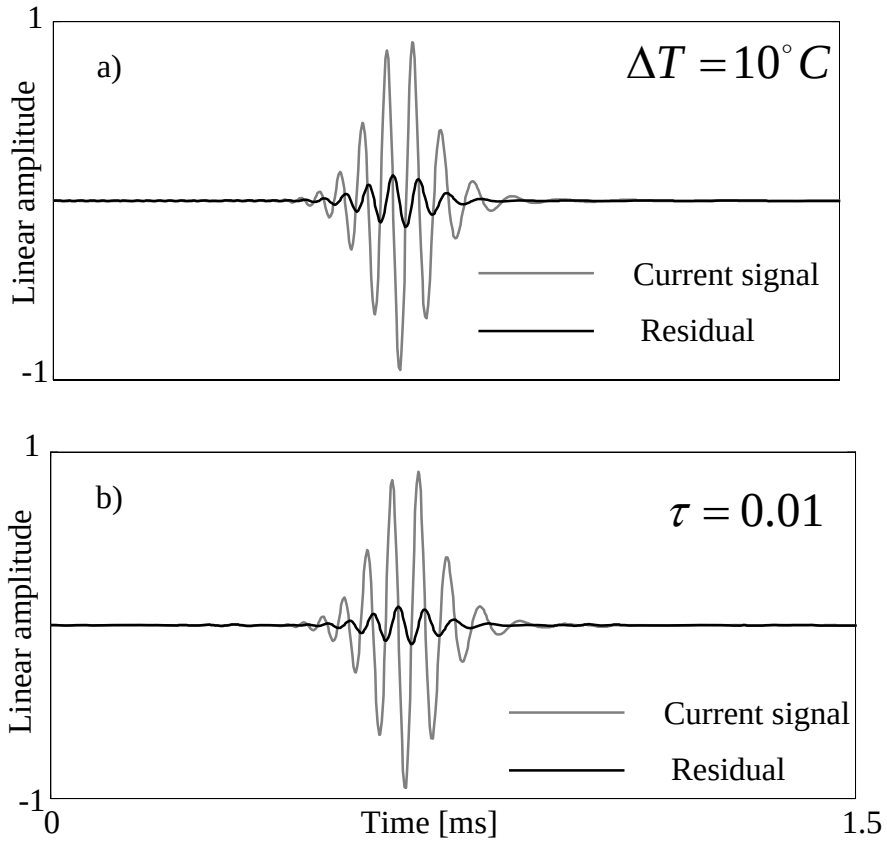

Figure 6.5: *a) Uncompensated subtraction for a 10 °C temperature change for the A_0 mode. The maximum residual is -16 dB. b) Uncompensated subtraction with liquid loading. The maximum residual is -19 dB.*

Figure 6.6 shows the dispersion curve for the unloaded plate at 20 and 30 °C and for the bilayer at 20 °C, zoomed around the centre frequency of the input signal (20kHz); the values of the phase velocities at centre frequency are indicated. Due to the high dispersion of the A_0 mode in the low frequency region, it is difficult to observe the relative velocity difference on this scale. The difference between the values of phase velocity for the free plate at 20 and 30 °C is 1.2 m/s, which corresponds to a percentage variation of -0.13 % (rather similar to the corresponding value for the S_0 mode). The phase velocity in the bilayer at centre frequency is closer to the value at 30 °C in the free plate.

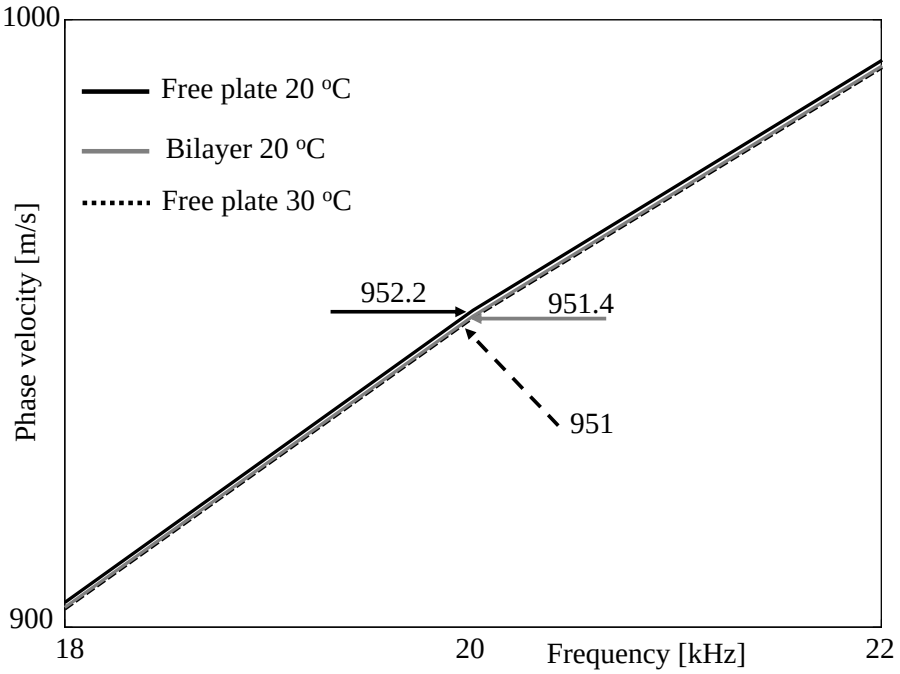

Figure 6.6: *A_0 mode. Comparison of the dispersion curve for the aluminium water bilayer at 20 °C with the dispersion curves for the free plate at 20 and 30° C. The values of the corresponding phase velocities at centre frequency are indicated.*

6.5 Performance of Optimal Baseline and Optimal Stretch with liquid loading

It is interesting to study whether the residual levels observed in figures 6.3b and 6.5b for the bilayer can be reduced using temperature compensation techniques. Our approach for the compensation of the effects of liquid loading on subtraction is based on the combined use of Optimal Baseline and Optimal Stretch [103, 109]. A wide set of baselines for different temperatures has been obtained in the range 20-30 °C for the unloaded aluminium plate and subsequently the Optimal Baseline and Optimal Stretch methods have been applied in order to find the best matching baseline and to further improve the result of the corresponding subtraction from the current signal. The baselines have been obtained simulating the propagated signal for different temperatures by varying density, shear and longitudinal velocities of aluminium as a function of temperature. These physical properties were obtained from data on the variation of elastic constants with temperature for monocrystalline

aluminium found in [121]. The physical properties were derived for each temperature in the range 20-30 °C with a temperature step of 0.1 °C. The values were used as input in DISPERSE to obtain the phase velocity versus frequency dispersion curves at different temperatures.

Figure 6.7 shows that the optimal baseline for the S_0 mode has been found at the temperature of 21.1 °C. Therefore the temperature of the optimal baseline is only 1.1 °C above the temperature of the current signal recorded in the bilayer. This result was expected considering that in figure 6.4 the dispersion curve in the bilayer is very close to the dispersion curve of the free plate at 20 °C. The phase velocity for the free plate at the temperature of the optimal baseline at centre frequency is 5273.06 m/s whereas the corresponding phase velocity for the bilayer at 20 °C is 5272.98 m/s. The corresponding percentage variations with respect to the phase velocity at centre frequency of the free plate at 20 °C are -0.023 % and -0.025 %, respectively. The subtraction between the current signal measured in the bilayer and the optimal baseline yields a maximum residual of -37.5 dB. After application of Optimal Stretch, the result is further improved and the residual is reduced to -43 dB.

The result for the A_0 mode is shown in figure 6.8. The maximum residual after Optimal Baseline is -39 dB, very close to the target residual level. The target residual level is achieved after using Optimal Stretch and the maximum residual level is reduced down to -45 dB. The optimal baseline has been found at 27.5 °C. This result is expected, since the residual in the subtraction from the reference signal at 20 °C is significantly higher than that observed for the S_0 mode. The phase velocity for the free plate at the temperature of the optimal baseline at centre frequency is 951.3 m/s whereas the corresponding phase velocity for the bilayer at 20 °C is 951.4 m/s. The corresponding percentage variations with respect to the phase velocity at centre frequency of the free plate at 20 °C are -0.094 % and -0.084 %, respectively.

These results suggest that Optimal Baseline and Optimal Stretch, although designed to compensate for temperature variations, can be used to compensate very satisfac-

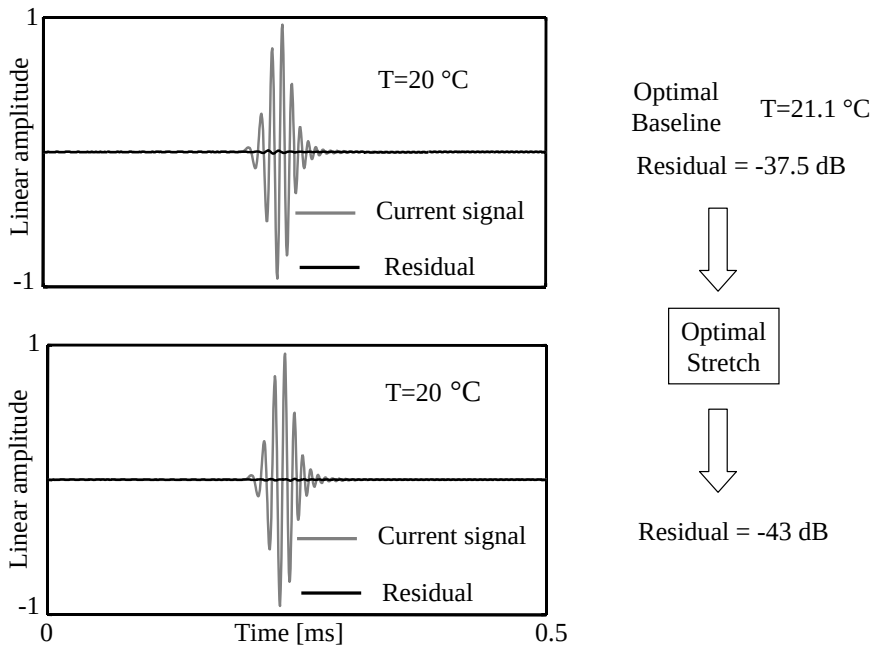

Figure 6.7: *Compensation of the subtraction for the S_0 mode. Performance of Optimal Baseline and Optimal Stretch in presence of a uniform water layer, $\tau = 0.01$, d=10mm.*

torily for the presence of a uniform thin liquid layer. The target of a residual level of approximately -40 dB has been achieved for the propagation of both the two fundamental S_0 and A_0 modes for very simple signals for a propagation distance of approximately 1 m.

6.6 Infinite water layer on an aluminium plate

Having shown that temperature compensation techniques can be applied for improving the result of subtraction also in presence of a thin liquid layer, it is reasonable to consider the same approach for the case of a plate bordered on one side with an infinite liquid layer. Due to the strong attenuation experienced by the A_0 mode in presence of liquid, the fundamental antisymmetric mode is not suitable for practical inspection applications in presence of liquid [122]. Therefore only the propagation of the S_0 mode will be considered for the case of an aluminium plate surrounded by an infinite water layer. This configuration can be considered representative of the inspection of fuel tanks in several industrial applications. The fluid-solid bilayer

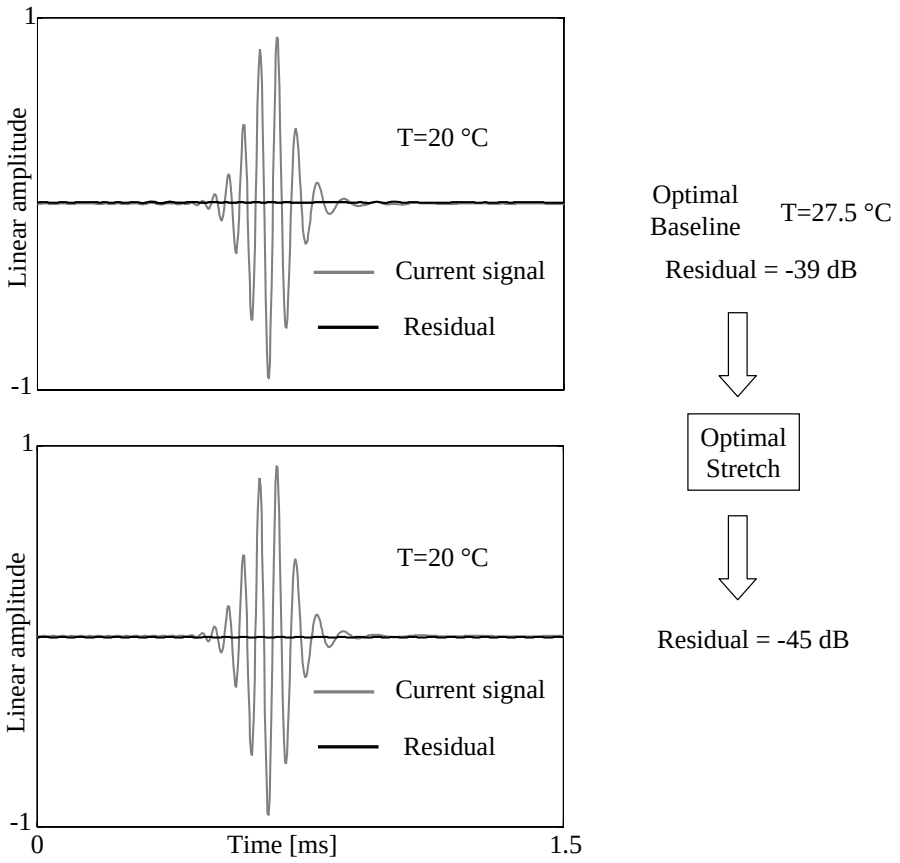

Figure 6.8: *Compensation of the subtraction for the A_0 mode. Performance of Optimal Baseline and Optimal Stretch in presence of a uniform water layer.*

considered has the same parameters defined in the subsection 6.4.1, except that now $\tau = \infty$. Figure 6.9 shows the attenuation curve for the typical frequency product range for S_0 mode inspection. The attenuation at $F = 0.1MHz$ is approximately 6 dB/m, significantly higher than the case of a thin water layer. A simple method to compensate for the attenuation of the S_0 mode is given in subsection 6.6.1.

6.6.1 Amplitude compensation for the S_0 mode

When guided waves are propagating in a medium surrounded by an infinite liquid layer, part of the energy radiates into the surrounding fluid and due to this leakage significant attenuation of the amplitude of the propagating mode is observed [123]. Therefore amplitude compensation is required in order to effectively apply the Sub-

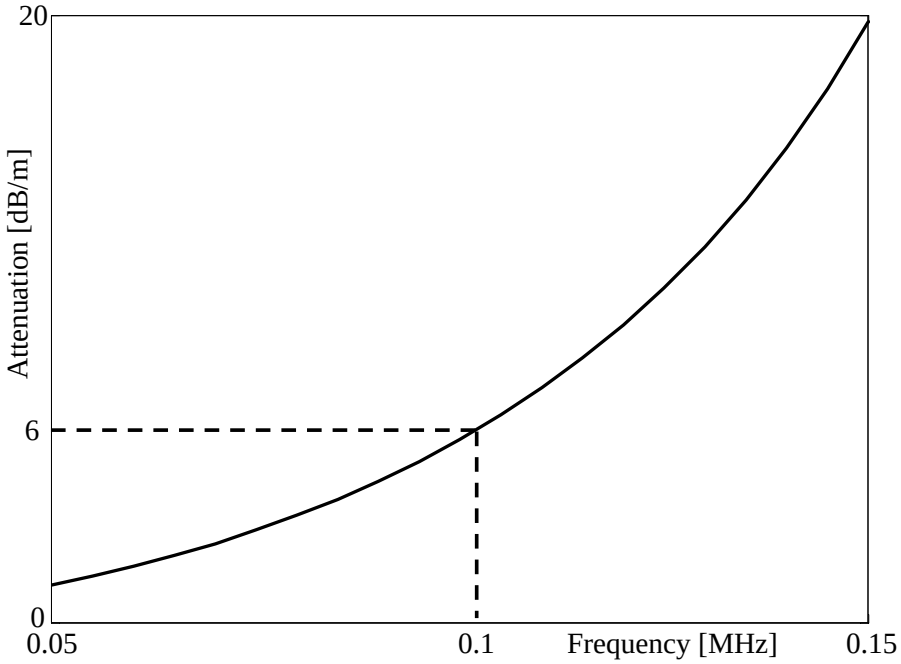

Figure 6.9: *Attenuation curve for a 10 mm thick aluminium plate bordered by an infinite water. The frequency range is shown is typical for S_0 mode inspection.*

traction approach. Once the current signal and the baseline signal have been obtained by DISPERSE as described in section 6.4, the amplitude compensation of the current signal is carried out in the frequency domain. Figure 6.10 illustrates our amplitude compensation approach.

In the top left corner the reference signal and the current signal are shown. Let $\rho_1(\omega)$ and $\rho_2(\omega)$ be the amplitude of the spectra of baseline and current signal, respectively (right hand side of figure 6.10). We can observe that higher frequencies are more attenuated; the reason for this is that increasing the frequency for the S_0 mode corresponds to increasing the out of plane displacements and therefore more energy is radiated towards the liquid layer [124]. The amplitude compensation of the current signal is obtained by simple multiplication of each frequency component by the ratio $\frac{\rho_1(\omega)}{\rho_2(\omega)}$. The phase of the current signal is left unchanged. Subsequently the current signal compensated for amplitude is obtained in time domain by means of the Inverse Fourier Transform. The amplitude compensated current signal is compared with the reference signal in the bottom left corner of figure 6.10.

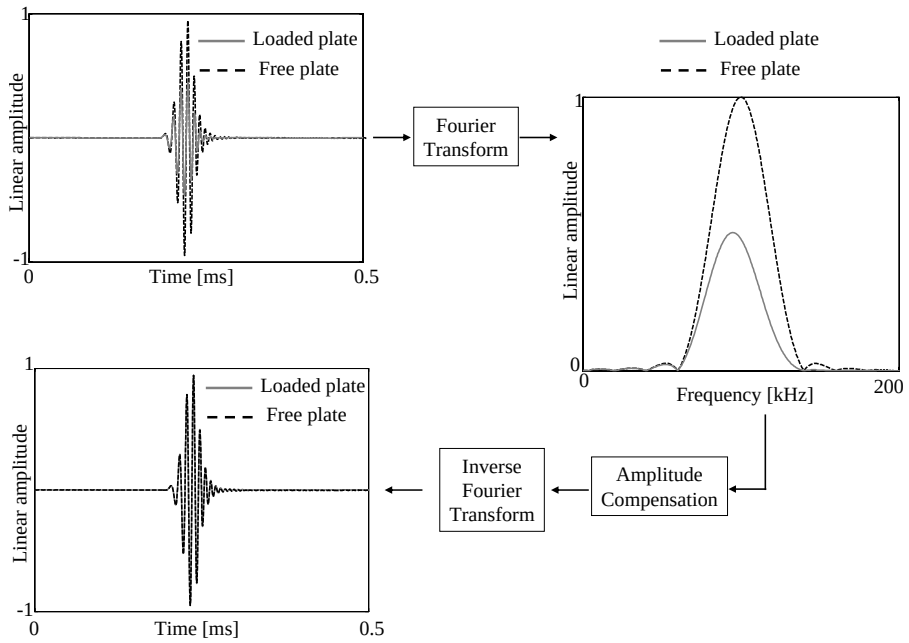

Figure 6.10: *Amplitude compensation in frequency domain. The original signals are shown on the top left corner. The amplitude of the signal measured in the liquid loaded plate is compensated in frequency domain (right). The amplitude compensated signal is compared with the reference signal obtained from the free plate (bottom left corner).*

6.6.2 Performance of Optimal Baseline and Optimal Stretch with liquid loading: Infinite water layer

Figure 6.11 shows the dispersion curve for the S_0 mode for an aluminium plate bordered with an infinite water layer at 20 °C compared with the dispersion curves for the unloaded plate at 20 and 30 °C. The dispersion curves are zoomed around the centre frequency of the input signal (0.1 MHz). The dispersion curve for the infinite bilayer is very close to the curve for the free plate at 20 °C, as already observed for the aluminium water bilayer characterized by $\tau = 0.01$. This suggests that the application of the Optimal Baseline method would yield a similar result in terms of the temperature of the best match.

Amplitude compensation was carried out by comparing the signal in the bilayer with the signal in the free plate at 20 °C. Subsequently it is possible to subtract the two signals in the bottom left corner of figure 6.10 and the compensation approach

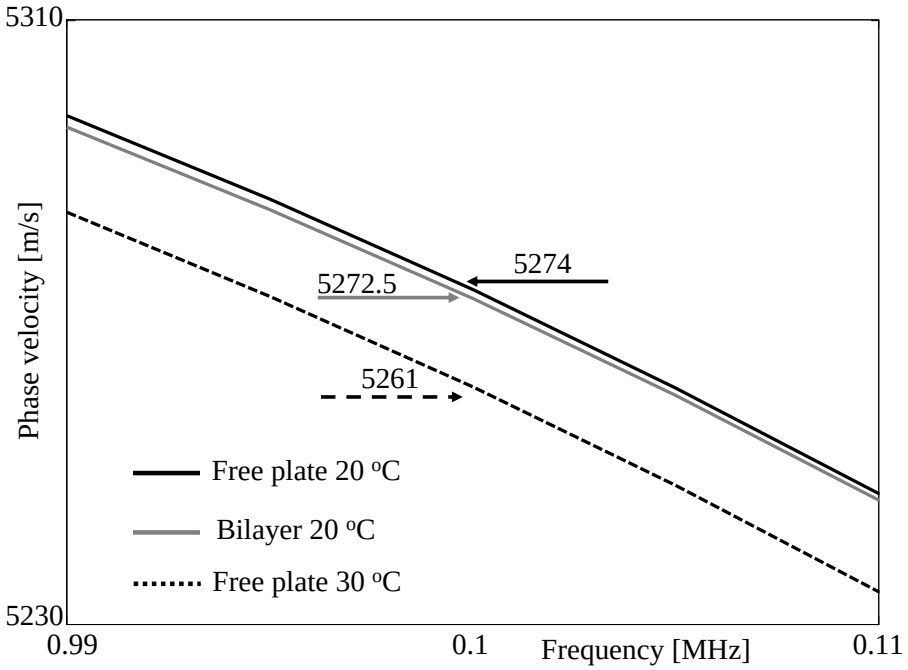

Figure 6.11: *S_0 mode. Comparison of the dispersion curve for the aluminium water bilayer ($\tau = \infty$) at 20 °C with the dispersion curves for the free plate at 20 and 30° C. The values of the corresponding phase velocities at centre frequency are indicated.*

described in section 6.5 has been adopted for reducing the amplitude of the residual. Figure 6.12 shows the result of the application of the compensation strategy. After Optimal Baseline the maximum residual is -39.5 dB. The best matching baseline signal was the time trace recorded at 21.5 °C. This temperature is very close to the temperature of the optimal baseline found in the case of a bilayer characterized by $\tau = 0.01$. Applying Optimal Stretch it is possible to further reduce the maximum residual down to -45 dB.

6.7 Subtraction approach in presence of an epoxy layer

In this section we will consider the case in which the fluid in the bilayer of figure 6.1 is a viscoelastic material. In particular we will consider the case of an aluminium plate bordered by a thin layer of epoxy. For the epoxy layer a hysteretic structural

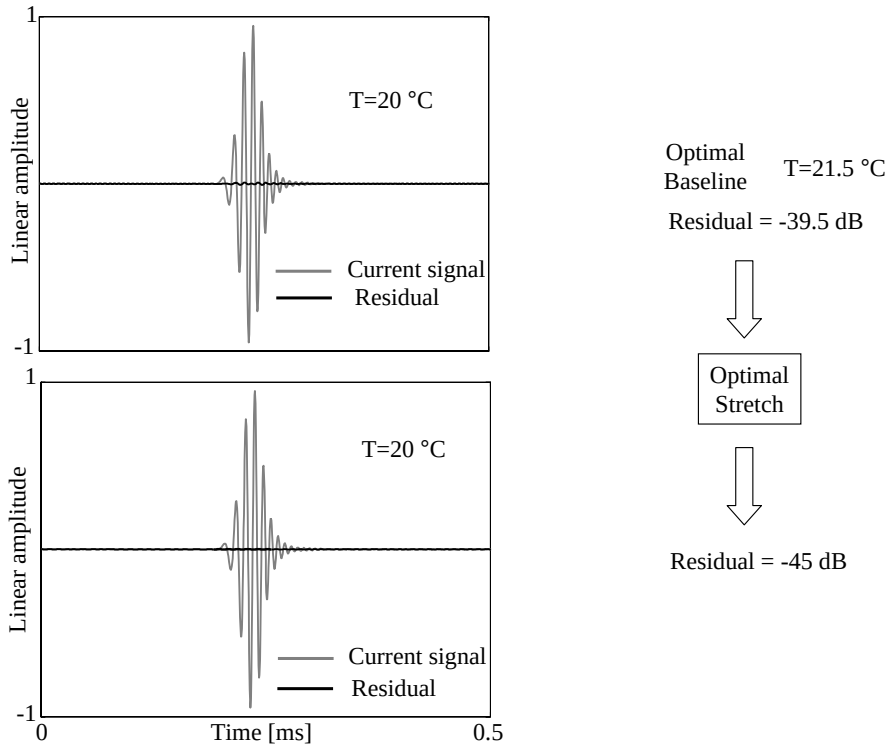

Figure 6.12: *Compensation of the subtraction for the S_0 mode. Performance of Optimal Baseline and Optimal Stretch in presence of an infinite water layer.*

damping model has been used with the longitudinal and shear damping coefficients equal to 0.01 and 0.1 np/λ, respectively [125]. This situation can be considered as a first approximation to the very similar case of painted plate-like structures in aerospace applications. We will evaluate the performance of Optimal Baseline and Optimal Stretch in presence of a thin layer of epoxy ($\tau = 0.01$) and for a propagation distance D=20λ, the value of F·d characterizing the bilayer being equivalent to that used previously for S_0 and A_0, respectively.

6.7.1 Performance of Optimal Baseline and Optimal Stretch with a thin epoxy layer

Figure 6.13 shows the result for the uncompensated subtraction for the S_0 mode between the current signal recorded in the bilayer and the baseline recorded in the free plate, both at 20 °C. The maximum residual is -12.5 dB which is comparable

to the corresponding residual for a 10 °C temperature change.

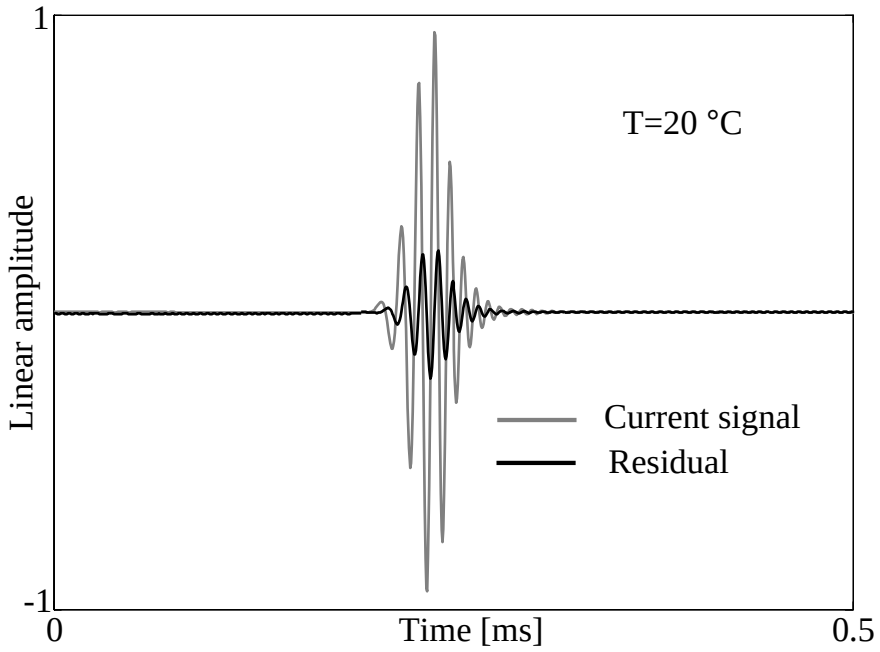

Figure 6.13: *Uncompensated subtraction for the propagation of the S_0 mode in presence of a thin epoxy layer ($\tau = 0.01$). The maximum residual is -12.5 dB.*

Figure 6.14 shows the dispersion curve for the bilayer at 20 °C compared with the dispersion curves for the unloaded plate at 20 and 30 °C, zoomed around the centre frequency of the input signal. It is possible to observe that the dispersion curve of the bilayer is closer to the curve of the free plate at 30 °C than to the curve at 20 °C. This suggests that the temperature of the best matching reference signal obtained by the Optimal Baseline method will be close to 30 °C.

The application of the compensation strategy is shown in figure 6.15. After using the Optimal Baseline method the residual is reduced to -38 dB and the temperature of the optimal baseline is equal to 27.5 °C. The phase velocity for the free plate at the temperature of the optimal baseline at centre frequency is 5264.9 m/s whereas the corresponding phase velocity for the bilayer at 20 °C is 5264.7 m/s. The corresponding percentage variations with respect to the phase velocity at centre frequency of the free plate at 20 °C are -0.178 % and -0.182 %, respectively. After application of the Optimal Stretch method the residual is further reduced to -45 dB.

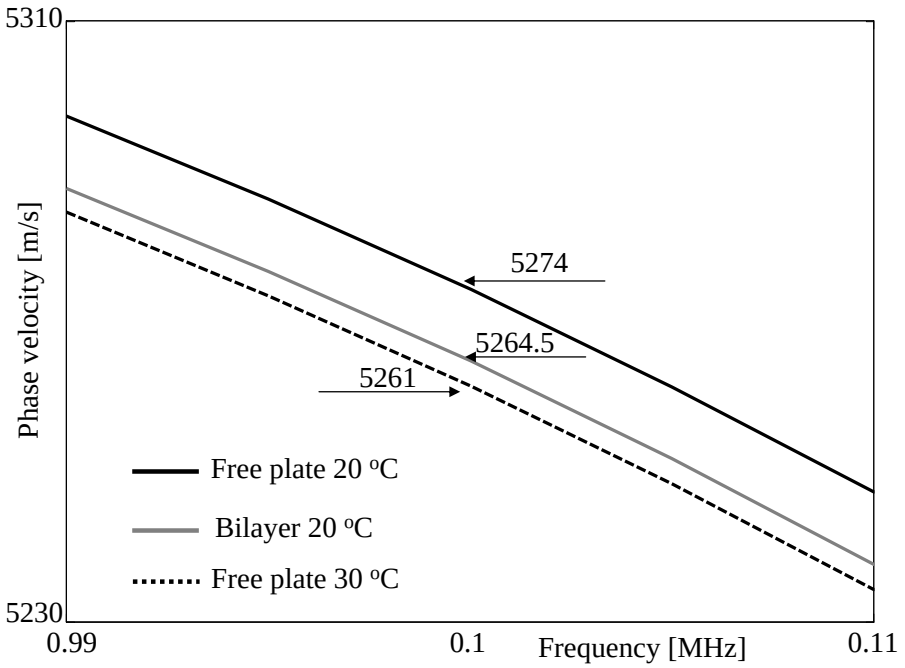

Figure 6.14: *S_0 mode. Comparison of the dispersion curve for the aluminium epoxy bilayer ($\tau = 0.01$) at 20 °C with the dispersion curves for the free plate at 20 and 30 °C. The values of the corresponding phase velocities at centre frequency are indicated.*

Figure 6.16 shows the result for the uncompensated subtraction for the A_0 mode. The maximum residual in the uncompensated subtraction is equal to -21 dB, which is lower than that for a 10 °C temperature change. Figure 6.17 shows the dispersion curve for the bilayer at 20 °C compared with the dispersion curves for the unloaded plate at 20 and 30 °C. Figure 6.18 shows the result of the application of Optimal Baseline and Optimal Stretch to the uncompensated data. The optimal baseline was found at 26 °C and the residual level after Optimal Baseline was -38.5 dB. The phase velocity for the free plate at the temperature of the optimal baseline at centre frequency is 951.48 m/s whereas the corresponding phase velocity for the bilayer at 20 °C is 951.5 m/s. The corresponding percentage variations with respect to the phase velocity at centre frequency of the free plate at 20 °C are -0.076 % and -0.073 %, respectively. The residual level was further reduced to -45.5 dB after application of Optimal Stretch.

It is important to observe that both for S_0 and A_0 modes the target residual level can be achieved and the temperature of the optimal baseline is in the range 20-30 °C.

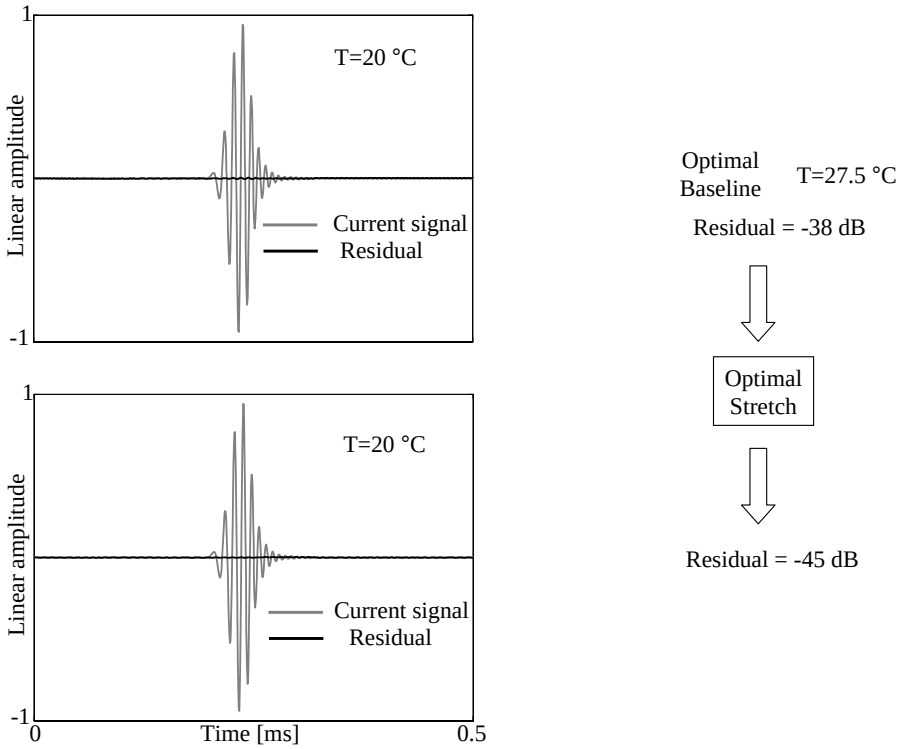

Figure 6.15: *Compensation of the subtraction for the S_0 mode. Performance of Optimal Baseline and Optimal Stretch in presence of a thin epoxy layer.*

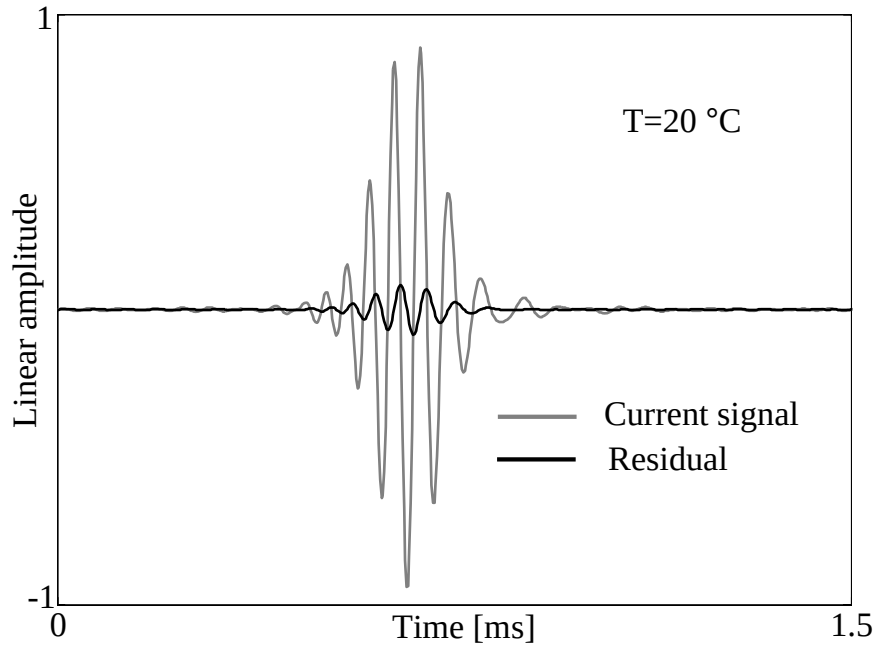

Figure 6.16: *Uncompensated subtraction for the propagation of the A_0 mode in presence of a thin epoxy layer ($\tau = 0.01$). The maximum residual is -21 dB.*

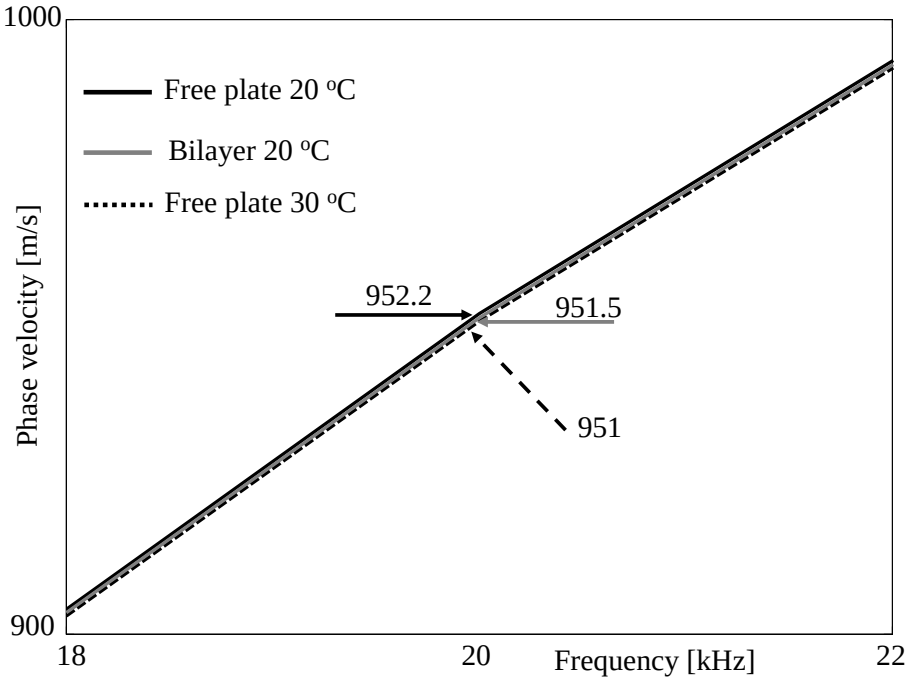

Figure 6.17: *A_0 mode. Comparison of the dispersion curve for the aluminium epoxy bilayer ($\tau = 0.01$) at 20 °C with the dispersion curves for the free plate at 20 and 30 °C. The values of the corresponding phase velocities at centre frequency are indicated.*

These results confirm that Optimal Baseline and Optimal Stretch can potentially also be used to compensate for detrimental effects that are not directly related to temperature variations.

6.8 Experimental work

Experimental tests have been carried out to validate the numerical results previously presented. Firstly, the situation of an aluminium plate immersed in a water tank will be considered, in order to simulate a plate surrounded by an infinite liquid layer. Subsequently the case of a thin uniform layer of epoxy will be examined. The results of these experiments are shown in the next sections.

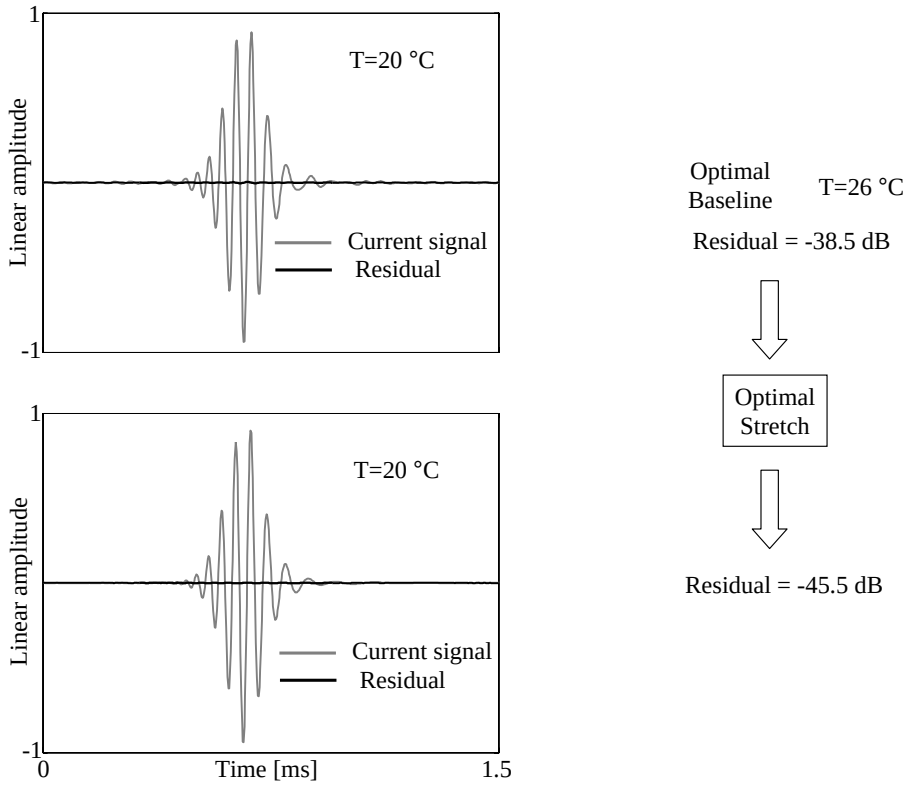

Figure 6.18: *Compensation of the subtraction for the A_0 mode. Performance of Optimal Baseline and Optimal Stretch in presence of a thin epoxy layer.*

6.9 Experiment with an infinite water layer

6.9.1 Experimental setup

The setup for this experiment was a 300 × 300 × 5 mm aluminium plate. Two piezoceramic PCM51 disc transducers for the excitation of the S_0 mode were attached to the plate and operated in pitch-catch mode, as shown in figure 6.19. The input signal was a 5 cycle Hanning windowed toneburst, 150 kHz centre frequency.

In order to keep each transducer electrically insulated from the plate, two thin plastic strips obtained from a 100 μm thick transparency film are used as spacers and inserted between each piezoelectric disc and the plate. The top surface of the strips was covered by a copper adhesive tape (60 μm thick); in this way it was possible to apply the electrical voltage which drives each transducer to its top and bottom surfaces, avoiding electrical contact between the transducers and the plate.

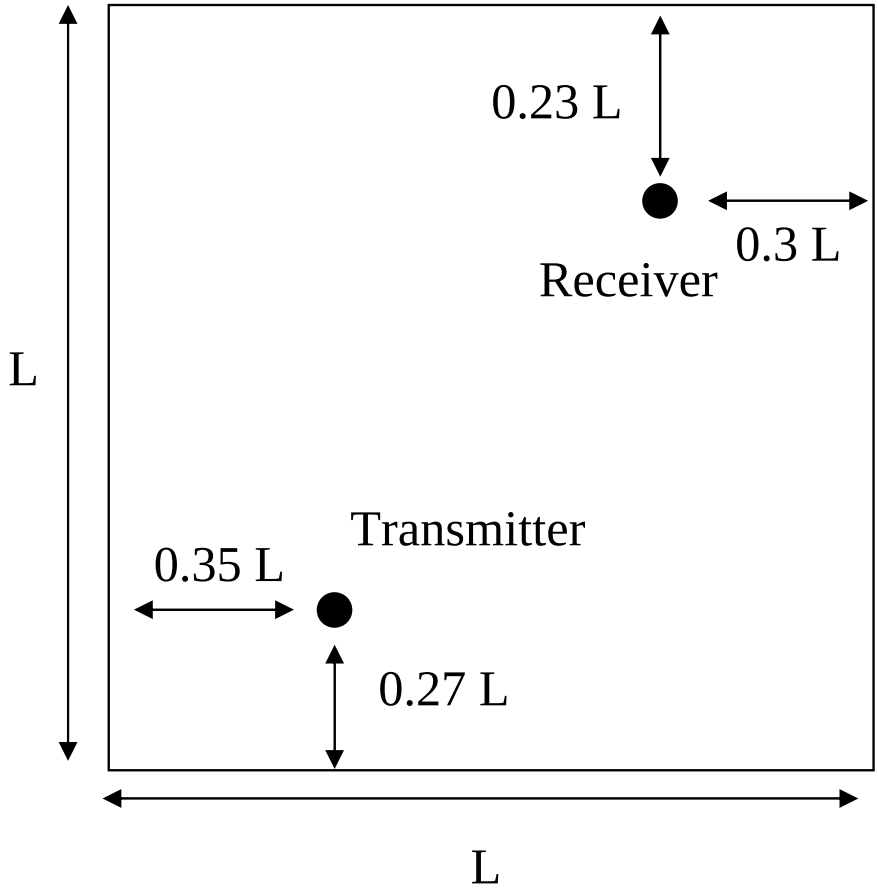

Figure 6.19: *Pitch-catch inspection of an aluminium plate.*

Once the transducers were wired, they were covered with a thin waterproof silicone layer to avoid contact between the transducer and the water. Figure 6.20 shows a schematic of the transducer used in this experiment.

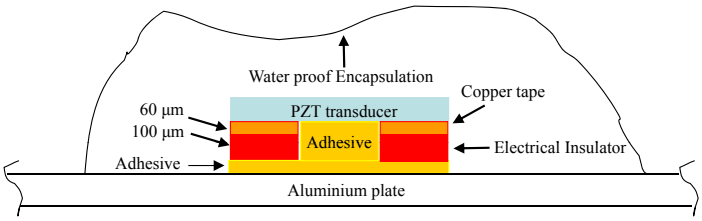

Figure 6.20: *Schematic of a piezoelectric transducer encapsulated with waterproof silicone. The electrical insulator avoids electrical contact between the transducer and the plate.*

6.9.2 Measurement procedure

In the first stage of the experiment, the aluminium plate instrumented with the piezoelectric transducers was placed on 3 adjustable height, point supports in an oven, where the temperature was slowly increased starting from room temperature, in order to allow the recording of reference signals with small temperature gap (the temperature differences between baselines was never greater than 0.2 °C). Figure 6.21 shows the position of the 3 point supports. Two thermocouples were connected to the plate in proximity of the transducers in order to continuously monitor the temperature during the acquisition of the baselines and no significant gradients were observed during the baselines acquisitions.

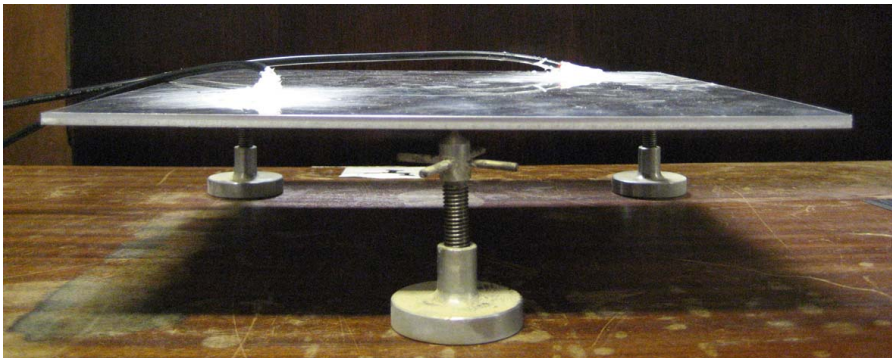

Figure 6.21: *Aluminium plate instrumented with transducers on 3 adjustable height, point supports.*

In the second stage of the experiment, the plate and the 3 adjustable height point supports were immersed in water in a cylindrical tank (diameter=660 mm, height=510 mm). The plate was placed equidistant from the bottom of the tank and from the free surface of the water, which was at 260 mm from the bottom of the tank (figure 6.22.

Let L be the side length of the square plate and c_{gr} the group velocity of the S_0 mode at the frequency of 150 kHz. The time it takes the guided waves to travel two plate transits in the aluminium plate is given by

$$t_{Al} = \frac{2L}{c_{gr}} \tag{6.1}$$

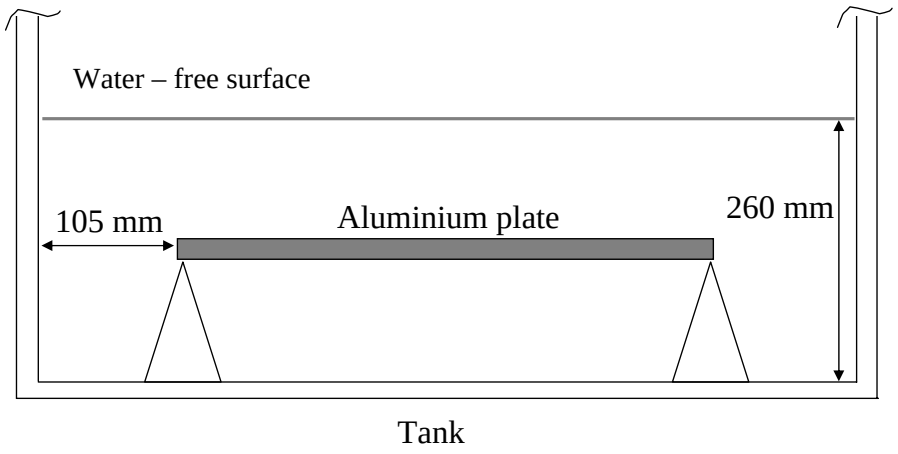

Figure 6.22: *Cross section of the experimental setup immersed in a water tank.*

During this time, the distance travelled by the leaky wave in the water is given by

$$d_{H_2O} = t_{Al} c_{H_2O} \tag{6.2}$$

where c_{H_2O} is the bulk velocity in water. Substituting the corresponding values for c_{gr} and c_{H_2O} a value of $d_{H_2O} \simeq 160\,mm$ is obtained. Figure 6.23 shows the leakage phenomenon for a plate immersed in water.

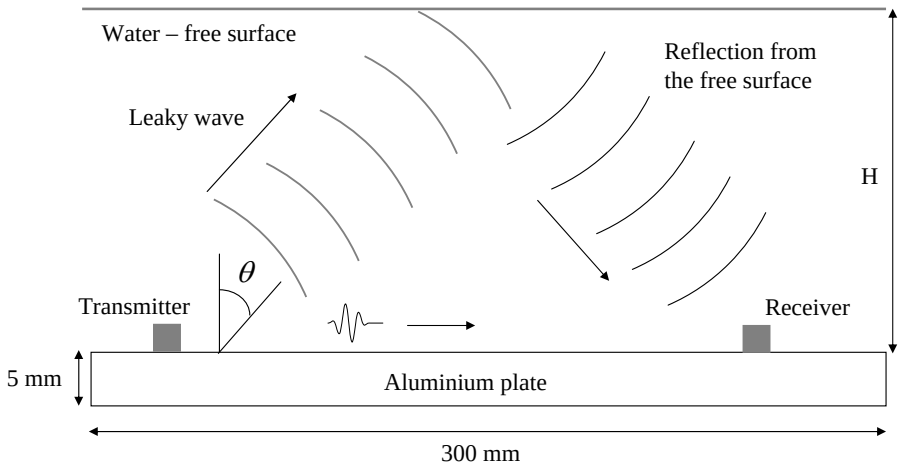

Figure 6.23: *Leakage phenomenon in a plate immersed by water. Energy radiates in the surrounding fluid creating a leaky bulk wave at a characteristic angle θ.*

The leakage angle θ can be found from the Snell's law and for the case of 5 mm thick aluminium plate immersed in water is

$$\theta = \arcsin \frac{c_{H_2O}}{c_{ph}} \simeq 16^\circ \tag{6.3}$$

where c_{ph} is the phase velocity of the S_0 mode at the frequency of 150 kHz. From equation 6.2 and considering figure 6.23 we can deduce that the minimum water level such that no reflection from the free surface of water is obtained before the time t_{Al} is

$$H = \frac{d_{H_2O}}{2} \simeq 80\,mm \tag{6.4}$$

The geometry of the experimental setup ensured that the reflections coming from the free surface of the water and from the tank were always received after the guided waves had propagated for two plate transits in the aluminium plate. In other words, the plate is surrounded by an equivalent infinite water layer for a propagation time corresponding to two plate transits. During the experiments, the temperature was monitored as during the baseline acquisition and the water was manually stirred to ensure that uniform temperatures were achieved in the tank before the acquisition of the signal.

6.9.3 Results

Figure 6.24 shows a time trace recorded in the plate immersed in the tank compared with a reference signal taken when the plate was in the oven at the same temperature of 31.5 °C.

The signal recorded in the water is attenuated compared to the baseline. The attenuation expressed in nepers as a function of time can be easily obtained and is represented by the solid grey curve in figure 6.25. The arrival time of the first pulse is indicated by the dashed vertical line; the part of the trend before this time corresponds to the ratio of the two parts of the original time traces where only noise is present. By comparison the attenuation trend obtained in DISPERSE for the S_0 mode propagating in a 5 mm thick aluminium plate bordered on its top and bottom surface by an infinite water layer is also shown (dashed black line in figure 6.25).

The actual amplitude ratio curve shows multiple peaks and troughs, caused by the multiple reverberations that are occurring in the plate and are responsible for

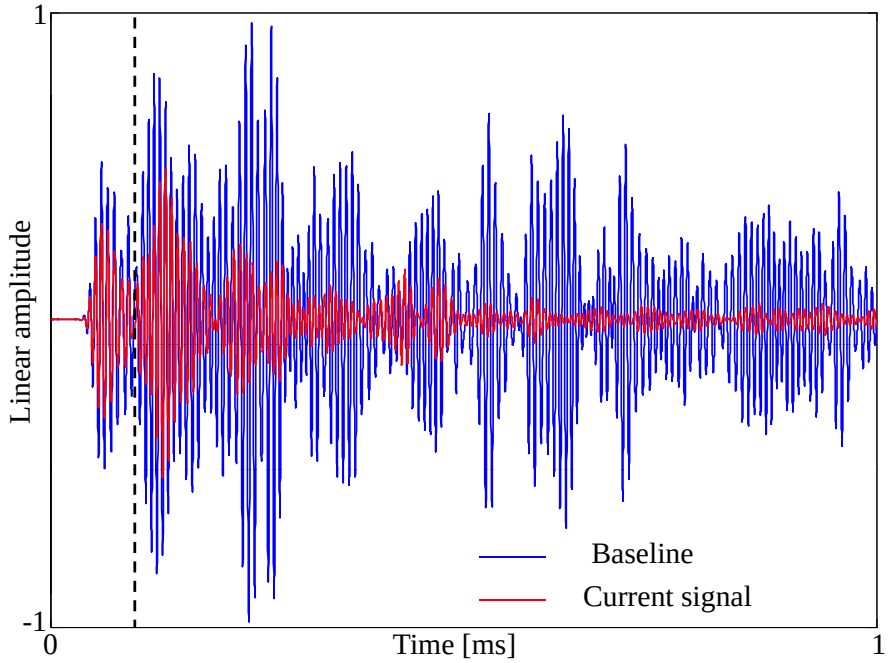

Figure 6.24: *Comparison of a current signal measured from the immersed plate with the reference signal recorded from the free plate at the same temperature. The dashed line represents the first arrival of the water surface reflection.*

interference between different wavepackets. By smoothing the original curve using a running average method it is possible to observe that the smoothed trend (solid black curve) shows a good agreement with the dispersion curve obtained with DISPERSE for the S_0 mode (dashed black line) in the part of the time trace immediately after the arrival time of the first pulse (area enclosed in the dashed rectangle of figure 6.25). For clarity a zoomed view of this area is shown in figure 6.26.

However, in the remaining part of the time trace the two trends are significantly different due to the fact that overlapping of multiple reflections is occurring. Since energy is coming back from the edges rather than propagating away as assumed in DISPERSE, the actual attenuation is lower than the attenuation predicted by DISPERSE for the S_0 mode. This issue prevents amplitude compensation from being efficiently applied to the entire time trace.

In order to verify the numerical results previously presented in section 6.6.2, only the first arrival due to the direct propagation of the S_0 mode from the transmitter

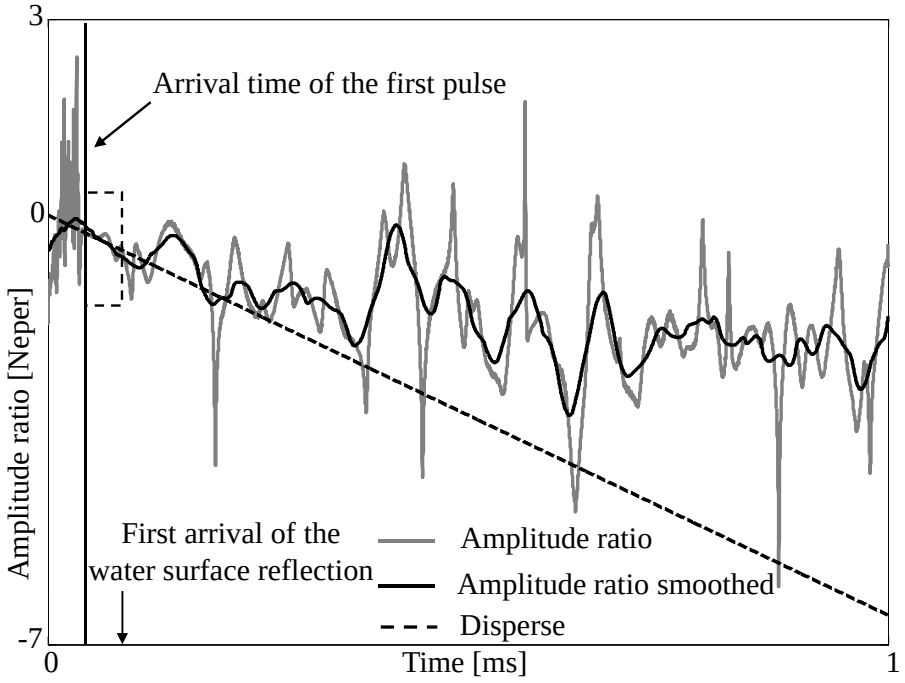

Figure 6.25: *Amplitude ratio between current signal measured from the immersed plate and baseline. Multiple reverberations are responsible for peaks and troughs in the actual trend. Running averages can be used to smooth the curve.*

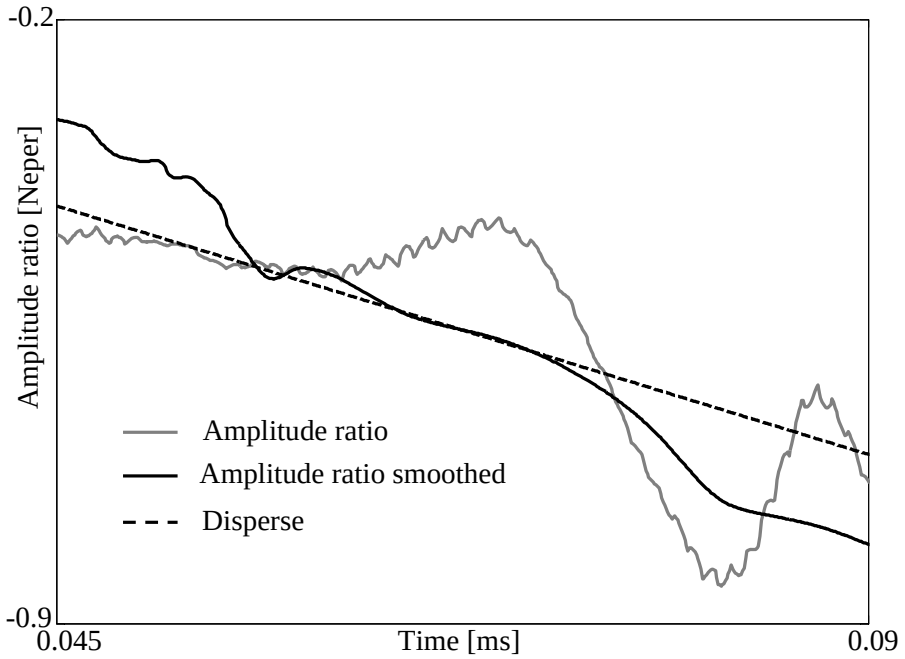

Figure 6.26: *Zoomed view of area enclosed in the dashed rectangle of figure 6.25.*

to the receiver will be considered. The first arrival in the time trace was chopped because reflections from the edge were received before whole first arrival was obtained. Amplitude compensation was applied to the first arrival using as reference signal the time trace recorded from the unloaded plate at the same temperature. Subsequently, Optimal Baseline and Optimal Stretch were applied to improve the result of the subtraction between the baseline and the amplitude compensated current signal. Figure 6.27 shows the performance of Optimal Baseline and Optimal Stretch in reducing the residual of the uncompensated subtraction of the reference signal from the current signal.

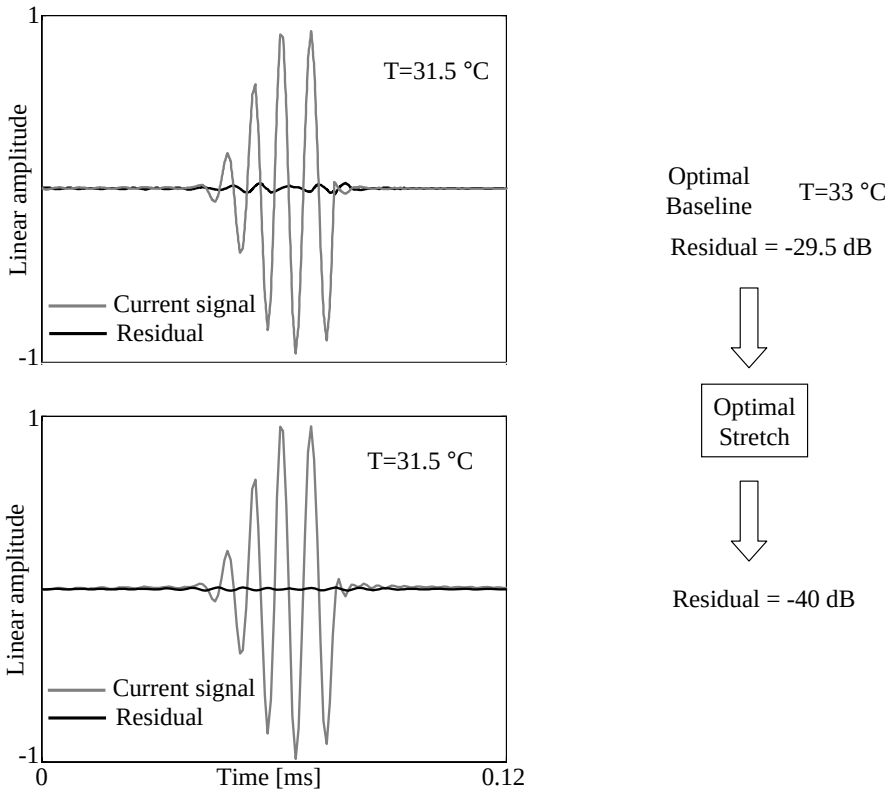

Figure 6.27: *Compensation of the subtraction for the S_0 mode. Performance of Optimal Baseline and Optimal Stretch in presence of an infinite water layer.*

The optimal baseline was found at the temperature of 33 °C, which was 1.6 °C higher than the temperature of the current signal. This result confirms the numerical prediction obtained with DISPERSE and presented in section 6.6, where the temperature of the optimal baseline was 1.5 °C higher than the temperature of the current signal measured in the bilayer. The maximum residual after application

of the Optimal Baseline method obtained in the experiment was -29.5 dB. After application of Optimal Stretch, the residual is further reduced to -40 dB.

6.10 Experiment with a thin uniform viscoelastic layer

For this experiment a plate identical to that one discussed for the experiment with the infinite water layer was used. The plate was instrumented with two piezoelectric transducers PCM51 and it was inspected in pitch-catch mode, in a configuration similar to that shown in figure 6.19. The input signal was a 5 cycle Hanning windowed toneburst, 150 kHz centre frequency. The acquisition of the baselines was done in the same way described in subsection 6.9.2 and the baselines were recorded with a temperature gap of 0.1 °C. In order to simulate a plate coated by a thin layer of viscoelastic material, a layer of uncured HEXCEL Redux 319®was placed on the free surface of the plate. Redux 319®is a supported epoxy film adhesive with a woven nylon carrier; the thickness of the adhesive layer is approximately 100 μm. Using epoxy film adhesive is convenient for keeping layer thickness constant.

Since film adhesives require high temperatures (150-250 °C) for the curing process, it was not possible to consider a similar test with a cured uniform layer of epoxy adhesive because the piezoelectric transducers would have been damaged by high temperatures. Therefore it would have been impossible to compare directly current signals (time traces obtained from the plate with cured epoxy adhesive) with baseline signals (time traces recorded from the unloaded plate).

Figure 6.28 shows a top view of the aluminium plate coated with the epoxy layer. The dotted circles represent the two transducers that were attached to the back surface of the plate.

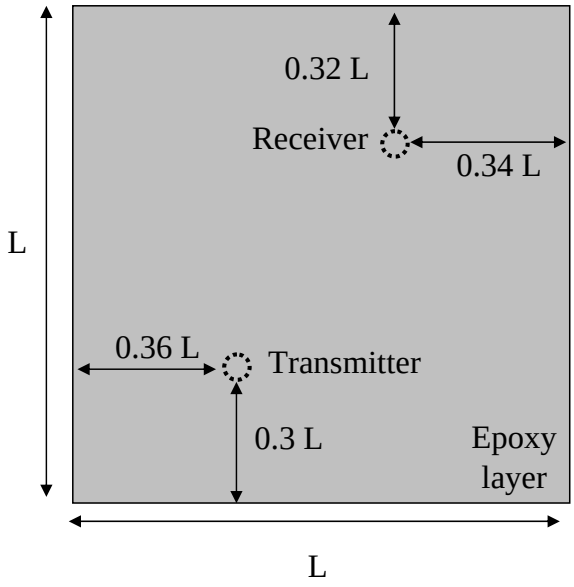

Figure 6.28: *Top view of the aluminium plate coated with a thin epoxy layer. The transducers (dotted circles) are bonded to the back surface of the plate.*

6.10.1 Results

Figure 6.29 shows a time trace recorded in the plate coated with the adhesive compared with a reference signal taken when the plate was in the oven at the same temperature. The current signal (measured in the plate coated with the adhesive) is attenuated compared to the reference signal (measured in the free plate). The attenuation expressed in nepers as a function of time has been obtained as in subsection 6.9.3 and is shown in figure 6.30. The first part of the trend before the arrival time of the first pulse corresponds to the ratio of the two parts of the original time traces where no signal is present. Since the uncured adhesive properties were unknown it was not possible to predict the attenuation trend in DISPERSE. The dashed black line shown in figure 6.30 only represents the best linear fit of the smoothed curve (solid black line).

The current signal was recorded at 28.4 °C and amplitude compensation is the first step required before applying the temperature compensation strategy. As was done in subsection 6.9.3 amplitude compensation was applied only to the first arrival. The amplitude of the current signal was compensated according to the method described

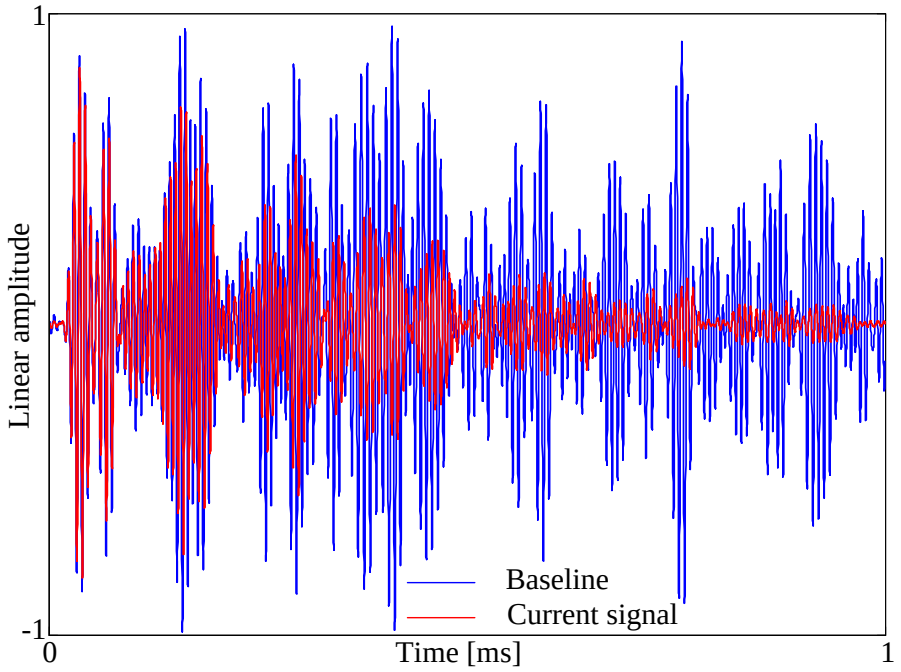

Figure 6.29: *Comparison of a current signal measured from the plate coated with a thin epoxy layer with the reference signal recorded from the free plate at the same temperature.*

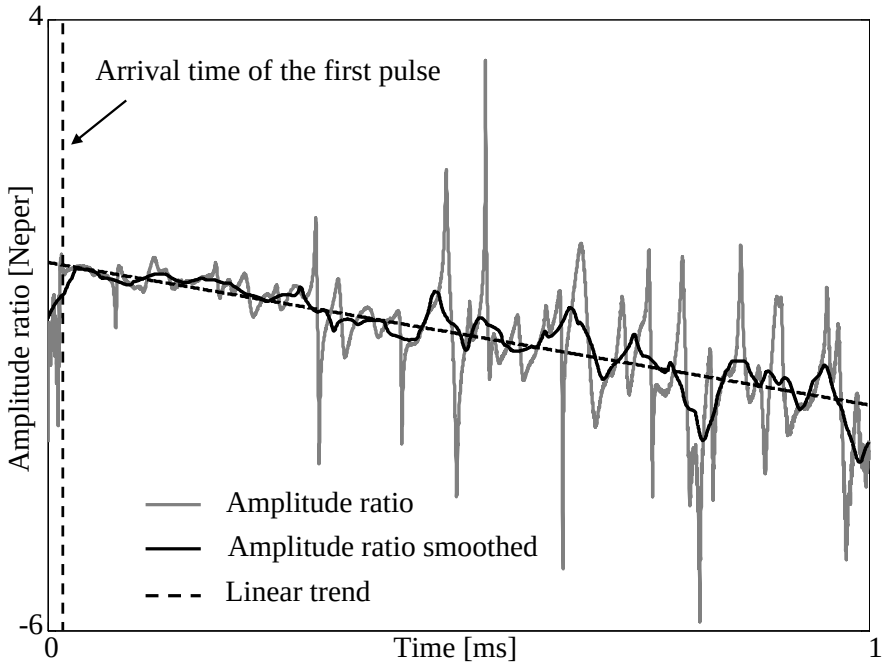

Figure 6.30: *Amplitude ratio between current signal measured from the plate coated with an epoxy layer and baseline. Multiple reverberations are responsible for peaks and troughs in the actual trend. Running averages can be used to smooth the curve.*

in section 6.6.1 using as reference signal the baseline obtained from the unloaded plate in the oven at the same temperature. Subsequently, the Optimal Baseline method was used to select the best matching baseline and Optimal Stretch was applied to further improve the result of the subtraction.

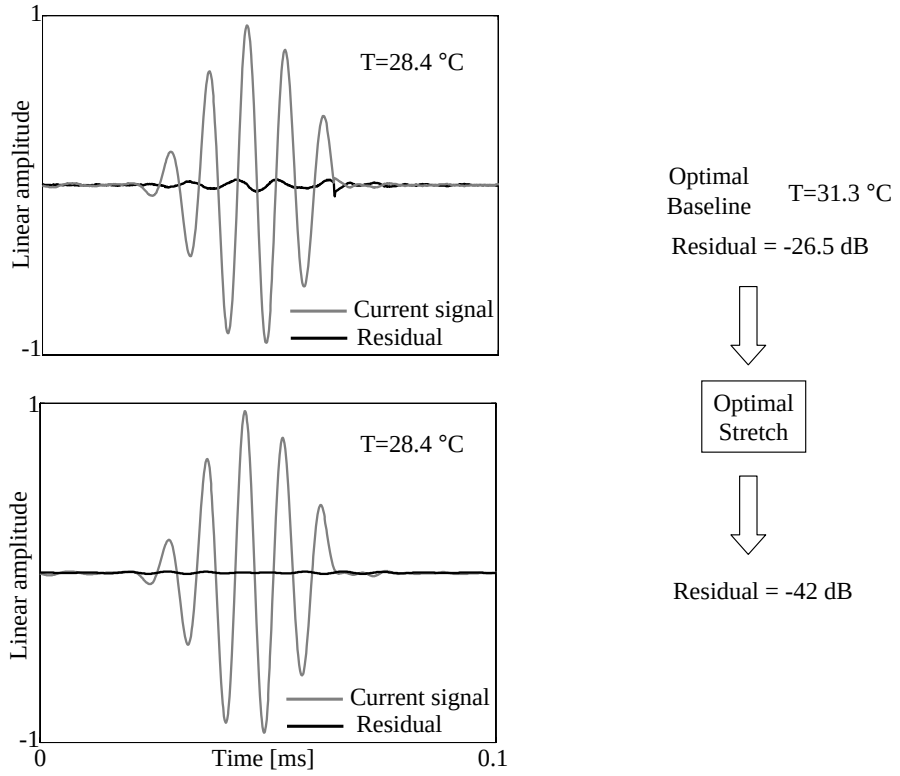

Figure 6.31: *Compensation of the subtraction for the S_0 mode. Performance of Optimal Baseline and Optimal Stretch in presence of a thin uniform epoxy layer.*

Figure 6.31 shows the results of the application of the temperature compensation strategy. After Optimal Baseline the residual level was -26.5 dB and the temperature of the best match was 31.3 °C (almost 3 °C higher than the temperature of the current signal). The residual level was further reduced to -42 dB by applying Optimal Stretch. Therefore, it was possible to achieve the target residual level in the subtraction by using Optimal Baseline and Optimal Stretch also in presence of a thin epoxy adhesive layer. However, it has to be stressed that this result was obtained with only the first arrival of the original time trace. In order to consider longer signals it is necessary to employ a different approach for amplitude compensation. A possible alternative method could rely on normalising the power content of the signals in the frequency domain.

6.11 Experiment with a non uniform viscoelastic layer

In order to study the performance of the compensation strategy with a non uniform epoxy layer, a square patch of the adhesive (side length 50 mm, equivalent to $0.17L$) was removed from the central area of the plate between the transducers. The patch of the adhesive removed is represented by the area enclosed in the dashed square of figure 6.32.

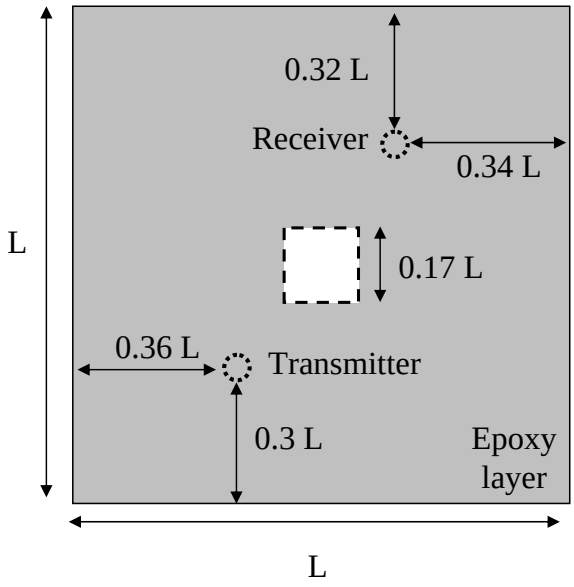

Figure 6.32: *Non uniform viscoelastic layer on an aluminium plate. The area enclosed in the dashed square represents the adhesive patch removed from the former uniform layer.*

The current signal obtained from the experimental setup after removing the patch of adhesive was recorded at 27.8 °C. Amplitude compensation was applied to the first arrival using as reference signal a time trace recorded from the unloaded at the same temperature. Subsequently Optimal Baseline and Optimal Stretch were applied. Figure 6.33 shows the performance of the compensation strategy. The Optimal Baseline was found at 29 °C and the maximum residual in the subtraction was -28 dB. The temperature difference between current signal and optimal baseline is 1.2 °C, whereas in the case of uniform epoxy layer it was almost 3 °C. This result is expected because from figure 6.32 it can be seen that removing the square patch

of adhesive in the area between the two transducers significantly reduces the area covered by epoxy encountered by the guided waves directly propagating from the transmitter to the receiver. Hence, the first arrival is less affected by the presence of the epoxy layer and, as result, the temperature of the optimal baseline is closer to the temperature of the current signal compared to the configuration of a uniform epoxy layer. After determining the optimal baseline, the maximum residual in the subtraction was further reduced to -38 dB (value very close to the target residual level), by using the Optimal Stretch method.

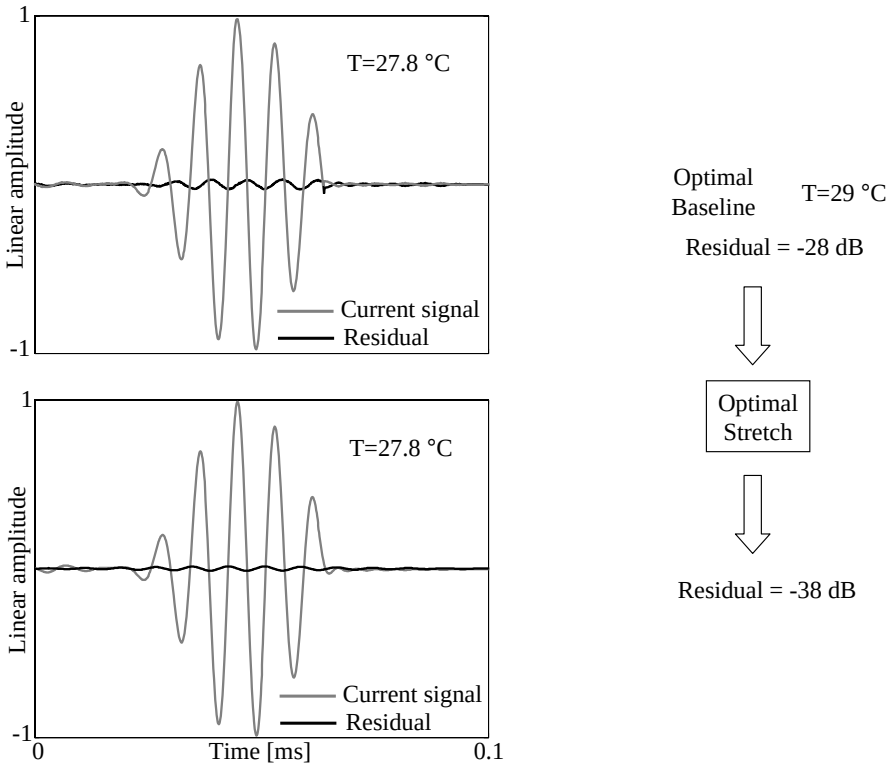

Figure 6.33: *Compensation of the subtraction for the S_0 mode. Performance of Optimal Baseline and Optimal Stretch in presence of a thin non uniform epoxy layer.*

6.12 Summary

This Chapter has investigated the possibility of employing Temperature Compensation techniques in presence of liquid loading on plates, in order to study whether methods developed for temperature compensation can also be used to compensate

for the presence of liquid loading. The effects of liquid loading have been compared with the effects of a 10 °C temperature change. Subsequently, Temperature Compensation techniques have been applied in numerical simulations for the fundamental S_0 and A_0 modes. The residual in the subtraction for the S_0 mode propagating in an aluminium water bilayer ($\tau = 0.01$) is negligible compared to the residual observed in the uncompensated subtraction for a 10 °C temperature change. The presence of a thin epoxy layer is responsible for a higher residual in the subtraction, both for the S_0 and A_0 modes. However, numerical simulations show that the compensation strategy based on the combined use of Optimal Baseline and Optimal Stretch was able to achieve the target residual level of -40 dB for the subtraction both in the presence of a thin and of an infinite water layer and in the presence of a thin viscoelastic layer, represented by a uniform thin layer of not cured epoxy adhesive.

Experiments have been conducted to evaluate the subtraction performance in real structures in presence of liquid loading. Tests were carried out for an aluminium plate bordered by an infinite water layer and for an aluminium plate coated with a thin layer of epoxy. In both series of experiments, a compensation strategy based on the combined use of Optimal Baseline and Optimal Stretch was used. The temperature of the optimal baseline was in both cases only a few degrees different from the temperature of the current signal. More importantly, the target residual level was achieved, confirming that temperature compensation techniques can be applied in principle also for the compensation of detrimental effects different from temperature variations. The situation of a non uniform epoxy layer was also considered and an experiment was conducted after removing a square patch of adhesive from the original uniform epoxy layer. Although Optimal Stretch has not been specifically designed for being applied to signals recorded in structures with non uniform temperature coefficient, a maximum residual very close to the target level was obtained.

Chapter 7

Effects of different temperature responses in adhesive joints on Subtraction approach

7.1 Background

Adhesive joints are extensively used in the aerospace industry and represent a crucial element for the structural integrity of an aircraft [126]. Several advantages derive from the use of adhesive joints compared to other fastening techniques. For instance an adhesive bond ensures a weight reduction in the bonded structure, with respect to mechanical fastening methods. The application of adhesive joints in several industrial fields has been continuously growing in parallel with the development of new polymers and basically all the structural adhesives used in the last few decades are polymer based [127].

There are three main components in the typical structure of an adhesive joint, represented by the adherends and the epoxy adhesive that is the bonding element of the structure. The adhesive is applied in the form of a thin viscoelastic layer in order to create an intimate contact with both the substrates [127]. Subsequently the bond

is cured and after the curing process, the epoxy becomes capable of withstanding the loads imposed by the structure [128]. The adhesive layer in aerospace applications is typically of the order of 100 $\mu\, m$ thick.

The adhesive layer has different temperature coefficients compared to the material of the adherends joined in the bond (e.g. thermal expansion, Young's modulus dependence on temperature). Therefore environmental changes, such as temperature variations will affect the adherends and the adhesive layer differently and this issue can be detrimental for the performance of the Subtraction approach applied to signals recorded from structures where materials with different temperature responses are present. In this Chapter our aim is to evaluate the performance of the Subtraction approach when temperature coefficients are not uniform over the structure under inspection. Specifically, the performance of the temperature compensation strategy already presented in the Chapters 5 and 6 will be evaluated both on numerical simulations and experiments. This study is important for specifying the applicability of the subtraction approach in configurations that can be considered representative of typical aircraft structures.

7.2 Different temperature responses of materials and Temperature Compensation techniques

The mechanical properties of the epoxy layer in an adhesive joint can be significantly different from the properties of the adherends, due to their different nature. For instance, the thermal expansion coefficient for aluminium is approximately $23 \cdot 10^{-6} K^{-1}$, whereas the corresponding coefficient for epoxy is typically in the range $40 - 60 \cdot 10^{-6} K^{-1}$ [129]. Therefore the adhesive in a bond will be much more affected than the adherends by the same temperature change. This issue is crucial for a reliable application of the temperature compensation strategy already considered in this work.

The Optimal Baseline method is not affected in principle by this issue since the

strategy behind this method is based on recording baselines at all the possible operating temperatures of the structure. Nevertheless, it is desirable to reduce the size of the database by increasing the temperature step between baselines and using the Optimal Stretch technique to effectively interpolate between the available baselines (Chapter 5). However, the Optimal Stretch technique implicitly assumes uniform temperature coefficients of modulus and expansion over the structure. Therefore the performance of the Optimal Stretch method in structures comprising materials with different temperature responses needs to be evaluated. Numerical FE simulations and experimental work were carried out to estimate the maximum temperature variation that Optimal Stretch can compensate, achieving the target residual level of -40 dB required for reliable applications of the subtraction approach. This evaluation is crucial for understanding the real effectiveness of the subtraction approach in structures where materials with different temperature responses are present.

7.3 Experimental setup and 3D FE model

7.3.1 Experimental setup

The experimental setup consisted of a 300 mm long L-shaped stringer bonded in the middle of a 900 × 300 × 5 mm aluminium plate by a thin layer of HEXCEL Redux 319®. This is a supported epoxy film adhesive with a woven nylon carrier to ensure reliable thickness control; the thickness of the adhesive layer is approximately 100 μm. Before the bond was created, the surfaces of the adherends were cleaned with acetone [130]. The adhesive layer was placed between the plate and the shortest side of the stringer. Figure 7.1 shows a view of the experimental setup zoomed around the region of the joint (the dimensions of the stringer are indicated).

In order to create the bond, a steel bar was placed on top of the area of the bond and the stringer was clamped to the plate using two G-clamps, one placed at each end of the stringer and the structure was then placed in an oven. The adhesive was cured at 180 °C for one hour, as required by the technical specifications of

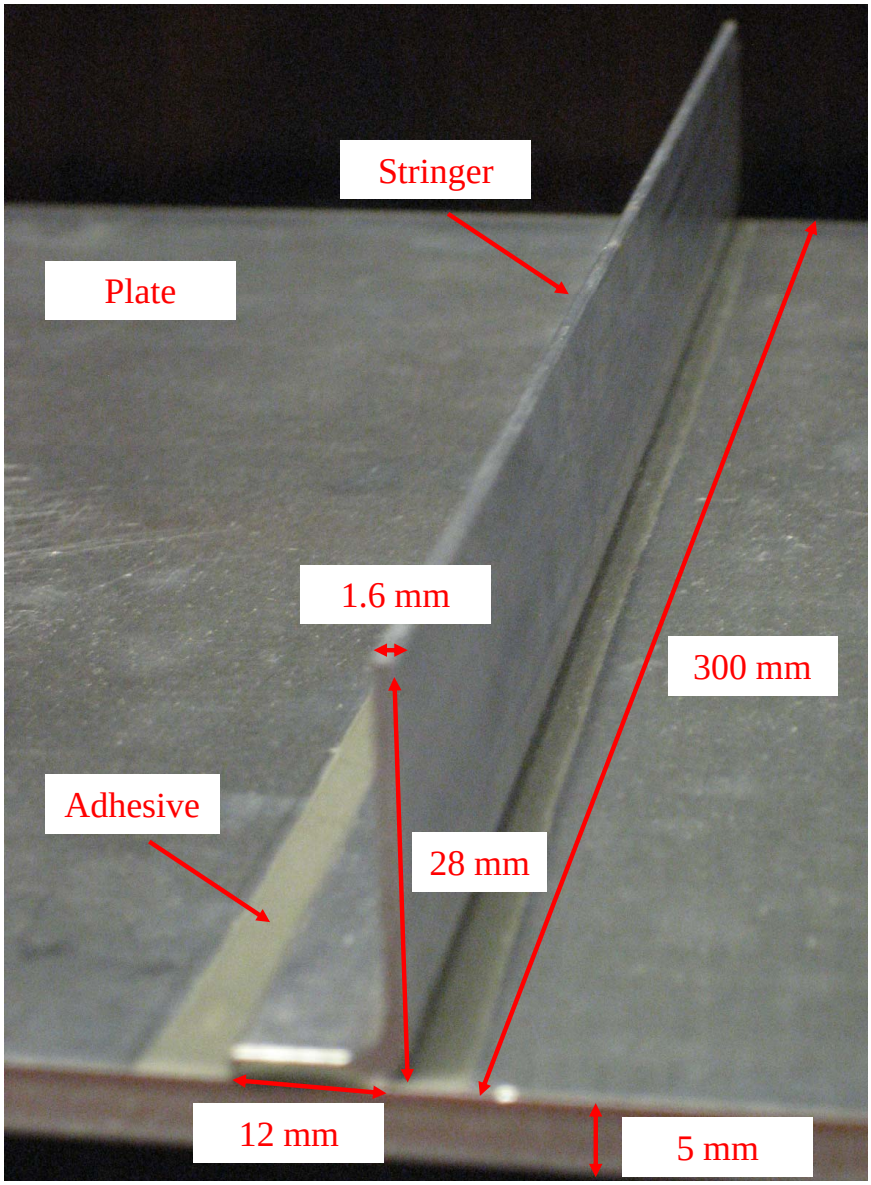

Figure 7.1: *Detailed view of the adhesive joint in the experimental setup.*

the adhesive. After the curing process, the G-clamps were removed and the setup was left to cool until it reached room temperature. Subsequently, two piezoceramic PCM51 disc transducers for the excitation of the S_0 mode were bonded to the plate and operated in pitch-catch mode, as shown in figure 7.2.

The input signal was a 5 cycle Hanning windowed toneburst, 150 kHz centre frequency. Two thermocouples were connected to the plate close to the transducers in order to continuously monitor the temperature during the acquisition of the signals.

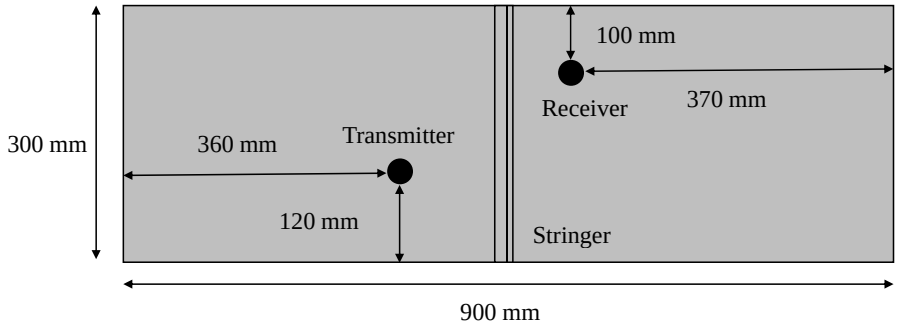

Figure 7.2: *Top view of the plate with bonded stringer. The transducers are operated in pitch-catch mode.*

7.3.2 3D FE model

A 3D FE model of the experimental setup has been designed in ABAQUS to simulate a stringer bonded by a 100 μm thick epoxy layer to a 900 $\times$ 300 $\times$ 5 mm aluminium plate. The model has been meshed with C3D8R elements from the ABAQUS element library [131]. For the propagation of the S_0 mode, a pointlike source, located at the same position as the transmitter in the experimental setup, was simulated by applying radial forces to 8 nodes symmetrically placed on a circle of the same diameter as the transducers used in the experimental setup. In this way approximately axisymmetric waves propagating outward in all directions were obtained [132]. The received signal was monitored at the same location as in the experimental tests and the in-plane displacements were combined to reconstruct the total in-plane displacement field of the propagating S_0 mode at the position where the receiver is located in the experimental setup. Numerical simulations were carried out to estimate the maximum temperature difference that could be compensated by Optimal Stretch. The monitoring time was 1 ms that at the excitation frequency of 150 kHz corresponds to approximately 5.3 m propagation distance for the S_0 mode in the plate. The results of the numerical simulations are summarized in section 7.4.

7.4 Results of numerical simulations

In order to evaluate the performance of Optimal Stretch in presence of materials with non uniform temperature responses, it was assumed that the Young's modulus of the epoxy decreased linearly at a rate of 1%/°C. This is at the top end of the variation seen in practice [133]. Subsequently, time traces were simulated at 20°C and upwards in 0.5 °C steps. The mechanical properties of plate and stringer were set to the corresponding values for the temperatures considered (section 6.5) and the Young's modulus of the epoxy has been reduced according to the linear approximation previously described; the Poisson's ratio of epoxy was assumed constant at 0.392. The signal at 20 °C was then taken as the baseline and the signals at higher temperatures were taken in turn as the current signal. The Optimal Stretch technique was then applied and the amplitude of the residual evaluated. Figure 7.3 shows the performance of Optimal Stretch for 2 °C temperature difference between baseline and current signal.

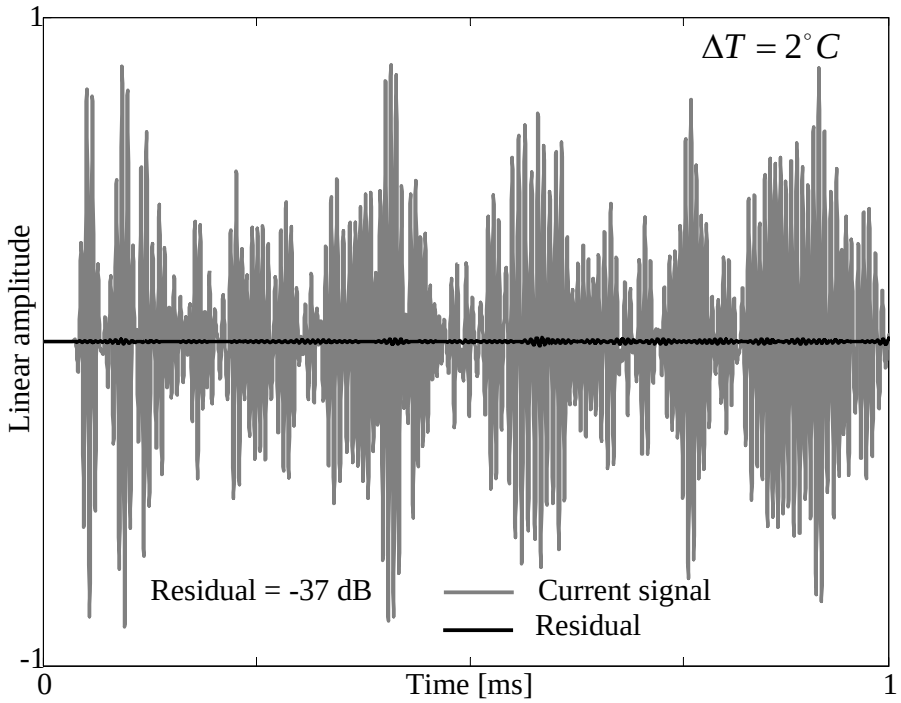

Figure 7.3: *Compensation by Optimal Stretch for the 3D FE model. Optimal Stretch can compensate for 2 °C temperature change, achieving a maximum residual level of -37 dB.*

The amplitude of the subtracted signal on a dB scale is shown in figure 7.4 (solid

grey line) where it is compared with the residual obtained for 1.5 and 3 °C temperature difference (solid black line and dashed black line, respectively). It can be

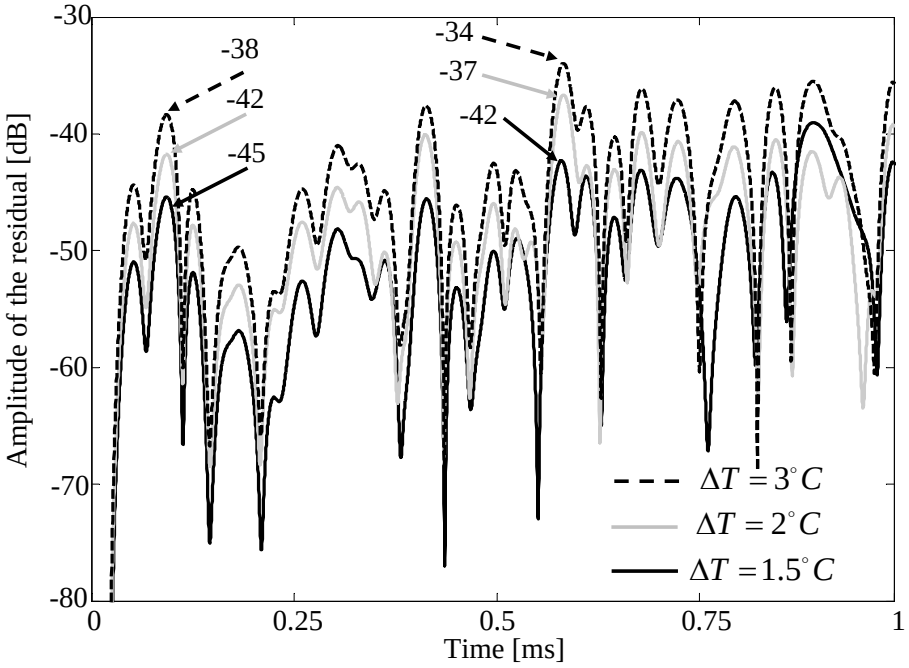

Figure 7.4: *Compensation by Optimal Stretch for the 3D FE model. In the presence of 1.5 °C temperature change, the maximum residual is always lower than -40 dB. Optimal Stretch can compensate for 2 °C temperature change, achieving a residual level of -37 dB.*

.

seen that the Optimal Stretch method is able to achieve the target residual level up to 1 ms (approximately 5.3 m propagation distance) for 1.5 °C temperature difference between current signal and baseline. The maximum residual in the subtraction for a 2 °C temperature difference is -37 dB and it was obtained at 0.6 ms, which corresponds to approximately 3.2 m propagation distance. Note that for 3 °C temperature difference the maximum residual level is already higher than the target residual level for the first arrival. The performance of Optimal Stretch was also tested on a FE model of a free plate with transmitter and receiver located as in the model of the plate with a bonded stringer. Considering the results obtained in the FE model of the bonded stringer, numerical simulations for the free plate were run starting with a temperature gap of 3 °C and upwards in 0.5 °C steps. Figure 7.5 shows the maximum residual up to 1 ms as function of the temperature difference, ΔT, between baseline and current signal for the plate with the bonded stringer and

the free plate. The maximum residual is increasing with the temperature gap and for the plate with bonded stringer the maximum residual is -34 dB in presence of a 3 °C temperature difference. For the free plate the target residual level was achieved up to 1 ms for 4 °C temperature change. Note that for the free plate the target residual level can be achieved for higher temperature gaps than for the plate with the bonded stringer. The marked points in the graph represent the values obtained in the numerical simulations; the two curves shown are only indicative of the trend of the maximum residual as function of the temperature gap between baseline and current signal. However, the maximum residual obtained is strongly dependent on the interference between different wave packets and, for this reason, the trends are not expected to be smooth.

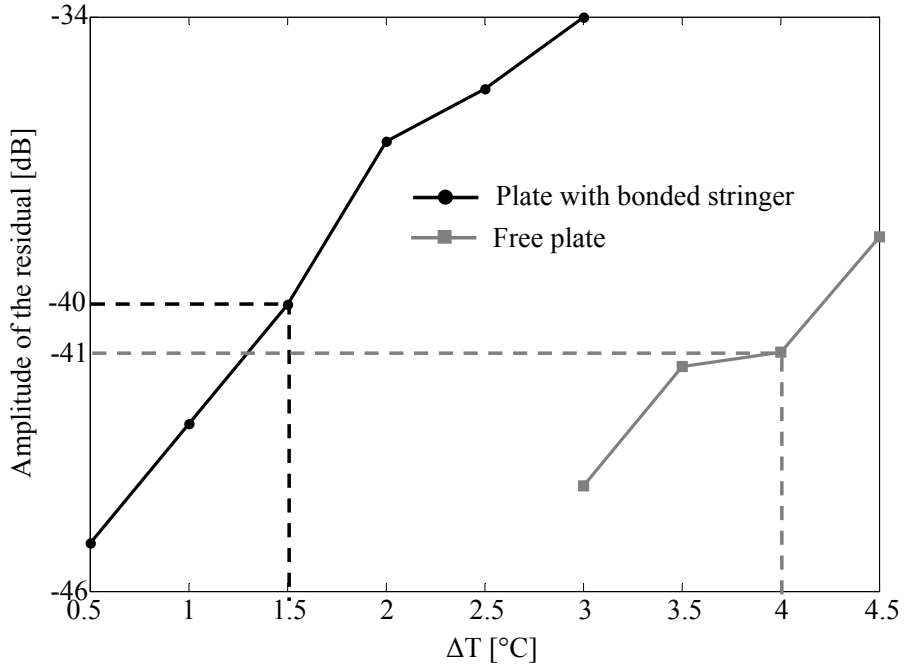

Figure 7.5: *Amplitude of the residual as function of the temperature difference between baseline and current signal for the FE model of a free plate and the FE model of a plate with bonded stringer.*

7.5 Preliminary experiments: performance of Optimal Stretch method

7.5.1 Optimal Stretch performance

The first series of measurements was conducted the day after the stringer was bonded to the parent plate. The acquisition of the signals was carried out for approximately 10 hours in a room where the temperature was varying in the range 14-16 °C. The temperature differences between baselines was never greater than 0.2 °C. The signal at lowest temperature was assumed as a baseline and signals at higher temperatures recorded in the same dataset were taken in turn as the current signal. Figure 7.6 shows that for 0.5 °C temperature difference between baseline and current signal, Optimal Stretch achieves a maximum residual of -36 dB, already higher than the target residual level.

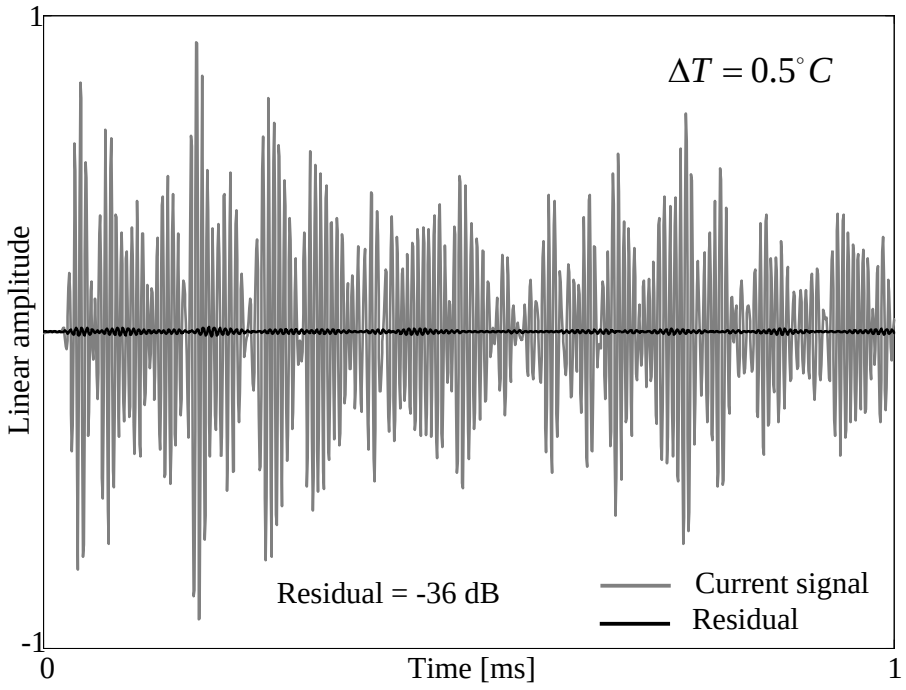

Figure 7.6: *Compensation by Optimal Stretch for the first series of experiments with the bonded stringer. Optimal Stretch can compensate for 0.5 °C temperature change, achieving a maximum residual level of -36 dB.*

This performance is not very satisfactory, considering that in the numerical simulations Optimal Stretch was able to compensate for a higher temperature difference between current signal and baseline. A possible explanation for this result is that irreversible changes in the structure were still occurring due to modifications in the adhesive layer during the acquisition of the time traces. Since the measurements were carried out only one day after the stringer was bonded to the plate, it is possible that changes in the structure of the adhesive bond were happening as result of the post-curing modifications in the structure of the epoxy.

In order to evaluate the best result achievable by Optimal Stretch in this geometry, the performance of Optimal Stretch was evaluated on a free aluminium plate (900 $\times$ 300 $\times$ 5 mm) identical to that one just discussed with two transducers placed in the same locations as shown in figure 7.2. Hence the performance of Optimal Stretch in the presence of materials with non uniform temperature responses can be directly compared with the performance obtained in the same plate geometry and transducers separation, but with uniform temperature response over the structure. The acquisition of the baselines from the free plate and the procedure for determining the Optimal Stretch performance were carried out as for the plate with a bonded stringer. Figure 7.7 shows the performance of the Optimal Stretch method on the free plate for a 2 °C temperature difference between the current signal and the baseline. The maximum residual level was -41 dB. The amplitude of the residual level on a dB scale is shown in figure 7.8 and it can be seen that the target residual level is achieved for all the time trace when the temperature gap is 2 °C. A maximum residual of -38 dB, very close to the target residual level, was achieved even when the temperature difference between the baseline and the current signal was 2.5 °C. These results can be considered as the highest performance achievable by the Optimal Stretch in this configuration, since it was obtained in a similar geometry and environmental conditions as in the experiment with the bonded stringer, but with only one material in the structure. Figure 7.9 shows the maximum amplitude of the residual up to 1 ms as function of the temperature difference between reference and current signal for the plate with bonded stringer and the free plate in the range 0.5-2 °C. The Optimal Stretch performance is significantly better for the free plate, the

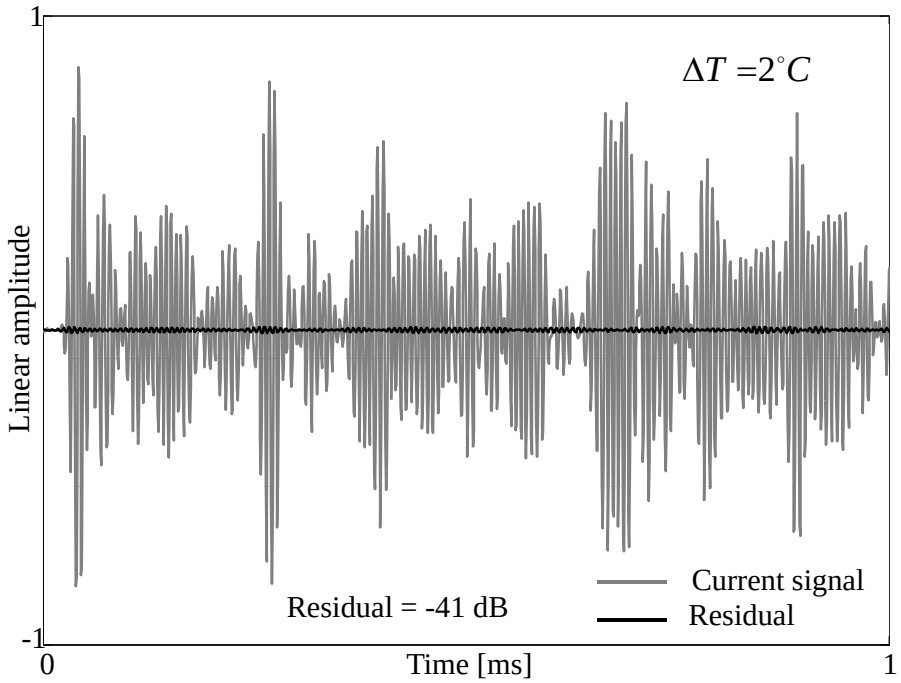

Figure 7.7: *Compensation by Optimal Stretch for the first series of experiments with the free plate. Optimal Stretch can compensate for 2 °C temperature change, achieving the target residual level.*

difference between the two trends being -20 dB for a 2 °C temperature difference.

7.5.2 Optimal Baseline performance

Evaluating the performance of Optimal Baseline, although not directly affected by the presence of materials with different temperature coefficients, is important for assessing the robustness of the Subtraction approach and is helpful for gaining an insight regarding irreversible changes occurring in the experimental setup described in section 7.3.1, due to modifications happening in the adhesive. The performance of the Optimal Baseline method was evaluated assuming as current signal a time trace recorded from the experimental setup at 15 °C, whereas the reference signals were represented by the time traces recorded in a previous dataset with temperatures in the range 14-16 °C. The temperature gap between baselines was never greater than 0.2 °C. Figure 7.10 shows the performance achieved by the Optimal Baseline method. The optimal baseline was found at the same temperature as the current signal and

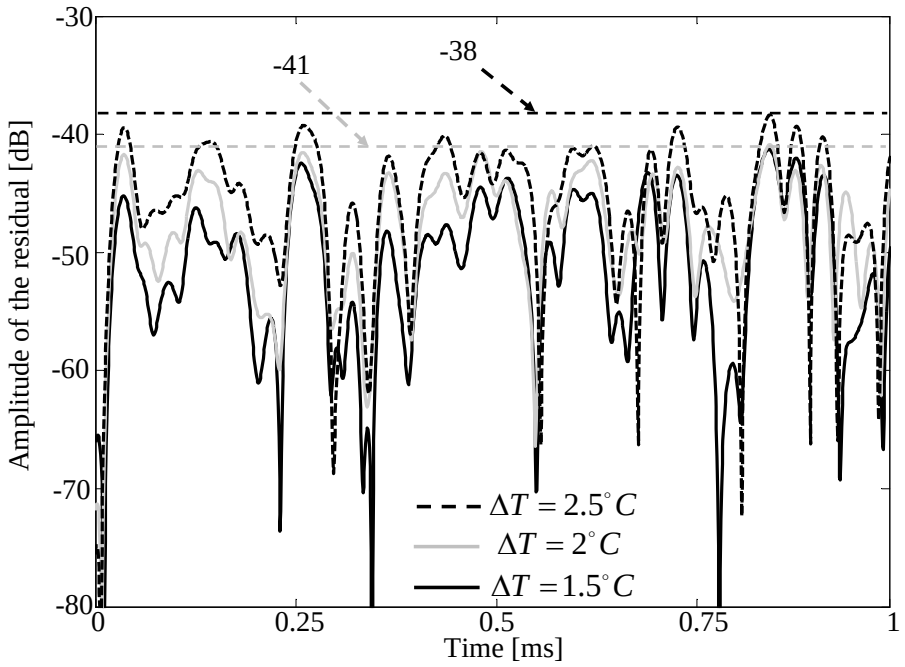

Figure 7.8: *Maximum residual in the subtraction as function of the temperature difference between baseline and current signal for the free plate. Optimal Stretch can compensate for 2 °C temperature variation, achieving the target residual level.*

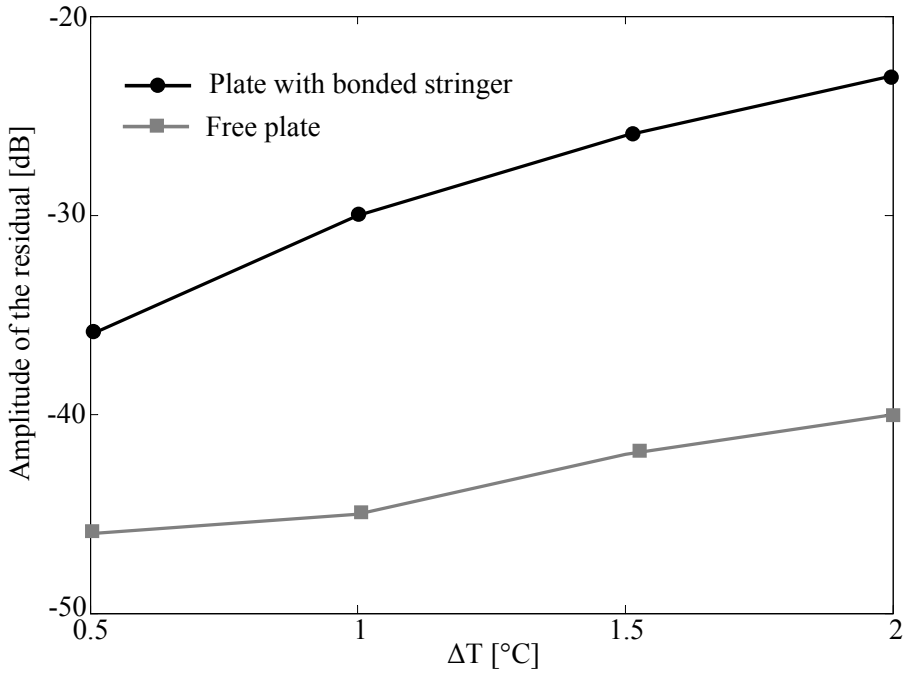

Figure 7.9: *Amplitude of the residual as function of the temperature difference between baseline and current signal for the free plate and the plate with bonded stringer.*

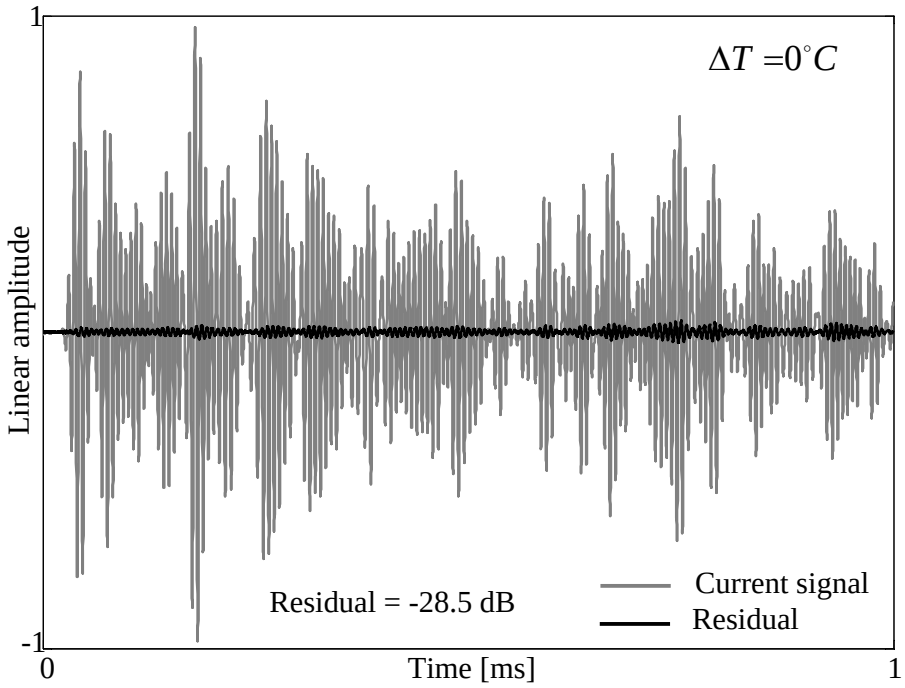

Figure 7.10: *Compensation by Optimal Baseline for experiment with the bonded stringer. Optimal Baseline can achieve a maximum residual of -28.5 dB. The temperature of the baseline and current signals was 15 °C.*

a maximum residual of - 28.5 dB was achieved in the subtraction. This performance is lower than that achieved by Optimal Baseline in a more complex structure with adhesive bonded stringers [103], inspected after irreversible changes had stopped. This shows that the performance of Temperature Compensation techniques shown in this section might be negatively affected by changes still occurring in the structure. The effects of these changes should decrease with time, as will be shown later.

7.6 Second series of experiments on the bonded stringer

In order to verify whether the performance of Temperature Compensation techniques was improving with time a second series of measurements was carried one month after the first series. The results are shown next for Optimal Stretch and Optimal Baseline, respectively.

7.6.1 Optimal Stretch performance

The acquisition of the signals was carried out in the same room where the first series of measurements was taken, but on this occasion the temperature was varying in the range 8-10 °C. Two datasets of time traces were recorded on two different days and the temperature difference between baselines was never greater than 0.1 °C for both datasets. The signal at the lowest temperature of the first dataset was used as the reference signal and the time traces of the second dataset were taken in turn as the current signal. The Optimal Stretch method was able to achieve a maximum residual level of -41 dB up to 1 ms in the presence of a 1 °C temperature change. The performance of Optimal Stretch in compensating for 1.5 °C temperature change was -38 dB, very close to the target residual level. This result is shown in figure 7.11. Figure 7.12 shows the amplitude of the residual on a dB scale relative to

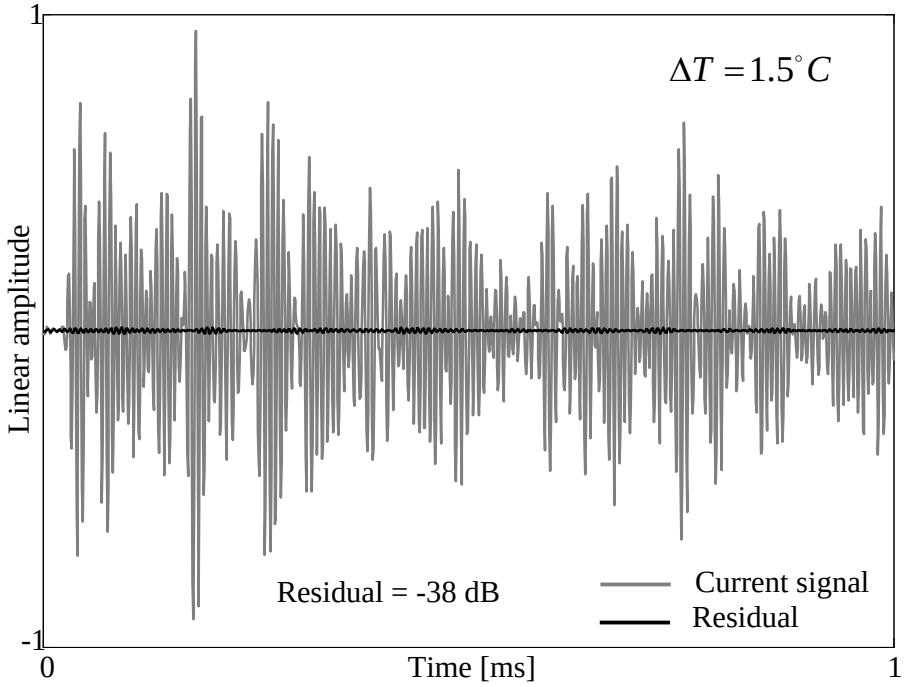

Figure 7.11: *Compensation by Optimal Stretch for the second series of experiments with the bonded stringer. Optimal Stretch can compensate for 1.5 °C temperature change, achieving a residual level of -38 dB.*

the amplitude of the first arrival for the cases of 1 °C and 1.5 °C temperature change. It is important to notice that the target residual level has been achieved over the

entire duration of the time trace in the presence of 1 °C temperature change; this is equivalent to a propagation distance of approximately 5.3 m. Hence this result is comparable with the performance obtained in the FE simulations in the presence of a 1.5 °C temperature change. In presence of 1.5 °C temperature change a maximum

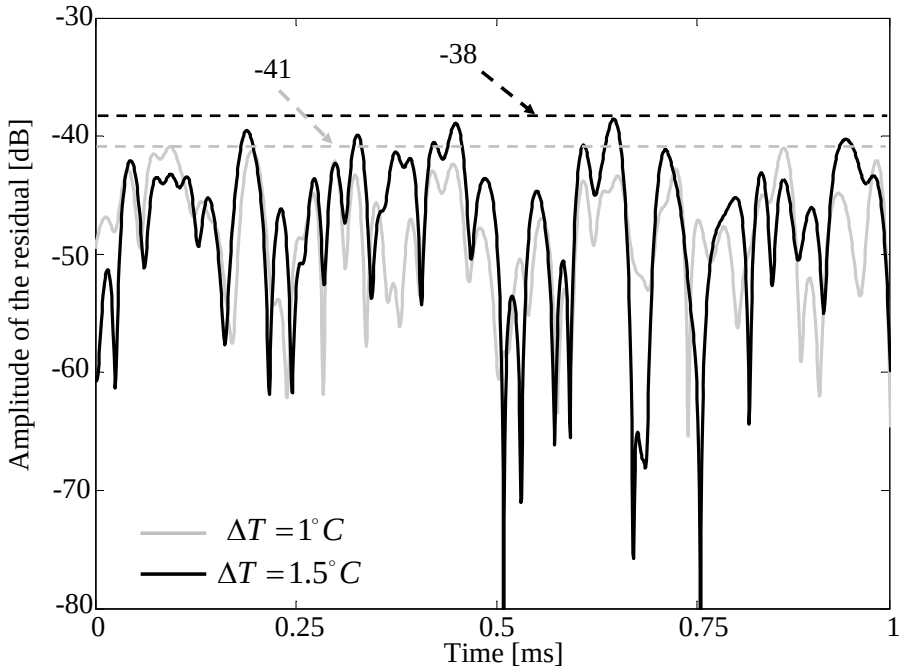

Figure 7.12: *Amplitude of the subtracted signal on a dB scale relative to the amplitude of the first arrival for the plate with bonded stringer. Optimal Stretch is able to achieve a residual level of -41 dB for the entire time trace in the presence of 1 °C temperature change. A maximum residual close to the target is achieved for 1.5 °C temperature change.*

residual of -38 dB, very close to the target residual level, was achieved over the entire length of the time trace.

The experimental results shown in this section represent a significant improvement compared to the results obtained in the first series of experiments, when in the presence of only 0.5 °C temperature difference the maximum residual achievable by Optimal Stretch was only -36 dB. Furthermore, it has been verified that the experimental performance of Optimal Stretch in the presence of a 1.5 °C temperature change is comparable with the result obtained in FE simulations when a 2 °C temperature difference between baseline and current signal and a 2 % reduction in the Young's modulus of the epoxy were considered.

7.6.2 Optimal Baseline performance

In this test the signals recorded during the first day of measurements were used as baselines and one of the signals of the second day was used as a current signal. As in the previous series of experiments, the temperature of the optimal baseline was found at the same temperature as the current signal. The maximum residual was -37 dB, which is 8.5 dB lower than the result obtained in the first series of experiments. This result represents a significant improvement of the performance of the Optimal Baseline method and it suggests that the effects of post-curing modifications in the adhesive were significantly reduced.

7.7 Temperature compensation strategy and damage detection [1]

Temperature Compensation techniques have performed well even in the presence of different temperature responses of materials over the structure under inspection. It is important to evaluate the response of the compensation strategy based on the combined use of Optimal Baseline and Optimal Stretch to a simulated defect. Specifically, it has to be verified that the modifications introduced by the presence of a defect are not removed by the compensation strategy. This is crucial to make it possible to detect defects in structures with non uniform temperature response. Considering the experimental setup of the aluminium plate with the bonded stringer, experiments were conducted to compare the performance of the compensation strategy in the presence of a simulated defect with the performance in the undamaged structure.

[1] The tests in section 7.7 were done in collaboration with Thomas Clarke of the NDT group, Imperial College London.

7.7.1 Compensation strategy performance: undamaged structure

In order to evaluate the performance of the temperature compensation strategy in the undamaged structure, the experimental setup was inspected in pitch-catch mode as described in section 7.3.1. In order to simulate a typical SHM inspection, the structure was monitored continuously for two days for the acquisition of the baselines and the time traces were recorded automatically every 20 minutes. The maximum temperature difference between the reference signals was never greater than 0.5 °C. Subsequently, another set of time traces was recorded over a period of one day in order to obtain a set of current signals. The Optimal Baseline method was used to select the best matching time traces from the set of the available baselines. Subsequently, Optimal Stretch was applied in order to further reduce the residual in the subtraction between the current signal and the optimal baseline. Figure 7.13 shows the compensation strategy performance for the undamaged structure. A maximum residual of -55 dB was achieved.

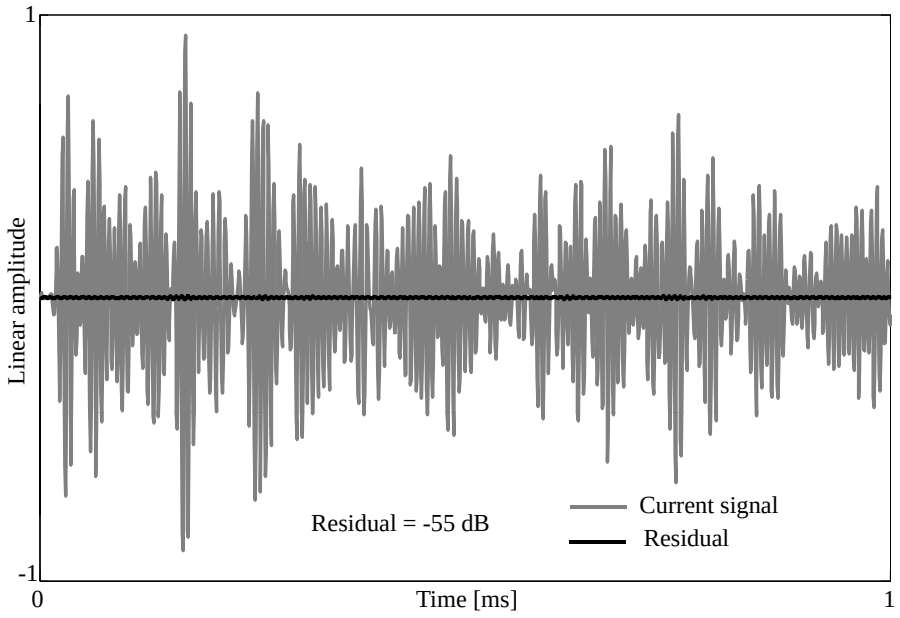

Figure 7.13: *Performance of the compensation strategy for the undamaged structure. A maximum residual of -55 dB was achieved.*

7.7.2 Compensation strategy performance: damaged structure

Before an artificial defect was introduced, a second pair of transducers were bonded to the structure, in order to consider more transmitter-receiver combinations. Subsequently, the presence of a defect in the structure was simulated by drilling a small circular hole in the region of the bond. Figure 7.14 shows the positions of the 4 transducers used in the experiment and the position of the drilled hole in the structure. The second pair of sensors is represented by the transducers 3 and 4.

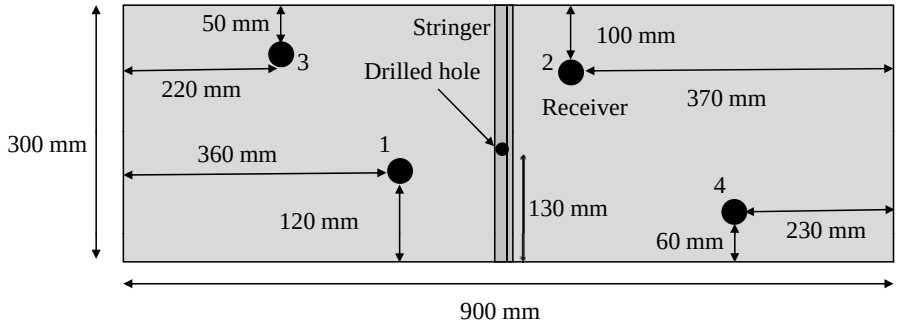

Figure 7.14: *Drilled hole in the region of the bond, simulating an artificial defect. The hole is placed at 130 mm from the bottom side of the plate.*

The initial diameter of the hole was 1 mm. Subsequently the diameter was increased to 3.5 and 5 mm. For each diameter of the hole, time traces were recorded in order to evaluate the performance of the compensation strategy as the size of the simulated defect was increased. The time traces recorded in the undamaged structure were used as a set of baselines and the Optimal Baseline was used to select the best matching signal, as previously done in subsection 7.7.1. Optimal Stretch was then used to improve the result of the subtraction between current signal and baseline and the performance of the subtraction approach was evaluated for the values of the hole diameter previously indicated. Figure 7.15 shows the performance of the compensation strategy in the damaged structure when diameter of the drilled hole was 5 mm and the inspection was carried out using the transducers pair 1-2. The maximum residual was -25 dB, significantly higher than the corresponding value obtained in the undamaged structure.

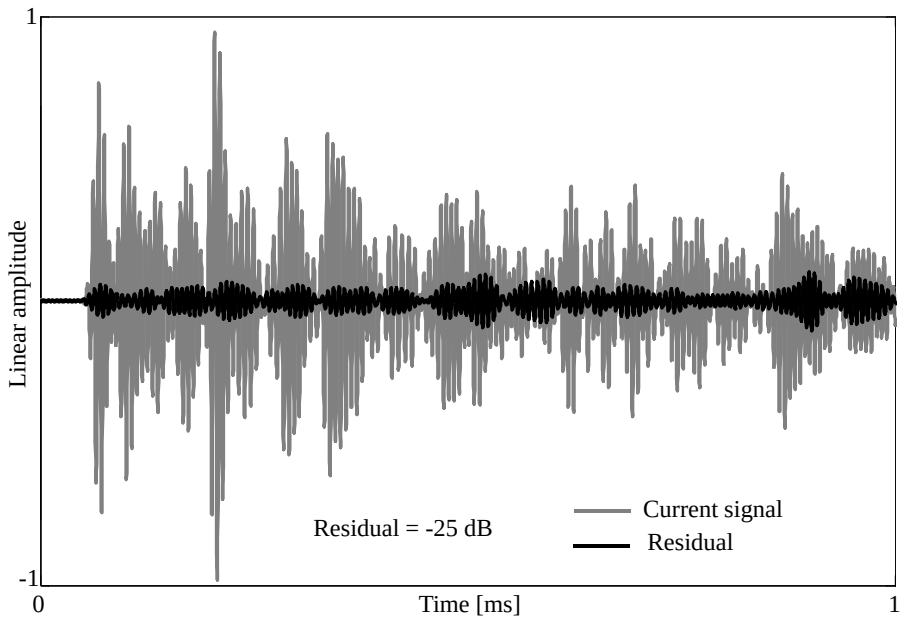

Figure 7.15: *Performance of the compensation strategy for the damaged structure with a 5 mm diameter drilled hole.*

Figure 7.16 shows the amplitude of the residual in the subtraction for the transducers pair 1-2. The residual in the subtraction for each value of the hole diameter is compared on a dB scale with the residual obtained when the structure was undamaged.

It can be seen that the presence of the hole is responsible for an increase in the residual level at the arrival time corresponding to the expected arrival of the first reflection from the defect. For instance, the presence of the 1 mm diameter hole is responsible for a residual level that at the expected arrival time of the first reflection from the hole is approximately 8 dB higher than the corresponding value for the undamaged structure. Furthermore, as the diameter of the hole is increased, the reflection coming from the hole increases as well and this leads to high amplitude of the subtracted signal. This is also observed in later parts of the time traces as a result of the shadowing effects caused by the presence of the defect [103]. The presence of the defect is responsible for alterations in the interference patterns between the reflections from the edges of the plate and the reflections from the stringer and therefore for an increased residual level in the subtraction also in the later part of the time traces when the signal measured in the defective structure is compared with

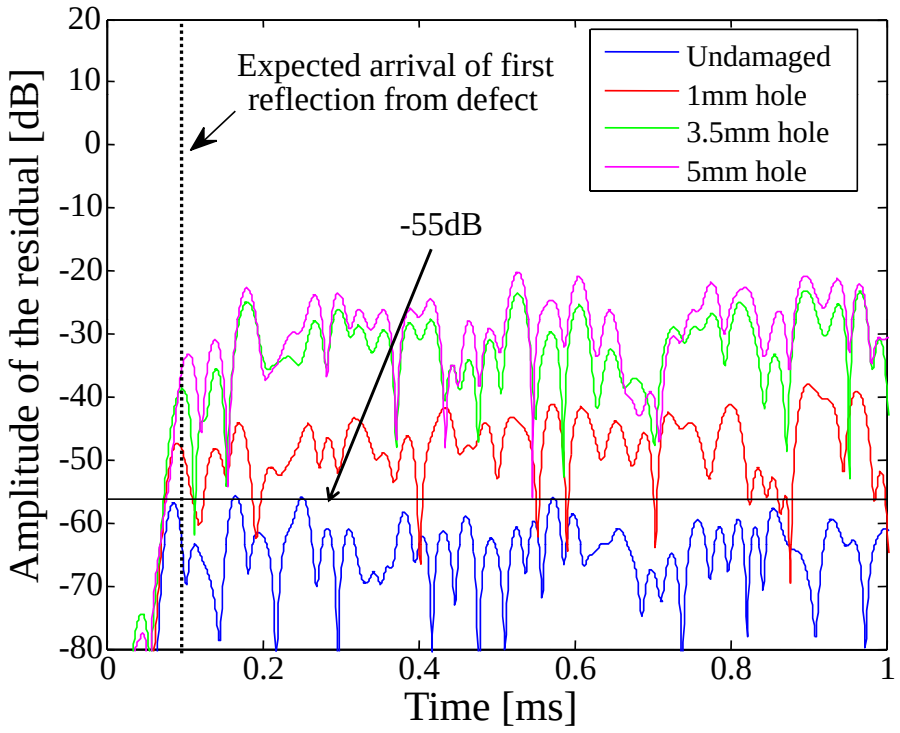

Figure 7.16: *Pitch-catch inspection using the transducers pair 1-2. Amplitude of the residual in the subtraction for different hole diameters compared to the residual for the undamaged structure. Increasing the defect size is responsible for higher residual level.*

the baseline recorded in the undamaged structure. After the 1 mm diameter hole was drilled, the maximum residual level measured over the entire time trace was -38 dB (17 dB higher than the residual level obtained for the undamaged structure). After the hole diameter was increased to 3.5 mm and 5 mm, the maximum residual increased to -23 dB and -20 dB, respectively. The increased residual level indicates that some change has happened and, therefore, can be useful for damage detection. These results show that the subtraction approach can achieve damage detection when the temperature coefficients of expansion and modulus are not uniform in the structure under inspection.

Experiments have been conducted considering other possible transmitter-receiver combinations, in order to demonstrate the generality of the results already presented. It has been observed that the considerations previously made can be considered valid also for other possible inspection strategies with the sensors used in the experiments. Figure 7.17 shows the amplitude of the residual in the subtraction for the transducers

pair 3-4. It can be seen that, even in this pitch-catch configuration of inspection, the presence of the artificial defect accounts for an increase of the residual level at the expected arrival of the first reflection from the defect. After the 1 mm diameter hole was introduced the maximum residual level was -39 dB (16 dB higher than the residual observed when the structure was without defects). After the hole diameter was increased to 3.5 mm and 5 mm, the maximum residual increased to -23.5 dB and -20 dB, respectively. Therefore the maximum values of the residual achieved for each diameter of the drilled hole are very similar to the corresponding values obtained in the pitch-catch inspection with the transducers pair 1-2. However, it has to be observed that the damage detection can be reliable only with a sensible distribution of the sensors of the array with respect to the defect location.

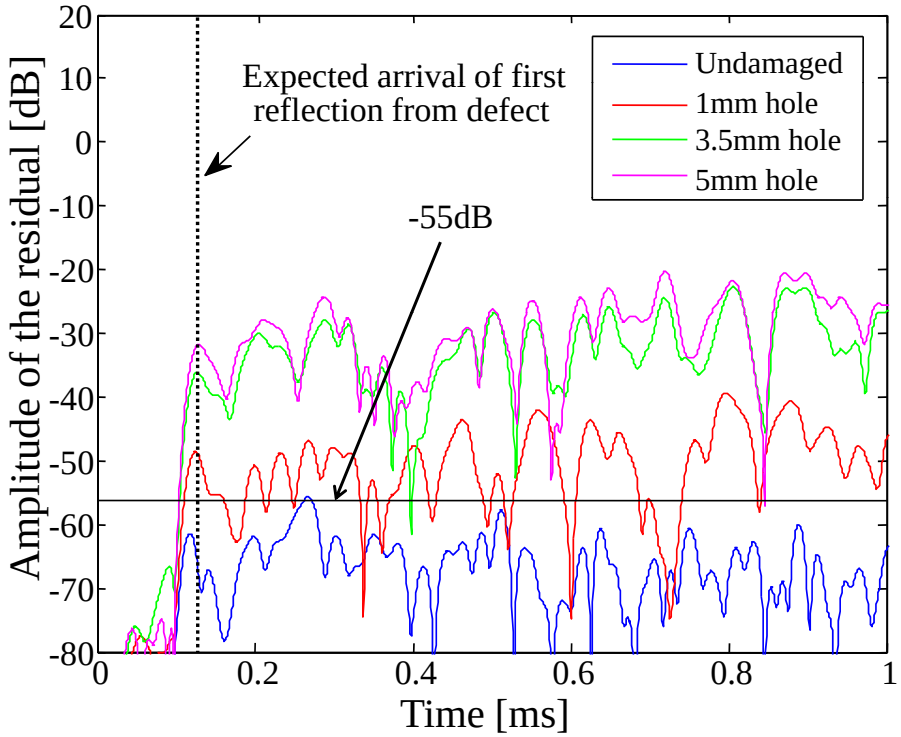

Figure 7.17: *Pitch-catch inspection using the transducers pair 3-4. Amplitude of the residual in the subtraction for different hole diameters compared to the residual for the undamaged structure.*

7.8 Summary

This Chapter has investigated the possibility of employing Temperature Compensation techniques in structures with materials having different temperature coefficients, in order to verify whether Subtraction approach can be reliably applied also in the presence of non uniform temperature responses over the structure. Optimal Stretch is the technique that would be most affected by this issue, since it assumes uniform temperature coefficient over the structure under inspection, whereas Optimal Baseline is not affected in principle by non uniform temperature responses over the structure. Numerical simulations and experiments have been carried out to assess the performance of the Optimal Stretch method. The performance of the Optimal Baseline technique has also been evaluated in the experiments in order to understand whether irreversible changes over the structure were occurring as a consequence of modifications in the adhesive during the post-curing.

A typical stringer for aerospace applications was bonded via an adhesive epoxy layer to a 5 mm thick aluminium plate, in order to evaluate the performance of Temperature Compensation techniques with ultrasonic signals recorded in a real structure comprising materials with different temperature responses. Numerical calculations on a 3D FE model of the experimental setup were also carried out to simulate the different temperature responses of aluminum and epoxy and to predict the performance achievable by the Optimal Stretch method for the S_0 mode.

It was observed experimentally that the performance of Temperature Compensation techniques in the experiments conducted immediately after bonding was negatively affected by irreversible changes occurring in the adhesive bond. The results obtained in subsequent tests showed a significant improvement both for Optimal Stretch and Optimal Baseline performance.

It has been shown that Optimal Stretch, although not specifically designed for dealing with signals recorded in structures where materials with different temperature responses are present, can compensate satisfactorily for temperature variations of approximately 1.5 °C, achieving the target residual level for efficient subtraction.

These results were obtained for large propagation distances, higher than those required for full coverage of inspected areas in practical SHM applications.

The capability of the Subtraction approach in detecting the presence of an artificial defect was evaluated and it was shown that, even in presence of materials with different temperature responses, damage detection was possible because a significant increase in the residual level of the subtracted signal was observed compared to the residual level obtained in the undamaged structure.

Chapter 8

Conclusions

8.1 Thesis Review

The development of an efficient guided wave SHM system requires robust signal processing techniques for the correct interpretation of the complicated ultrasonic time traces that would be recorded in the inspection of a complex structure. Therefore the availability of suitable signal processing techniques is crucial for making damage detection possible and extensive research has been conducted in this field. The main objective of this thesis has been the investigation of two possible approaches, namely Deconvolution and Subtraction, for achieving damage detection. Firstly, Deconvolution has been considered as a possible method for enhancing the resolution of ultrasonic time traces, by reducing the time duration of the individual wavepackets in a time trace. Subsequently, the Subtraction approach has been considered and compensation techniques have been used to reduce the residual in the subtraction between the current signal and the reference signal obtained from the undamaged structure.

The subject of the research and the framework in which this project is set were introduced in Chapter 1. A summary of this work and of the results obtained is given here; for convenience the main findings of this thesis are summarized in the next section.

Chapter 2 described the concept of Structural Health Monitoring, as well as the impact that SHM can have on the operation and maintenance of complex structures. The advantages of sparse distributed arrays for SHM are also introduced and the main requirements for robust signal processing for guided wave SHM were discussed.

The fundamentals of the most widely used deconvolution techniques were briefly reviewed in Chapter 3. Among the several deconvolution methods proposed in the literature Wiener filter and SMLR algorithm appeared as the most suitable techniques for enhancing the resolution of ultrasonic time traces and therefore were chosen as potential deconvolution methods for SHM.

The performance of Wiener filter and SMLR algorithm was evaluated in Chapter 4. It was demonstrated that the effects of noise on the bandwidth of the input wavelet and the effects of the phase shift due to interaction of the input wavelet with structural features are detrimental for the feasibility of a Deconvolution approach for SHM. With respect to the first issue, the Wiener filter performed well when a broadband input waveform was used, but the performance was significantly reduced when a typical narrowband input signal for NDE was considered. The SMLR algorithm was able to achieve perfect deconvolution with a better resolution than the Wiener filter even with very noisy signals, providing zero width spikes as the result of the deconvolution. Considering the effects of phase shift, it was observed that although frequency independent phase shift could be overcome, little improvement in resolution was obtained using the Wiener filter in presence of frequency dependent phase shift. The application of the SMLR algorithm to the deconvolution of a frequency independent phase shifted signal showed that this technique is very sensitive to modifications of the form of the original wavelet. These considerations suggest that Deconvolution is unlikely to be useful for guided wave SHM applications, because the relatively narrow bandwidth of the input wavelet and phase shifts between different reflections would limit significantly the benefits obtained from deconvolution.

The Subtraction approach was introduced in Chapter 5 and the detrimental effects of temperature variations had been examined in detail. It has been shown that the

residual in the subtraction of two signals recorded at different temperature can be related to the temperature difference. Subsequently, Temperature Compensation techniques were introduced and a brief review of their application in SHM was presented.

In Chapter 6 the effects of liquid loading on Subtraction were evaluated and a comparison with the effects of temperature change was made. Numerical simulations were carried out to compare the effects of liquid loading with the effects of temperature variations. It was shown that Temperature Compensation techniques can compensate satisfactorily also for the presence of a thin liquid layer. Experiments on a plate immersed in a water tank and on a plate coated with a thin layer of epoxy adhesive were conducted, confirming that Temperature Compensation techniques can be employed in principle to compensate for detrimental effects different from temperature changes.

In Chapter 7 the performance of the Temperature Compensation techniques were evaluated in the presence of materials with different temperature responses. Numerical simulations and experimental work were conducted on an aluminium plate with a stringer bonded by an epoxy adhesive. It was shown experimentally that, although Optimal Stretch assumes uniform temperature responses over the structure, it was possible to compensate for 1 °C temperature change, achieving the target residual level for Subtraction. A maximum residual in the subtraction very close to the target residual level was achieved also up to 1.5 °C temperature change. By comparison the maximum temperature difference between current signal and baseline that Optimal Stretch was able to compensate in the same configuration in a free aluminium plate was 2.5 °C.

8.2 Brief summary of the main contributions

The main contributions and findings of this thesis can be briefly summarized as follows:

- It was demonstrated that the Deconvolution approach, although promising for enhancing the resolution of ultrasonic time traces in simple configurations, does not appear suitable for SHM applications since the relatively narrow bandwidth of the input signal used in SHM and the sensitivity to modifications of the shape of the input signal (e.g. phase shift) represent strong limitations to the effectiveness of this approach;

- The effects of uniform liquid loading on a plate were compared to the effects of temperature change, showing that the presence of a uniform liquid layer on a plate can be related to an equivalent temperature variation of the free plate;

- Temperature compensation techniques were tested also in the presence of "uniform non-temperature effects". It was demonstrated that these detrimental effects can also be overcome in principle using compensation methods designed for temperature changes;

- It was shown that the compensation strategy based on the combined use of Optimal Baseline and Optimal Stretch can achieve the target residual level in the presence of uniform liquid loading. This was verified with simple signals in numerical simulations and in experimental tests on a aluminium plate immersed in water and on an aluminium plate coated with a viscoelastic epoxy layer;

- It was shown that Temperature Compensation techniques can also be employed to improve subtraction performance in structures comprising materials with different temperature responses. It was possible to compensate for reasonable temperature changes using only the Optimal Stretch method, achieving the target residual level of -40 dB for subtraction;

- It was shown that the compensation strategy based on the combined use of Optimal Baseline and Optimal Stretch can detect the presence of an artificial defect even in the presence of non uniform temperature responses over the structure under inspection.

Most of these results have been presented at international NDT conferences and published as proceedings. A paper on the evaluation of Deconvolution approach is currently in press in Journal of Structural Health Monitoring and papers are being prepared for submission to refereed journals.

8.3 Future work

Deconvolution performance was shown to be negatively affected by modifications of the original shape of the input wavelet. Although it was concluded that Deconvolution has limited applicability to SHM, it could be interesting to investigate the possibility of overcoming the effects of the interaction of the input wavelet with typical structural features of interest for SHM, to verify whether the results presented in this work on the application of Deconvolution could be improved.

The Subtraction approach appears promising for practical guided waves SHM applications. However, the feasibility of this approach depends on environmental conditions and further work is necessary to make this method effectively applicable to real SHM problems.

With respect to the application of Temperature Compensation techniques to overcome the detrimental effects of liquid loading, it would be interesting to study some configurations of non uniform liquid loading on plate-like structures. For instance partial coverage of plate-like structures with water or other low viscosity liquid is often encountered in practice and the modeling or the experimental representation of this kind of problems are not straightforward.

Temperature Compensation techniques performed well also in presence of a viscoelastic liquid layer, represented by an uncured epoxy adhesive and the case of a non uniform adhesive layer was also considered. More investigation can be conducted on this topic and for instance it would be interesting to study the performance of Subtraction in the case of partially painted plate-like structures and in presence of varying thickness of the paint layer. Furthermore the situation of a cured adhesive

epoxy (representing the effects of paint) should be considered.

Considering the monitoring of structures with non uniform temperature responses, the performance of Temperature Compensation techniques could be characterized in more complex configurations (e.g. more stringers bonded to a plate to simulate an airframe panel) and in the presence of temperature gradients in the structure. Furthermore the combined effects of non uniform temperature responses and liquid loading could be simultaneously taken into account in evaluating the performance of the Subtraction approach.

References

[1] D. Balageas, C. P. Fritzen, and A. Güemes. *Structural Health Monitoring*. ISTE Ltd, London, UK, 2006.

[2] C. Boller. Next generation structural health monitoring and its integration into aircraft design. *International Journal of Systems Science*, 31(11):1333–1349, 2000.

[3] R. P. Dalton, P. Cawley, and M. J. S. Lowe. Propagation of acoustic emission signals in metallic fuselage structure. *IEE Proc.-Sci. Meas. Technol.*, 148(4):169–177, 2001.

[4] R. P. Dalton, P. Cawley, and M. J. S. Lowe. The potential of guided waves for monitoring large areas of metallic aircraft fuselage structure. *Journal of Nondestructive Evaluation*, 20(1):29–46, 2001.

[5] A. J. Croxford, P. D. Wilcox, B. W. Drinkwater, and G. Konstantinidis. Strategies for guided-wave structural health monitoring. *Proc. Royal Society A*, 463:2961–2981, 2007.

[6] A. J. Croxford, P. D. Wilcox, G. Konstantinidis, and B. W. Drinkwater. Strategies for overcoming the effect of temperature on guided wave structural health monitoring. volume 6532, pages 65321T–1 – 65321T–10, 2007.

[7] Y. Lu and J. E. Michaels. A methodology for structural health monitoring with diffuse ultrasonic waves in the presence of temperature variations. *Ultrasonics*, 43(9):717–731, 2005.

[8] C. P. Frizten. Recent developments in vibration-based structural health monitoring. In Fu-Kuo Chang, editor, *Proc. of the 5th International Workshop on Structural Health Monitoring, Stanford University*, pages 42–60. DES*tech* Publications, Inc., 2005.

[9] R. V. Williams. *Acoustic Emission.* Adam Hilger, Bristol, UK, 1980.

[10] A. V. Bakulin, S. N. Isaev, and A. P. Tishkin. Acoustic-emission location of corrosion centers. *Protection of metals*, 24(6):806–809, 1988.

[11] M. R. Gorman. Plate waves acoustic emission. *J. Acoust. Soc. Am.*, 90(1):358–364, 1991.

[12] B. N. Pavlakovic, M. J. S. Lowe, D. N. Alleyne, and P. Cawley. Disperse: A general purpose program for creating dispersion curves. In D. O. Thompson and D. E. Chimenti, editors, *Review of Progress in Quantitative NDE*, volume 16, pages 185–192. Plenum Press, New York, 1997.

[13] R. Geng and J. L. Rose. Modern acoustic emission technique and its application in aviation industry. *Ultrasonics*, 44:e1025–e1029, 2006.

[14] E. I. Madaras, W. H. Prosser, G. Studor, M. R. Gorman, and S. M. Ziola. Structural health monitoring of the space shuttle's wing leading edge. In D. O. Thompson and D. E. Chimenti, editors, *Review of Progress in Quantitative NDE*, volume 25B, pages 1756–1763. Plenum Press, New York, 2006.

[15] N. N. Hsu and W. H. Sachse. Characterization of acoustic emission sources, sensors, and propagation structures. *J. Acoust. Soc. Am.*, 64:S154, 1978.

[16] P.D. Wilcox. Omni-directional guided wave transducer arrays for the rapid inpsection of large areas of plate structures. *IEEE Trans. Ultrason. Ferroelectr. Freq. Control*, 50(6):699–709, 2003.

[17] P.D. Wilcox, M. J. S. Lowe, and P. Cawley. An EMAT array for the rapid inspection of large structures using guided waves. In D. O. Thompson and D. E. Chimenti, editors, *Review of Progress in Quantitative NDE*, volume 22A, pages 814–821. Plenum Press, New York, 2003.

[18] S. Beard and F. K. Chang. Active damage detection in filament wound composite tubes using built-in sensors and actuators. *Journal of Intelligent Material Systems and Structures*, 8(10):891–897, 1997.

[19] D. N. Alleyne, B. Pavlakovic, M. J. S. Lowe, and P. Cawley. Rapid, long range inspection of chemical plant pipework using guided waves. *Insight*, 43:93–96,101, 2001.

[20] P.D. Wilcox, M. Evans, B. Pavlakovic, D. N. Alleyne, K. Vine, P. Cawley, and M. J. S. Lowe. Guided wave testing of rail. *Insight*, 45(6):413–420, 2003.

[21] P. Cawley, M. J. S Lowe, D. N. Alleyne, B. Pavlakovic, and P. Wilcox. Practical long range guided wave testing: application to pipes and rail. *Materials Evaluation*, 61(1):66–74, 2003.

[22] P. Fromme, P. Wilcox, and P. Cawley. Remote monitoring of plate-like structures using guided wave arrays. In D. O. Thompson and D. E. Chimenti, editors, *Review of Progress in Quantitative NDE*, volume 22A, pages 157–164. American Institute of Physics, New York, 2003.

[23] P. Fromme, P. Wilcox, M. J. S. Lowe, and P. Cawley. On the development and testing of a guided ultrasonic wave array for structural health monitoring. *IEEE Trans. Ultrason. Ferroelectr. Freq. Control*, 53(4):777–785, 2006.

[24] P.D. Wilcox. A signal processing technique to remove the effect of dispersion from guided wave signals. *IEEE Trans. Ultrason. Ferroelectr. Freq. Control*, 50(4):419–427, 2003.

[25] J. Rajagopalan, K. Balasubramaniam, and C. V. Krishnamurthy. A single transmitter multi-receiver (stmr) pzt array for guided ultrasonic wave based structural health monitoring of large isotropic plate structures. *Smart Materials and Structures*, 15(5):1190–1196, 2006.

[26] P. S. Tua, S. T. Quek, and Q. Wang. Detection of cracks in plates using piezo-actuated lamb waves. *Smart Materials and Structures*, 13(4):643–660, 2004.

[27] G. Konstantinidis, B. W. Drinkwater, and P. D. Wilcox. The long term stability of guided wave structural health monitoring systems. In D. O. Thompson and D. E. Chimenti, editors, *Review of Progress in Quantitative NDE*, volume 25B, pages 1702–1709. Plenum Press, New York, 2006.

[28] H. Gao and J. L. Rose. Ultrasonic sensor placement optimization in structural health monitoring using evolutionary strategy. In D. O. Thompson and D. E. Chimenti, editors, *Review of Progress in Quantitative NDE*, volume 25B, pages 1687–1693. Plenum Press, New York, 2006.

[29] T. E. Michaels, J. E. Michaels, B. Mi, and M. Ruzzene. Damage detection in plate structures using sparse ultrasonic transducers arrays and acoustic wavefield imaging. In D. O. Thompson and D. E. Chimenti, editors, *Review of Progress in Quantitative NDE*, volume 24A, pages 938–945. Plenum Press, New York, 2005.

[30] J. E. Michaels and T. E. Michaels. Guided wave signal processing and image fusion for in situ damage localization in plates. *Wave Motion*, 44(6):482–492, 2007.

[31] J. E. Michaels and T. E. Michaels. Enhanced differential methods for guided wave phased array imaging using spatially distributed piezoelectric transducers. In D. O. Thompson and D. E. Chimenti, editors, *Review of Progress in Quantitative NDE*, volume 25B, pages 837–844. Plenum Press, New York, 2006.

[32] H. Gao, Y. Shi, and J. L. Rose. Guided wave tomography on an aircraft wing with leave in place sensors. In D. O. Thompson and D. E. Chimenti, editors, *Review of Progress in Quantitative NDE*, volume 24B, pages 1788–1794. Plenum Press, New York, 2005.

[33] X. Zhao, H. Gao, G. Zhang, B. Ayhan, F. Yan, C. Kwan, and J. L. Rose. Active health monitoring of an aircraft wing with embedded piezoelectric sensor/actuator network: I. defect detection, localization and growth monitoring. *Smart Materials and Structures*, 16(4):1208–1217, 2007.

[34] V. Giurgiutiu. Lamb-wave embedded nde with piezoelectric wafer active sensors for structural health monitoring of thin-wall structures. In D. O. Thompson and D. E. Chimenti, editors, *Review of Progress in Quantitative NDE*, volume 23B, pages 1452–1459. American Institute of Physics, New York, 2004.

[35] V. Giurgiutiu, A. Zagrai, and J. J. Bao. Piezoelectric wafer embedded active sensors for aging aircraft structural health monitoring. *Structural Health Monitoring*, 1(1):41–62, 2002.

[36] M. Lin and F. K. Chang. The manufacturing of composite structures with a built in network of piezoceramics. *Compos. Sci. Technol.*, 62(7-8):919–939, 2002.

[37] M. Lin, X. Qing, A. Kumar, and S. J. Beard. Smart layer and smart suitcase for structural health monitoring applications. In D. O. Thompson and D. E. Chimenti, editors, *Proc. SPIE on Smart Structures and Materials*, volume 4332. SPIE Optical Engineering Press, 2001.

[38] X. Qing, A. Kumar, C. Zhang, I. G. Gonzalez, G. Guo, and F. K. Chang. A hybrid piezoelectric/fiber optic diagnostic system for structural health monitoring. *Smart Materials and Structures*, 14(3):S98–S103, 2005.

[39] G. Gorinevsky and G. Gordon. Spatio-temporal filter for structural health monitoring. In *Proc. of the 2006 American Control Conference*, pages 3743–3748, 2006.

[40] P. Gaydecki. *Foundations of Digital Signal Processing: Theory, Algorithms and Hardware Design*. The institution of Electrical Engineers, London, 2004.

[41] R. E. Challis, R. J. Freemantle, G. P. Wilkinson, and J. D. H. White. Compression wave NDE of adhered metal lap joints: uncertainties and echo feature extaction. *Ultrasonics*, 34:315–319, 1996.

[42] E. A. Robinson and T. S. Durrani. *Geophysical Signal Processing*. Prentice-Hall, Englewood Cliffs, NJ, 1986.

[43] E. A. Robinson and S. Treitel. *Geophysical Signal Analysis*. Prentice-Hall, Englewood Cliffs, NJ, 1980.

[44] O. Yilmaz and S. M. Doherty. *Seismic Data Processing*. Society of Exploration Geophysicists, Tulsa, Oklahoma, 1987.

[45] N. Wiener. *Extrapolation, Interpolation and Smoothing of stationary time series*. John Wiley and sons, New York, 1949.

[46] J. Leinbach. Wiener spiking deconvolution and minimum phase wavelets: A tutorial. *The Leading Edge*, 14(3):189–192, 1995.

[47] K. L. Peacock and S. Treitel. Predictive deconvolution: Theory and practice. *Geophysics*, 34(2):155–169, 1969.

[48] E. A. Robinson and S. Treitel. Principles of digital Wiener filtering. *Geophysical Prospecting*, 15(3):311–332, 1967.

[49] N. Levinson. The Wiener rms error criterion in filter design and prediction. *J. Math. Phys.*, 25:261–278, 1947.

[50] A. Jurkevics and R. Wiggins. A critique of seismic deconvolution methods. *Geophysics*, 49(12):2109–2116, 1984.

[51] A. J. Berkhout. Least-squares inverse filtering and wavelet deconvolution. *Geophysics*, 42(7):1369–1383, 1977.

[52] A. J. Bickel and D. R. Martinez. Resolution performance of Wiener filter. *Geophysics*, 48(7):887–899, 1983.

[53] A. D. Hillery and R. T. Chin. Iterative Wiener filters for image restoration. *IEEE Trans. Signal Processing*, 39(8):1892–1899, 1991.

[54] J. L. Starck and E. Pantin. Deconvolution in astronomy: A review. *Publications of the Astronomical Society of the Pacific*, 114:105–1068, 2002.

[55] E. Sekko, G. Thomas, and A. Boukrouche. A deconvolution technique using optimal Wiener filtering and regularization. *IEEE Trans. Signal Processing*, 72(1):23–32, 1999.

[56] J. S. Lim and A. V. Oppenheim. Enhancement and bandwidth compression of noisy speech. *Proceedings of the IEEE*, 67(12):1586–1604, 1979.

[57] L. M. Arslan. Modified Wiener filtering. *Signal Processing*, 86(2):267–272, 2006.

[58] S. P. Neal, P. L. Speckman, and M. A. Enright. Flaw signature estimation in ultrasonic nondestructive evaluation using the Wiener filter with limited prior information. *IEEE Trans. Ultrason. Ferroelectr. Freq. Control*, 40(4):347–353, 1993.

[59] P. Karpur, B. G. Frock, and P. K. Bhagat. Wiener filtering for image enhancement in ultrasonic nondestructive evaluation. *Materials Evaluation*, 48(11):1374–1379, 1990.

[60] F. Honarvar, H. Sheikhzadeh, M. Moles, and A. N. Sinclair. Improving the time-resolution and signal-to-noise ratio of ultrasonic nde signals. *Ultrasonics*, 41(9):755–763, 2004.

[61] T. Miyashita, H. Schwetlick, and W. Kessel. Recovery of ultrasonic impulse response by spectral extrapolation. *Acoustica Imaging*, 14:247–256, 1985.

[62] C. A. Zala, I. Barrodale, and K. I. McRae. High resolution deconvolution of ultrasonic traces. In *Proceedings of a NATO Advanced Research Workshop held within the activities of the NATO Special Programme on Sensory Systems for Robotic Control on Signal processing and pattern recognition in nondestructive evaluation of materials*, pages 101–108. Springer-Verlag New York, Inc., 1988.

[63] S. K. Sin and C. H. Chen. A comparison of deconvolution techniques for the ultrasonic nondestructive testing evaluation of material. *IEEE Trans. on Image Processing*, 1(1):3–10, 1992.

[64] M. H. Hayes. *Statistical digital signal processing and modeling.* John Wiley & Sons, Inc., USA, 1996.

[65] J. M. Mendel. *Optimal Seismic Deconvolution: An Estimation Based Approach.* Academic Press, New York, 1983.

[66] J. J. Kormylo and J. M. Mendel. Maximum-likelihood detection and estimation of Bernoulli-Gaussian processes. *IEEE Trans. Information Theory*, 28(3):482–488, 1982.

[67] C. Y. Chi and J. M. Mendel. Improved maximum-likelihood detection and estimation of Bernoulli Gaussian processes. *IEEE Trans. Information Theory*, 30(2):429–435, 1984.

[68] J. Goutsias and J. M. Mendel. Maximum-likelihood deconvolution: An optimization theory perspective. *Geophysics*, 51(6):1206–1220, 1986.

[69] G. B. Giannakis, J. M. Mendel, and X. Zhao. A fast prediction-error detector for estimating sparse-spike sequences. *IEEE Trans. Geoscience and Remote Sensing*, 27(3):344–351, 1989.

[70] K. F. Kaaresen. Deconvolution of sparse spike trains by iterated window maximization. *IEEE Trans. Signal Processing*, 45(5):1173–1183, 1997.

[71] K. F. Kaaresen and E. Bolviken. Blind deconvolution of ultrasonic traces accounting for pulse variance. *IEEE Trans. Ultrason. Ferroelectr. Freq. Control*, 46(3):564–573, 1999.

[72] R. A. Wiggins. Minimum entropy deconvolution. *Geoexploration*, 16(1):21–35, 1978.

[73] M. Ooe and T.J. Ulrych. Minimum entropy deconvolution with an exponential transformation. *Geophysical Prospecting*, 27(2):458–473, 1979.

[74] C. A. Cabrelli. Minimum entropy deconvolution and simplicity: A noniterative algorithm. *Geophysics*, 50(3):394–413, 1985.

[75] C.-S. Wang, J. Tang, and B. Zhao. An improvement on d norm deconvolution: A fast algorithm and the related procedure. *Geophysics*, 56(5):675–680, 1991.

[76] T. J. Ulrych and C. Walker. Analytic minimum entropy deconvolution. *Geophysics*, 47(9):1295–1302, 1982.

[77] R. Wiggins. Entropy guided deconvolution. *Geophysics*, 50(12):2720–2726, 1985.

[78] P.H. Van Cittert. Zum einfluss der spaltbreite auf die itensitatswerteilung in spektrallinien. *Z. Phys.*, 69:298–308, 1931.

[79] L. J. B. LaCoste. Deconvolution by successive approximations. *Geophysics*, 47(12):1724–1730, 1982.

[80] E. O. Brigham, H. W. Smith, F. X. Bostick, and W. C. Duesterhoeft. An iterative technique for determining inverse filters. *IEEE Trans. Geoscience Electronics*, 6(2):86–96, 1968.

[81] B. Alessandrini and M. Gasperini. The deconvolution of marine seismic source: An iterative approach. *Geophysics*, 54(6):780–784, 1989.

[82] H. W. J. Debeye and P. Van Riel. l_P-norm deconvolution. *Geophysical Prospecting*, 38(4):381–403, 1990.

[83] H. L. Taylor, S. C. Banks, and J. F. McCoy. Deconvolution with the l_1 norm. *Geophysics*, 44(1):39–52, 1979.

[84] O. J. Karst. Linear curve fitting using least deviations. *Journal of the American Statistical Association*, 53(281):118–132, 1958.

[85] H. M. Wagner. Linear curve fitting using least deviations. *Journal of the American Statistical Association*, 54(285):206–212, 1959.

[86] I. Barrodale, C. A. Zala, and N. R. Chapman. Comparison of the l_1 and l_2 norms applied to one-at-a-time spike extraction from seismic traces. *Geophysics*, 49(11):2048–2052, 1984.

[87] S. Levy and D. W. Oldenburg. The deconvolution of phase-shifted wavelets. *Geophysics*, 47(9):1285–1294, 1982.

[88] D. W. Oldenburg. A comprehensive solution to the linear deconvolution problem. *Geophysics*, 65(2):331–357, 1981.

[89] T. Clarke, F. Simonetti, S. Rokhlin, and P. Cawley. Evaluation of the temperature stability of a low frequency a0 mode transducer developed for shm applications. In D. O. Thompson and D. E. Chimenti, editors, *Review of Progress in Quantitative NDE*, volume 27A, pages 910–917. American Institute of Physics, 2008.

[90] P. Gaydecki. A versatile real-time deconvolution dsp system implemented using a time domain inverse filter. *Measurement Science Technology*, 12(1):82–88, 2001.

[91] D. N. Alleyne and P. Cawley. Optimization of Lamb wave inspection techniques. *NDT&E International*, 25(1):11–22, 1992.

[92] P. J. Torvik. Reflection of wave trains in semi-infinite plates. *J. Acoust. Soc. Am.*, 41(2):346–353, 1967.

[93] M. J. S. Lowe, P. Cawley, J. Y. Kao, and O. Diligent. The low frequency reflection characteristics of the fundamental antisymmetric Lamb wave a_0 from a rectangular notch in a plate. *J. Acoust. Soc. Am.*, 112(6):2612–2622, 2002.

[94] G. L. Choy and P. G. Richards. Pulse distortion and Hilbert transformation in multiply reflected and refracted body waves. *Bulletin of the Seismological Society of America*, 65(1):55–70, 1975.

[95] R. N. Bracewell. *The Fourier transform and its applications*. McGraw-Hill Book Co., New York, 1965.

[96] J. M. Mendel. White-noise estimators for seismic data processing in oil exploration. *IEEE Trans. on Automatic Control*, 22(5):694–706, 1977.

[97] J. M. Mendel. *Maximum-Likelihood Deconvolution: a Journey into Model-Based Signal Processing*. Springer, New York, 1990.

[98] J. J. Kormylo and J. M. Mendel. Maximum-likelihood seismic deconvolution. *IEEE Trans. Geoscience and Remote Sensing*, 21(1):72–82, 1983.

[99] J. A. Högbom. Aperture synthesis with a non-regular distribution of interferometer baselines. *Astron. Astrophys. Suppl.*, 15:417–426, 1974.

[100] G. Konstantinidis, B. W. Drinkwater, and P. D. Wilcox. The temperature stability of guided wave structural health monitoring systems. *Smart Materials and Structures*, 15(4):967–976, 2006.

[101] O. Diligent, T. Grahn, A. Boström, P. Cawley, and M. Lowe. The low-frequency reflection and scattering of the s_0 Lamb mode from a circular through-thickness hole in a plate: Finite element, analytical and experimental studies. *J. Acoust. Soc. Am.*, 112(6):2589–2601, 2002.

[102] R. L. Weaver and O. I. Lobkis. Temperature dependence of diffuse field phase. *Ultrasonics*, 38(1-8):491–494, 2000.

[103] T. Clarke, F. Simonetti, and P. Cawley. Guided wave health monitoring of complex structures by sparse array systems: influence of temperature changes on performance. *Journal of Sound and Vibration*, 2009 in press.

[104] A. Mazzeranghi and D. Vangi. Methodology for minimizing effects of temperature in monitoring with the acousto-ultrasonic technique. *Experimental Mechanics*, 39(2):86–91, 1999.

[105] S. E. Olson, M. P. DeSimio, and M. M. Derriso. Structural health monitoring incorporating temperature compensation. In Fu-Kuo Chang, editor, *Proc. of the 5th International Workshop on Structural Health Monitoring, Stanford University*, pages 1635–1642. DES*tech* Publications, Inc., 2005.

[106] P. D. Wilcox, G. Konstantinidis, and B. W. Drinkwater. Structural health monitoring using sparse distributed networks of guided wave sensors. *Proceedings of SPIE on Smart Structures and Integrated Systems*, 6173:469–480, 2006.

[107] O. I. Lobkis and R. L. Weaver. Coda-wave interferometry in finite solids: Recovery of P-to-S conversions rates in an elastodynamic billiard. *Physical Review Letters*, 90(25), 2003.

[108] G. Konstantinidis, P. D. Wilcox, and B. W. Drinkwater. An investigation into the temperature stability of a guided wave structural health monitoring

system using permanently attached sensors. *IEEE Sensors Journal*, 7(5):905–912, 2007.

[109] P. D. Wilcox, A. J. Croxford, J. E. Michaels, Y. Lu, and B. W. Drinkwater. A comparison of temperature compensation methods for guided wave structural health monitoring. In D. O. Thompson and D. E. Chimenti, editors, *Review of Progress in Quantitative NDE*, volume 27B, pages 1453–1460. American Institute of Physics, 2008.

[110] A. J. Croxford, P. D. Wilcox, Y. Lu, J. Michaels, and B. W. Drinkwater. Quantification of environmental compensation strategies for guided wave structural health monitoring. volume 6935, 2008 in press.

[111] T. Clarke, F. Simonetti, and P. Cawley. Evaluation of a strategy to minimize temperature effects during sparse-array guided wave SHM of real complex structures. In D. O. Thompson and D. E. Chimenti, editors, *Review of Progress in Quantitative NDE*, volume 28. American Institute of Physics, 2009 in press.

[112] J. E. Michaels and T. E. Michaels. Detection of structural damage from the local temporal coherence of diffuse ultrasonic signals. *IEEE Trans. Ultrason. Ferroelectr. Freq. Control*, 52(10):1769–1782, 2005.

[113] J. E. Michaels and T. E. Michaels. An integrated strategy for detection and imaging of damage using a spatially distributed array of piezoelectric sensors. volume 6532, pages 653203:1–12, 2007.

[114] J. E. Michaels. Detection, localization and characterization of damage in plates with an *in situ* array of spatially distributed ultrasonic sensors. *Smart Materials and Structures*, 17(3):035035 (15pp), 2008.

[115] H. Sohn. Effects of environmental and operational variability on structural health monitoring. *Philosofical Transations Royal Society A*, 365:539–560, 2007.

[116] Y. Lu and J. E. Michaels. Discriminating damage from surface wetting via feature analysis for ultrasonic structural health monitoring systems. In D. O.

Thompson and D. E. Chimenti, editors, *Review of Progress in Quantitative NDE*, volume 27B, pages 1420–1427. American Institute of Physics, 2008.

[117] F. Simonetti and P. Cawley. On the nature of shear horizontal wave propagation in elastic plates coated with viscoelastic materials. *Proc. Royal Society A*, 460:2197–2221, 2004.

[118] C. L. Yapura and V. K. Kinra. Guided waves in a fluid-solid bilayer. *Wave motion*, 21:35–46, 1995.

[119] Z. Zhu and J. Wu. The propagation of Lamb waves in a plate bordered with a viscous liquid. *J. Acoust. Soc. Am.*, 98:1057–1064, 1995.

[120] B. Pavlakovic and M. J. S. Lowe. Disperse User's Manual. 2003.

[121] P. M. Sutton. The variation of the elastic constants of crystalline aluminum with temperature between 63°K and 773°K. *Physical Review*, 91(4):816–821, 1953.

[122] F. B. Cegla, P. Cawley, and M. J. S. Lowe. Fluid bulk velocity and attenuation measurements in non-newtonian liquids using a dipstick sensor. *Measurement Science Technology*, 17(2):264–274, 2006.

[123] P. B. Nagy and R. M. Kent. Ultrasonic assessment of Poisson's ratio in thin rods. *J. Acoust. Soc. Am.*, 98(5):2694–2701, 1995.

[124] T. Vogt, M.J.S. Lowe, and P. Cawley. Ultrasonic waveguide techniques for the measurement of material properties. In D. O. Thompson and D. E. Chimenti, editors, *Review of Progress in Quantitative NDE*, volume 21B, pages 1742–1749. American Institue of Physics, New York, 2002.

[125] R. J. Freemantle and R. E. Challis. Combined compression and shear wave ultrasonic measurements on curing adhesive. *Measurement Science and Technology*, 9:1291–1302, 1998.

[126] A. J. Kinloch. *Durability of Structural Adhesives*. Applied Science Publishers, London, UK, 1983.

[127] K. A. Vine. *The Non-destructive Testing of Adhesive Joints for Environmental Degradation*. PhD thesis, University of London, 1999.

[128] B. D. Zeller, A. J. Kinloch, and P. Cawley. Characterization of epoxy-coated oxide films using acoustic microscopy,. In D. O. Thompson and D. E. Chimenti, editors, *Review of Progress in Quantitative NDE*, volume 17B, pages 1261–1268. Plenum Press, New York, 1998.

[129] G. W. C. Kaye and T. H. Laby. *Tables of Physical and Chemical Constants*. Longman, Essex, England, 1995.

[130] http://www.hexcel.com/. *Redux Bonding Technology*. 2003.

[131] *http://abaqus.cc.ic.ac.uk/v6.5/index.html*.

[132] J. Zhang, B. W. Drinkwater, and P. D. Wilcox. Defect characterization using an ultrasonic array to measure the scattering coefficient matrix. *IEEE Trans. Ultrason. Ferroelectr. Freq. Control*, 55(10):2254–2265, 2008.

[133] C. V. Cagle, H. Lee, and K. Neville. *Handbook of Adhesive bonding*. McGraw-Hill, USA, 1973.

List of Publications

[P1] T. Cicero, P. Cawley, F. Simonetti, and S.I. Rokhlin. Potential and Limitations of a Deconvolution Approach for Guided Wave Structural Health Monitoring. Journal of Structural Health Monitoring. In press.

[P2] T. Cicero, P. Cawley, M. Lowe and F. Simonetti. Effects of liquid loading and change of properties of adhesive joints on subtraction techniques for Structural Health Monitoring. In D. O. Thompson and D. E. Chimenti, editors, *Review of Progress in Quantitative NDE*, volume 28. American Institute of Physics, Melville, New York, 2009. In press.

[P3] T. Cicero, P. Cawley, M. Lowe, F. Simonetti, and S.I. Rokhlin. Deconvolution approach for sparse sensor arrays in Structural Health Monitoring. In D. O. Thompson and D. E. Chimenti, editors, *Review of Progress in Quantitative NDE*, volume 27A, pages 571-578. American Institute of Physics, Melville, New York, 2008.